

# The effect of dynamical speed of light theories in Palatini formalism on the cosmic evolution

Dissertation  
zur Erlangung des Doktorgrades  
an der Fakultät für Mathematik, Informatik und Naturwissenschaften  
Fachbereich Physik  
der Universität Hamburg

vorgelegt von  
Shadi Sajedi Shacker

Hamburg  
2018

Gutachter/innen der Dissertation: Prof. Dr. Robi Banerjee  
Prof. Dr. Mariafelicia De Laurentis

Zusammensetzung der Prüfungskommission: Prof. Dr. Robi Banerjee  
Prof. Dr. Peter Hauschildt  
Prof. Dr. Jochen Liske  
Prof. Dr. Marco Zagermann  
Prof. Dr. Geraldine Servant

Vorsitzende/r der Prüfungskommission: Prof. Dr. Jochen Liske

Datum der Disputation: 19.03.2018

Vorsitzender Fach-Promotionsausschusses PHYSIK:  
Prof. Dr. Wolfgang Hansen

Leiter des Fachbereiches Physik: Prof. Dr. Michael Potthoff

Dekan der Fakultät MIN: Prof. Dr. Heinrich Graener



FIRST, I would like to thank Robi Banerjee for providing me with the opportunity of doing my PhD in his research group. I am sincerely thankful for his encouragement, motivation and support.

Working in this group has been a great pleasure for me and I am also extremely thankful for my colleges' support during this time.

I would also like to acknowledge the support of a very nice friend and collaborator, Azam Izadi, from whom I learned a lot. Her patience and kindness made working with her really easy for me.

My special gratitude goes to Gonzalo Olmo, as one of the first people I always bother by asking my questions from. I learned a lot about modified gravity models from him and this work was not possible without his great feedback and extreme help.

I am also grateful to Jochen Liske for patiently guiding me through different observational data. I know it was quit a new field for me and he had to start teaching me all from the basics. I am totally thankful for the time he spent on our discussions.

I would also like to express my gratitude to my encouraging family; specially my parents, my aunts, my two brothers, my two cousins who are like sisters to me.

They have always tolerated my bad moods, given me hope and never let me feel lonely. I can count on them at any time, although we live far apart. I am so grateful for all the love and kindness they have always given me. I should also mention our new sweet member of the family, Kian, who has brought me a world full of joy.

LAST but not least, I would like to mention my high school sweetheart, aka my husband! Time passes so quickly and I cannot believe it has been years since he helped me decide to choose physics as my major. Since then, we have been through a lot and he was always there for me. I am truly grateful for all his inspiration and love.

To

MY GRANDMOTHER,  
WHOSE FAITH ENLIGHTENED MY LIFE

AND

MY MOTHER,  
WHOSE SMILE MOTIVATED ME TO CONTINUE



# The effect of dynamical speed of light theories in Palatini formalism on the cosmic evolution

## ABSTRACT

Motivated by the presence of the cosmological constant or Dark Energy as a huge part of the energy content of the universe, a lot of modified gravity models have been proposed. On the other hand, the constancy or dynamics of fundamental constants is of doubt in some theories.

Here, I study the dynamics of different facets of the speed of light in Palatini theories of gravity, where metric and connection are regarded to be independent from each other. It has been shown before that in such theories, in a local frame with a vanishing affine connection, the usual degeneracy between different manifestations of the speed of light is broken. I use this broken degeneracy in a  $f(\mathcal{R}^{\mu\nu}\mathcal{R}_{\mu\nu})$  model to check if different observations and constraints are in agreement with this claim.

In particular, I study the effect of a  $f(\mathcal{R}^{\mu\nu}\mathcal{R}_{\mu\nu})$  model on the Hubble parameter. Then using this modified Hubble parameter, I use the impact of the dynamics of the causal structure constant ( $c_{ST}$ ) on the distance modulus of Supernovae Ia and the predictions of the redshift drift without assuming cosmological constant (or Dark Energy) in the energy content of the universe. On the other hand, using the constraints given by quasar absorption lines and also the recent LIGO-Virgo observation on the dynamics of the speed of electromagnetic waves ( $c_{EM}$ ), I show that in this model a degeneracy between  $c_{EM}$  and  $c_{ST}$  is also favored by data.

At the end, using the fact that the speed of gravitational waves is constant in such model, I show  $c_{GW} \leq c_{EM} < c_{ST}$  in each redshift, within the redshift range I studied.

## ZUSAMMENFASSUNG

Der wesentliche Teil des Energiebudgets unseres Universums besteht aus einer noch unbekanntem Energieform, welche als Dunkle Energie oder kosmologische Konstante bezeichnet wird. Ihre Existenz hat zahlreiche Modifikationsansätze für die bestehenden Modelle der Gravitation motiviert. In einigen Theorien wird die zeitliche Konstanz der fundamentalen Naturkonstanten in Zweifel gezogen.

In dieser Arbeit untersuche ich die Dynamik verschiedener Facetten der Lichtgeschwindigkeit im Rahmen der Palatini-Gravitationstheorie, welche die Raumzeit-Metrik sowie die affine Verbindung zwischen Raumzeitpunkten als voneinander unabhängige Größen betrachtet. Es

wurde bereits gezeigt, dass in solche Theorien in einem lokalen Bezugssystem mit einer verschwindenden affinen Verbindung die sonst vorliegende Entartung zwischen den verschiedenen Manifestationen der Lichtgeschwindigkeit aufgelöst wird.

Basierend auf dieser Auflösung der Entartung prüfe ich in einem  $f(\mathcal{R}^{\mu\nu}\mathcal{R}_{\mu\nu})$ -Modell, inwiefern verschiedene Beobachtungen und Beobachtungsvorhersagen mit dieser Annahme übereinstimmen. Speziell untersuche ich die Auswirkungen eines  $f(\mathcal{R}^{\mu\nu}\mathcal{R}_{\mu\nu})$ -Modells auf den Hubble-Parameter. In einem solchen Ansatz kann die Dynamik der Kausalitätsstrukturkonstante  $c_{ST}$  und ihre Auswirkungen auf das Entfernungsmodul von Typ Ia Supernovae sowie ihren Rotverschiebungsdrift gänzlich ohne die Annahme einer kosmologischen Konstante (oder ohne Dunkle Energie) studiert werden. Beobachtungen von Absorptionslinien in Quasaren und der zeitlichen Variabilität der Geschwindigkeit elektromagnetischer Wellen ( $c_{EM}$ ) durch LIGO-Virgo zeigen, dass die vorliegenden Daten eine Entartung zwischen  $c_{EM}$  und  $c_{ST}$  favorisieren. Abschließend leite ich für den gesamten untersuchten Parameterraum der Rotverschiebung her, dass für Gravitationswellen, die in einem  $f(\mathcal{R}^{\mu\nu}\mathcal{R}_{\mu\nu})$ -Modell eine konstante Geschwindigkeit haben, der Zusammenhang  $c_{GW} \leq c_{EM} < c_{ST}$  gilt.

## LIST OF PUBLICATIONS

Izadi, A., **Sajedi Shacker, S.**, Olmo, G. J., & Banerjee, R., Observational effects of varying speed of light in quadratic gravity cosmological models. 2017, ArXiv e-prints

## Eidesstattliche Versicherung / Declaration on oath

Hiermit versichere ich an Eides statt, die vorliegende Dissertationsschrift selbst verfasst und keine anderen als die angegebenen Hilfsmittel und Quellen benutzt zu haben.

Die eingereichte schriftliche Fassung entspricht der auf dem elektronischen Speichermedium.

Die Dissertation wurde in der vorgelegten oder einer ähnlichen Form nicht schon einmal in einem früheren Promotionsverfahren angenommen oder als ungenügend beurteilt.

Hamburg, den 04.04.2018

---

Unterschrift der Doktorandin / des Doktoranden

# Contents

1	INTRODUCTION	3
2	STANDARD GENERAL RELATIVITY VERSUS OBSERVATIONS	7
2.1	Standard General Relativity	7
2.1.1	A short review on $\Lambda$ CDM model	8
2.1.2	The Observable Hubble Data (OHD)	9
2.1.3	The luminosity distance of Supernovae Ia	10
2.1.4	The redshift drift	13
2.1.5	Gravitational waves	17
2.2	$\Lambda$ CDM model challenges	18
2.3	Summary	19
3	DYNAMICAL FUNDAMENTAL COUPLINGS	21
3.1	Dynamical fine structure constant	22
3.1.1	Quasar absorption lines	22
3.2	Speed of light: different origins, different notions	24
3.3	Dynamical Speed of Light theories	26
3.3.1	Cosmological questions and dynamical speed of light	26
3.3.2	A model, as an example	27
4	EXTENDED THEORIES OF GRAVITY	31
4.1	EPS framework	32
4.2	A brief review on the Palatini formalism	34
4.2.1	Palatini $f(\mathcal{R})$ gravity	35
4.2.2	The equivalence between Brans-Dicke and $f(\mathcal{R})$ theories	36
4.2.3	Palatini $f(\mathcal{R}^{\mu\nu}\mathcal{R}_{\mu\nu})$ gravity	37
4.3	Different local frames in Palatini formalism	41
4.4	Different facets of the speed of light in the local frame ( $\Gamma$ LF)	41
4.4.1	The spacetime matter constant	41
4.4.2	Causal structure constant in the FRW spacetime	42
4.4.3	Speed of electromagnetic waves in FRW spacetime	43

4.4.4	Speed of the gravitational waves . . . . .	45
4.5	Summary . . . . .	46
5	A DETAILED INVESTIGATION OF THE $f(\mathcal{R}^{\mu\nu}\mathcal{R}_{\mu\nu})$ MODEL IN THE LOCAL FRAME, $\Gamma$ LF . . . . .	47
5.1	Approach and model ( $\mathcal{L} = \mathcal{R} + F\mathcal{R}^{\mu\nu}\mathcal{R}_{\mu\nu}$ ) . . . . .	48
5.2	Fitting the model parameter, $\gamma$ . . . . .	50
5.2.1	Observable Hubble Data and different models . . . . .	51
5.2.2	The causal structure constant ( $c_{\text{ST}}$ ) . . . . .	53
5.2.3	Studying the effect of a varying $c_{\text{ST}}$ on SN Ia luminosity distance . . . . .	54
5.2.4	The redshift drift . . . . .	59
5.3	A new fit for the model parameter . . . . .	61
5.3.1	The Hubble parameter with $\gamma(z)$ . . . . .	64
5.3.2	The distance modulus of SN Ia with $\gamma(z)$ . . . . .	66
5.3.3	The redshift drift with $\gamma(z)$ . . . . .	67
5.4	Dynamics of the speed of electromagnetic waves . . . . .	71
5.4.1	The quasar absorption lines and $c_{\text{EM}}$ . . . . .	72
5.4.2	Comparing the dynamics of $c_{\text{ST}}$ and $c_{\text{EM}}$ . . . . .	75
5.5	Speed of gravitational waves . . . . .	77
5.5.1	Constraints on $c_{\text{EM}}$ using gravitational wave observations . . . . .	80
5.6	Summary . . . . .	83
6	CONCLUSION AND OUTLOOK . . . . .	87
	BIBLIOGRAPHY . . . . .	90



## Numerical values used for fitting the model

Parameter	Value	Uncertainty	Reference
$H_0$	$65.1 \text{ km s}^{-1} \text{ Mpc}^{-1}$	$+1.7 / -1.9$	<a href="#">Planck Collaboration et al. 2015</a>
	$2.1097 \times 10^{-18} \text{ s}^{-1}$	$+2.1648 / -2.0482$ ( $\times 10^{-18} \text{ s}^{-1}$ )	
$l_p$	$1.6162 \times 10^{-35} \text{ m}$		<a href="#">Mohr et al. 2016</a>
$c_0$	$2.9979 \times 10^8 \text{ m s}^{-1}$	exact	<a href="#">Mohr et al. 2016</a>
$G$	$6.6741 \times 10^{-11} \text{ m}^3 \text{ kg}^{-1} \text{ s}^{-2}$	$31 \times 10^{-16}$	<a href="#">Mohr et al. 2016</a>
$\kappa = \frac{8\pi G}{c_0^2}$	$2.0766 \times 10^{-43}$		
$\Omega_m^0$	0.3289		Planck+WMAP 68% limits <a href="#">Planck Collaboration et al. 2015</a>
$\rho_{m,LCDM}^0 = \frac{3H_0^2 \Omega_m^0}{8\pi G}$	$2.6179 \times 10^{-27} \text{ kg m}^{-3}$		
$\rho_{m,EdS}^0 = \frac{3H_0^2}{8\pi G}$	$7.9607 \times 10^{-27} \text{ kg m}^{-3}$		
$\Omega_\Lambda^0 = 1 - \Omega_m^0$	0.6711		

## Frequently used symbols

---

Symbol	
$a(t)$	scale factor ( $\frac{a(t)}{a_0} = \frac{1}{1+z}$ )
$z$	redshift
$H$	Hubble parameter ( $\frac{\dot{a}}{a}$ )
$d_L$	Luminosity distance
$\Omega_i$	Density parameter of the $i$ component (matter, radiation,...)
$\Lambda$	Cosmological constant
$\Lambda$ CDM	$\Lambda$ Cold Dark Matter
$\Gamma_{\mu\nu}^{\alpha}$	Affine connection
$\left\{ \begin{smallmatrix} \alpha \\ \mu\nu \end{smallmatrix} \right\}$	Christoffel symbol
$R$	Ricci scalar made from Christoffel symbols
$R_{\mu\nu}$	Curvature tensor made from Christoffel symbols
$\mathcal{R}$	Ricci scalar made from Affine connections
$\mathcal{R}_{\mu\nu}$	Curvature tensor made from Affine connections
DSL	Dynamical Speed of Light
VSL	Varying Speed of Light
FRW	Friedmann–Lemaitre–Robertson–Walker

---

# 1

## Introduction

The standard  $\Lambda$ CDM model<sup>1</sup>, is perhaps one of the simplest and most prominent cosmological models that we had until now. The success of this model, cannot be denied. However, man's scientific spirit can never stop him from looking for knowing it “*all*”. The presence of the cosmological constant ( $\Lambda$ ) as an unknown constant, has motivated a lot of scientists not only to study the origin and meaning of it, but also examine extended models (e.g. (Amendola & Tsujikawa, 2010; Li et al., 2007; Tsujikawa, 2010)). Mentioning this at the beginning of this thesis helps me in expressing that although a lot of physicists believe in the  $\Lambda$ CDM model as a well founded theory, the attempt to explore other theories more has never stopped. Having a pile of extended models, shows that these models have to be studied further and their strength and also shortcomings must be compared and reviewed. In fact it shows that it is worth exploring different possible models, finding their advantages and drawbacks and finally be able to at least make the possible models, a smaller number and keep the ones with more benefits. Any of these conclusions would help in going one step forward in order to get the ultimate perfect model.

The success of  $\Lambda$ CDM model, has been revealed by several distinct observations. This model consists of Dark Matter and also the cosmological constant which plays the role of Dark Energy<sup>2</sup> (Amendola & Tsujikawa, 2010).

Among these observations, the luminosity distance of *Supernovae type Ia* (SN Ia) showed our universe has recently gone through an expansion phase (Perlmutter et al., 1999; Riess et al., 1998); and confirms that it can be well explained with a  $\Lambda$ CDM universe. Also,  $\Lambda$ CDM model can explain the shift of the position of *Cosmic Microwave Background* (CMB) acoustic peaks, also

---

<sup>1</sup>Also known as the concordance model.

<sup>2</sup>Based on Planck observations  $H_0 = 65.1^{+1.7}_{-1.9}$ ,  $\Omega_b h^2 = 0.02207$  and  $\Omega_c h^2 = 0.1173$  (Planck Collaboration et al., 2015)

known as the CMB shift parameter (Amendola & Tsujikawa, 2010; Tsujikawa, 2013).

However apart from all the advantages and simplicity, this model suffers from ambiguities such as the *cosmological constant problem*, *fine tuning problem* and the *coincidence problem*. Such problems are the main motivations to look for alternative models (e.g (Amendola & Tsujikawa, 2010; Joyce et al., 2015)). To put it another way, not knowing what the so called cosmological constant is, can be a reasonable motivation to look if  $\Lambda$ CDM model is just some other way of expressing another model which is less ambiguous. Another alternative to the standard theory is modifying the standard gravitational theory. Here, the Lagrangian is modified by adding extra geometric terms; e.g. terms which are made of the curvature tensor or modifying the matter content of the universe (Olmo, 2012). These models can be considered both in metric and Palatini formalism.

Unlike the metric formalism, Palatini formalism considers the Christoffel symbol and the affine connection to be independent from each other; therefore it gives a more generic description of the space time geometry (Fatibene & Francaviglia, 2012).

On the other hand, the constancy of the usual constants used in physical theories has been of doubt for a while now (e.g. (Magueijo, 2003)). Although the standard theory assumes some of the fundamental constants (such as the speed of light ) to be non-dynamical, there is no good reason not to explore more.

This doubt, resulted in several theoretical and experimental studies on the possibility and consequences of the existence of dynamical fundamental constants in recent years(e.g. (Barrow, 2003; Barrow & Lip, 2012; Magueijo, 2003; Murphy et al., 2001a; Uzan, 2004, 2011; Webb et al., 1999, 2001; Balcerzak & Dabrowski, 2014; Zhang & Meng, 2014)). Among these studies, here in this thesis we favor the ones studying either dynamics of the fine structure constant which can be translated to the dynamic of the electromagnetic waves, or the dynamics of speed of light in general. Of course a varying fine structure constant can be supposed to be the result of a varying  $c$ ,  $e$ ,  $\hbar$ , or a combination of these.

Basically, dynamical speed of light models can be used to solve some of the standard cosmological theory's problems, such as the horizon enigmas, which is related to the causal connection between different points in the sky; and can be solved by considering an inflationary era in the early universe. Similarly, a larger speed of light in the earlier times can enlarge the horizon and locate different parts of the universe in each other's horizons (Magueijo, 2003).

Furthermore, speed of light has different facets and it enters different physical equations with different origins (Ellis & Uzan, 2005), such as the causal structure constant ( $c_{ST}$ ) or the speed of the gravitational waves ( $c_{GW}$ ). In fact, there is no compelling reason to assume all these facets to not only be constant in cosmic time, but also be the same. Of course this is the case in the standard theory, but it has been shown that this may not hold in non-standard models (Izadi & Shojai, 2009).

The independency between the Christoffel symbol and the affine connection in Palatini formalism, results in two different local frames; one with the Christoffel symbol vanishing and the other one with vanishing affine connection. Interestingly in the frame in which the affine connection vanishes, if we consider different origins for the speed of light, they can in principle not only be-

come different from each other, but also become variable (Izadi & Shojai, 2009). Unlike many dynamical speed of light models which predefine speed of light as a function of redshift (time) (e.g. (Qi et al., 2014)), this approach results in varying different facets of the speed of light without predefining the form of variation.

In this thesis, we consider the approach mentioned above and study how different facets of the speed of light change in cosmic time, using different observational data.

In terms of time, when studying this model, we focus on the change of different facets of speed of light in recent era; i.e. we do not consider these changes in the very early universe.

Our main goal is first to study how different facets of speed of light change and if they are comparable to each other or not, and second to examine how considering such deviations between different facets of the speed of light can be helpful in eliminating Dark Energy at least in explaining some cosmological observations.



# 2

## Standard General Relativity versus observations

### 2.1 Standard General Relativity

As discussed before, the validity of General Relativity (GR) has been shown with great precision in small ranges to large ones. Hence, we dedicate this section to this revolutionary theory.

As it will be discussed in chapter 4, GR puts a lot of constraints on the geometry of the manifold, such that the connection is the metric connection and the Lagrangian is taken to be Einstein Hilbert Lagrangian. We will review this idea in chapter 4. In GR (when considering no cosmological constant), the action is given by

$$S = \frac{1}{2\kappa} \int d^4x \sqrt{-g} R + S_m(g_{\mu\nu}, \psi), \quad (2.1)$$

in which  $g_{\mu\nu}$  is the metric,  $R$  is the Ricci scalar,  $S_m$  is the matter action and  $\psi$  is the matter field. Using the action principle, varying (2.1) with respect to the metric and also  $\delta S_m = -1/2 \int d^4x \sqrt{-g} T_{\mu\nu} \delta g^{\mu\nu}$ , we get to Einstein field equations.

$$R_{\mu\nu} - \frac{1}{2} g_{\mu\nu} R = \kappa T_{\mu\nu} \quad (2.2)$$

This is the Einstein field equations from standard GR without a cosmological constant (see e.g. (D'Inverno, 1992)).

## 2.1.1 A short review on $\Lambda$ CDM model

Discovering the accelerated expansion of the universe (Perlmutter et al., 1999; Riess et al., 1998), revealed the need for considering an exotic kind of reason for this expansion in the content of our universe. This unknown expansion source, can either be a constant energy throughout the cosmic history or a variable which has changed to the present amount we observe indirectly today. The constant energy added to the total amount of the universe's energy, is coming from the so called *cosmological constant*. This constant can make a negative pressure which can dominate the universe in recent years and win over the attraction force of matter (see e.g. (Amendola & Tsujikawa, 2010; Weinberg, 2008)).

Despite several remained questions about the cosmological constant, the  $\Lambda$ CDM model is still the simplest cosmological model presented until now (e.g. (Tsujikawa, 2011)). Due to the fact that Hubble's law (performed by Hubble and Slipher (Amendola & Tsujikawa, 2010)), have shown that Einstein-Hilbert Lagrangian is not satisfactory, an extra term is needed to justify an accelerated expansion of our universe. If our universe is dominated only by matter, we expect its expansion to be decelerating; therefore, observing an accelerated expansion means we need something different to have a negative pressure and accelerate the expansion of the universe (see e.g. (Tsujikawa, 2011; Izadi et al., 2017; Farooq & Ratra, 2013)).

Hence as the standard  $\Lambda$ CDM model we need to modify Einstein field equations, either by adding an extra sentence either to the left hand side of (2.2) as a geometric term or to the right hand side of (2.2) as an extra term to the matter terms. This means the Einstein-Hilbert action must be modified by adding an extra term to it as

$$S = \frac{1}{2\kappa} \int d^4x \sqrt{-g} (R - 2\Lambda) + S_m(g_{\mu\nu}, \psi) \quad (2.3)$$

and by varying this action with respect to the metric we have

$$R_{\mu\nu} + g_{\mu\nu}(\Lambda - \frac{1}{2}R) = \kappa T_{\mu\nu} \quad (2.4)$$

This is what we call the Einstein field equations of the  $\Lambda$ CDM model. At first Einstein entered this constant  $\Lambda$  to have a static universe, although after a while it was proven that not only our universe is not static, but it also is in an accelerated expansion phase. For a more detailed historical points see (Amendola & Tsujikawa, 2010).

On the other hand, the *Friedmann-Lemaître-Robertson-Walker* (FRW) metric (Amendola & Tsujikawa, 2010), which shows a homogeneous and isotropic universe is given by

$$g_{\mu\nu} = \begin{pmatrix} 1 & 0 & 0 & 0 \\ 0 & -\frac{a^2}{1-Kr^2} & 0 & 0 \\ 0 & 0 & -a^2r^2 & 0 \\ 0 & 0 & 0 & -a^2r^2 \sin^2 \theta \end{pmatrix} \quad (2.5)$$

Here,  $a = a(t)$  is the scale factor of the universe and  $K$  is the curvature of the universe. Using this metric, the  $00$  and  $ii$  components of the field equations in (2.4), give the Friedmann equations

$$\begin{aligned} H^2 &= \frac{8\pi G}{3}\rho - \frac{Kc^2}{a^2} - \frac{\Lambda c^2}{3} \\ \frac{\ddot{a}}{a} &= -\frac{4\pi G}{3}\left(\rho + \frac{3p}{c^2}\right) + \frac{\Lambda c^2}{3} \end{aligned} \quad (2.6)$$

in which  $H = \dot{a}/a$  is the Hubble parameter,  $\rho$  is the energy density of the fluid and  $p$  is the pressure of the fluid. In terms of the density parameters, the Hubble parameter of the  $\Lambda$ CDM model in the recent universe in which the radiation is negligible, is given as<sup>1</sup>

$$H = H_0 \sqrt{\Omega_m^0 (1+z)^3 + \Omega_\Lambda^0} \quad (2.7)$$

in which  $\Omega_m^0 + \Omega_\Lambda^0 = 1$ . The standard cosmological model discussed here (the  $\Lambda$ CDM model), agrees with different observations (e.g. (Amendola & Tsujikawa, 2010)). In what follows we talk about few of them.

### 2.1.2 The Observable Hubble Data (OHD)

One of the methods which is used to investigate the value of the Hubble parameter in different redshifts is the differential age method.

Defining the Hubble parameter as  $H = \dot{a}/a$ , one rewrites this equation in terms of the redshift,

$$H(z) = -\frac{1}{1+z} \frac{dz}{dt}. \quad (2.8)$$

Then by observing old passive galaxies, one can calculate the variation of the age ( $dt$ ) in a redshift range ( $dz$ ) (Zhang et al., 2010). Figure 2.1 shows the Hubble parameter of the  $\Lambda$ CDM model together with the Observable Hubble Data. For the observable data, we selected the data related to the differential age method from Table 1 of Ref. (Farooq & Ratra, 2013).

---

<sup>1</sup> $H_0 = 65.1 \text{ kms}^{-1}\text{Mpc}^{-1}$ ,  $\Omega_m^0 = 0.3289$  (Planck Collaboration et al., 2015)

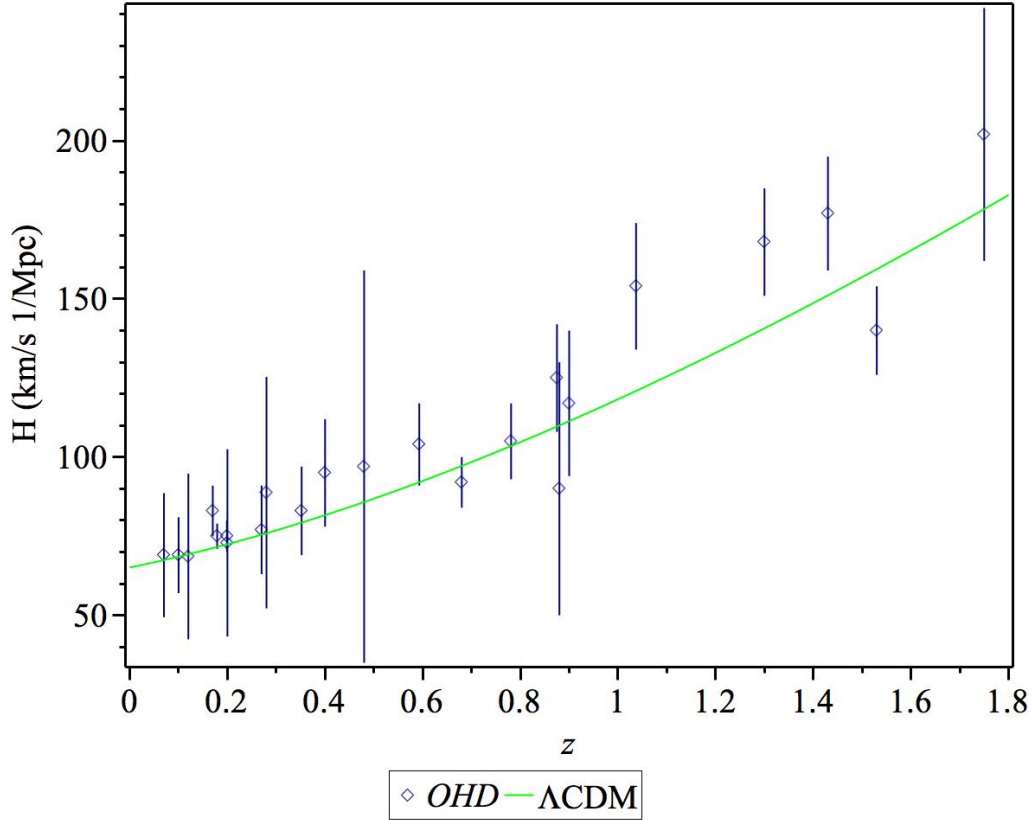


**Figure 2.1:** The Hubble parameter vs. redshift for  $\Lambda$ CDM model (Planck Collaboration et al., 2015) and Observable Hubble Data (selected data from measurements of differential age method) (Farooq & Ratra, 2013), which is in the redshift range  $0.070 < z < 1.750$ .

As it is clear here, the  $\Lambda$ CDM model agrees with the OHD. Considering no cosmological constant, the value of the Hubble parameter would become so much larger that it does not agree with these data points anymore. Also, as shown here, the Hubble parameter increases with redshift.

### 2.1.3 The luminosity distance of Supernovae Ia

The observations of the luminosity distance of Supernovae Ia, showing the recent acceleration of the universe (Perlmutter et al., 1999; Riess et al., 1998), is one of the evidences which proves that the standard gravitational model, in which one only considers the Einstein-Hilbert Lagrangian and only matter and radiation in the energy content of the universe, cannot give a satisfactory form of the universe's evolution. This shows that a large part of the energy content of our universe has to be of something unknown that we call : Dark Energy (or the cosmological constant) (see e.g. (Amendola & Tsujikawa, 2010)).

The luminosity distance is given by (Amendola & Tsujikawa, 2010)

$$d_L^2 = \frac{L_s}{4\pi\mathcal{F}} \quad (2.9)$$

in which,  $L_s$  is the absolute luminosity and  $\mathcal{F}$  is the observed flux :

$$\mathcal{F} = \frac{L_o}{4\pi(a_0 f(\chi))^2} \quad (2.10)$$

here  $L_o$  is the observed luminosity and  $f(\chi)$  is given by

$$\begin{aligned} f(\chi) &= \frac{1}{\sqrt{-K}} \sinh(\sqrt{-K}\chi) \\ &= \begin{cases} \sin \chi & \text{for } K = +1 \\ \chi & \text{for } K = 0 \\ \sinh \chi & \text{for } K = -1 \end{cases} \end{aligned} \quad (2.11)$$

$K$  shows the curvature of the universe which can be  $+1, 0, -1$  for a closed, flat or open universe<sup>2</sup>. Also,

$$\chi = \int_0^z c \frac{dz}{H} \quad (2.12)$$

Considering  $a_0 = 1$ , equation (2.9) can then be written as

$$d_L = f(\chi) \sqrt{\frac{L_s}{L_o}} \quad (2.13)$$

On the other hand, considering  $L$  as the luminosity of light which has been emitted in a time interval  $\Delta t$  with energy  $\Delta E$ , we have  $L = \Delta E / \Delta t$  which results in

$$\begin{aligned} d_L &= f(\chi)(1+z) \\ &= \chi(1+z) \\ &= (1+z) \int_0^z c \frac{dz}{H} \end{aligned} \quad (2.14)$$

$H$  is the Hubble parameter which is set according to the model we choose. For instance, for the  $\Lambda$ CDM model we take  $H = H_0 \sqrt{\Omega_m^0 (1+z)^3 + \Omega_\Lambda^0}$ . From the observational point of view, the luminosity distance is written in parsec<sup>3</sup> as

$$d_L = 10^{1+\mu/5} \text{ pc}, \quad (2.15)$$

<sup>2</sup>Here in this thesis, we always consider a flat universe; so  $K = 0$ .

<sup>3</sup>1pc =  $3.0857 \times 10^{16}$  m.

in which  $\mu = m - M$  is the distance modulus,  $m$  is the apparent magnitude, and  $M$  is the absolute magnitude. Figure 2.2, shows the SN distance modulus for observational points (Suzuki & et. al., 2012) and also the  $\Lambda$ CDM model.

In this thesis, we use the data points of (Suzuki & et. al., 2012) as observational data of the SN distance modulus. We are aware of the fact that this data set is corresponding to  $h = 0.7$  ( $H_0 = 70 \text{ km s}^{-1} \text{ Mpc}^{-1}$ ). However, only for the sake of comparison between different models and showing the correct trend of the models, we use these data points.

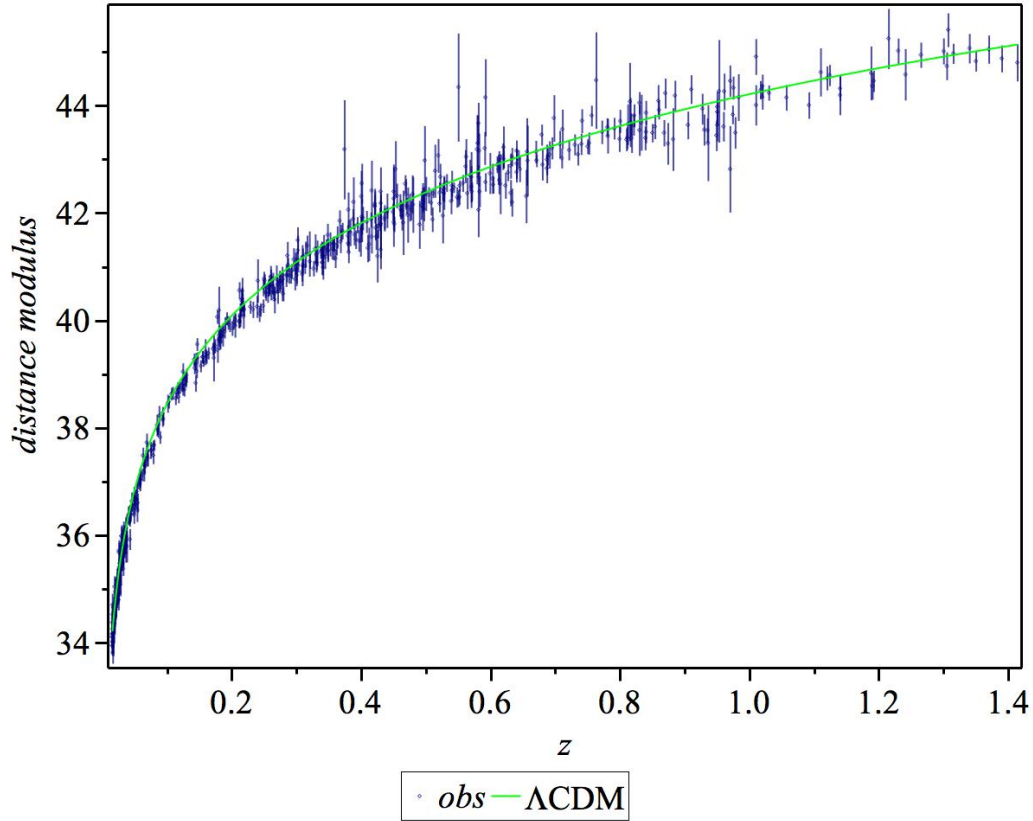


**Figure 2.2:** The SN Ia distance modulus vs. redshift for  $\Lambda$ CDM model (Planck Collaboration et al., 2015) and observational points (Suzuki & et. al., 2012).

As it is shown in Figure 2.2, the SN distance modulus, increases with redshift. In models which only consider matter for this redshift range and no modifications, this distance modulus has an increase which is not enough to match observations. This means such models, show the distance much less than we observe. This is simply one of the reasons we need Dark Energy: to make the distances larger enough to match with the observations (Tsujikawa, 2011).

### 2.1.4 The redshift drift

Theoretically, the expansion of the universe, changes the observed redshift of a source in a given time. This change is of course very small and has not been yet detected. However, observing of the redshift drift in future is not only going to be a direct way to observe the Hubble parameter, but it is also going to be model independent which is a great advantage. Briefly, the method is to observe a source and take its spectrum, take the spectrum again in a future time; and at the end compare these two and look for the shifts in the spectral features (Sandage, 1962; Liske et al., 2008a; Amendola & Tsujikawa, 2010). One of the suitable targets for this method are probably the quasars, as bright sources observed in wide redshift ranges (similar to the method of constraining possible variation of the fine structure constant which is explained in Chapter 3). They also have a lot of sharp absorption lines which would help in increasing the collected information from the spectrum and the precision of the observations (Liske et al., 2008a,b).

When a source emits light at  $t$ , its observed redshift at  $t_0$  is given by

$$z(t_0) = \frac{a_0}{a} - 1 \quad (2.16)$$

in which  $z(t_0)$  is the observed redshift of the source,  $a$  and  $a_0$  are the scale factors at  $t$  and  $t_0$  respectively. When the observer spends  $\Delta t_0$  time, the observed redshift will be

$$z(t_0 + \Delta t_0) = \frac{a(t_0 + \Delta t_0)}{a(t + \Delta t)} - 1 \quad (2.17)$$

The redshift of the source then varies by subtracting equation (2.16) from (2.17).

$$\begin{aligned} \Delta z &= z(t_0 + \Delta t_0) - z(t_0) \\ &\simeq \frac{\Delta t_0}{a} (\dot{a}_0 - \dot{a}) \\ &= H_0 \Delta t_0 \left( (1 + z) - \frac{H}{H_0} \right) \end{aligned} \quad (2.18)$$

According to this equation, if one observes the change in the redshift of some distant objects for a time duration  $\Delta t_0$ , then the Hubble parameter is directly calculated at that redshift (Amendola & Tsujikawa, 2010). As it is shown in this equation, the Hubble parameter can be simply calculated without assuming any kind of cosmological model for the universe. This is one of the advantages of this observation because the result is model independent (Liske et al., 2008b).

As we stated before, this change in the redshift of the quasar can also be translated in the change of the apparent velocity.

If we consider two points  $p$  and  $p'$  with an infinitesimal distance of  $\Delta l$  from each other, then the relative velocity of  $p'$  with respect to  $p$  due to the expansion of the universe would be

$$\begin{aligned} \Delta v &= v_p - v_{p'} \\ &= -H \, dl \end{aligned} \quad (2.19)$$

then, it takes

$$\Delta t = \frac{\Delta l}{c} \quad (2.20)$$

for a signal from  $p'$  to arrive at  $p$ . This leads to

$$\begin{aligned} \Delta t &= \frac{\Delta v}{H c} \\ H \Delta t &= \frac{\Delta v}{c} \\ \Delta v &= \frac{c \Delta z}{1 + z} \end{aligned} \quad (2.21)$$

which shows the relation between the change in the the apparent velocity of the source and the change in its redshift due to the expansion of the universe (Coles & Lucchin, 2002).

The overall precision of this velocity shift,  $\sigma_{\Delta v}$ , for observing 30 quasars at  $z = 4$  with a signal to noise ratio (S/N) of 2370 is going to be  $a_1$ ;  $a_1 = 2$  for using only the Ly $\alpha$  forest lines or  $a_1 = 1.35$  for using Ly $\alpha$  and Ly $\beta$  forest lines and also metal absorption lines. This accuracy is given by (Liske et al., 2008a)

$$\sigma_{\Delta v} = a_1 \left( \frac{2370}{S/N} \right) \left( \frac{30}{N_{\text{QSO}}} \right)^{1/2} \left( \frac{5}{1 + z_{\text{QSO}}} \right)^q \text{ cm/s} \quad (2.22)$$

The number of the lines, depends on the density of the cloud (which is in average a known property of the universe) and also the redshift. The higher the redshift, the denser the Ly $\alpha$  lines will be. Therefore, there are more spectral lines and the precision increases. This can be easily seen in the inverse dependence to the redshift in equation (2.22).

As stated earlier, the number of the spectral features increases with redshift. However at redshift around 4, there are so many spectral lines that they overlap each other and result in decreasing the amount of information. Therefore, from this redshift, the spectral features do not increase the same as before. This is why  $q$ , changes at  $z = 4$ :  $q = 0.9$  at  $z > 4$  and  $q = 1.7$  at  $z < 4$  (Liske et al., 2008a).

The error bars considered for the velocity shift, can be translated to the error bars in redshift drift:  $\sigma_{\Delta v} = c/(1 + z)\sigma_{\Delta z}$ . Using equation (2.18), redshift drift is plotted in Figure 2.3.

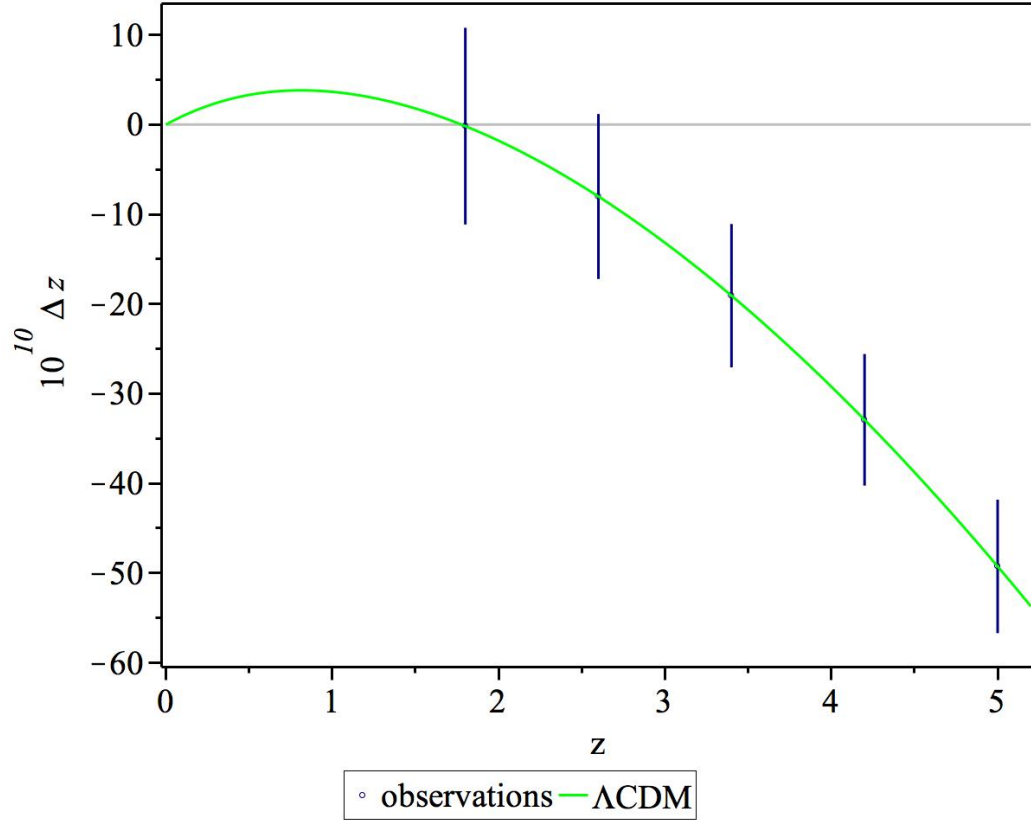


**Figure 2.3:**  $10^{10}\Delta z$  vs. redshift for  $\Lambda$ CDM model (Planck Collaboration et al., 2015) and theoretical observational points. As it is shown in this plot, in this redshift range  $\Delta z$  has a small value of the order of  $\approx 10^{-9}$ , therefore we plot  $10^{10}\Delta z$ . Here we used  $\Delta t_0 = 30$  yr,  $N_{QSO} = 20$ ,  $S/N = 2000$ ,  $a_1 = 1.35$  for the simulated observational points and their uncertainties. For the error bars we used  $\sigma_{\Delta v} = c/(1+z)\sigma_{\Delta z}$ .

As it is shown in Figure 2.3, redshift drift is a very small effect. That is the reason that  $10^{10}\Delta z$  is plotted here. Also, the shift of the redshift in the spectrum experiences an increase, reaches a maximum positive value and then decreases to zero<sup>4</sup> and in  $z = z_{\text{cross}}$  it crosses the zero line which means no shift in the redshift of the quasars is observable. After this redshift, again the redshift of the quasars changes.

The  $z \sim 2$  is an important redshift for us, in the sense that it is near the place in which  $\Delta v$  crosses the zero line. Among all the cosmological models, only the ones which result in accelerated expansion are positive at first and then cross the zero line (Liske et al., 2008a). For the  $\Lambda$ CDM model, the redshift drift crosses the zero line at  $z = 0, 1.7760$ . Other cosmological models, may show a different value for the redshifts at which the redshift drift crosses the zero line. This can be a key to show observational differences between the new models and the  $\Lambda$ CDM model. We will use this feature later.

<sup>4</sup>We call this redshift  $z_{\text{cross}}$ .

As said before,  $\Delta z$  can also be shown as the change in the velocity of the source,  $\Delta v$ .  $\Delta v$  is plotted in Figure 2.4 both for the  $\Lambda$ CDM model and simulated observational points. Again we emphasize that the redshift drift has not been detected yet and the so called “observation” points are taken from simulations with error bars shown in equation (2.22).

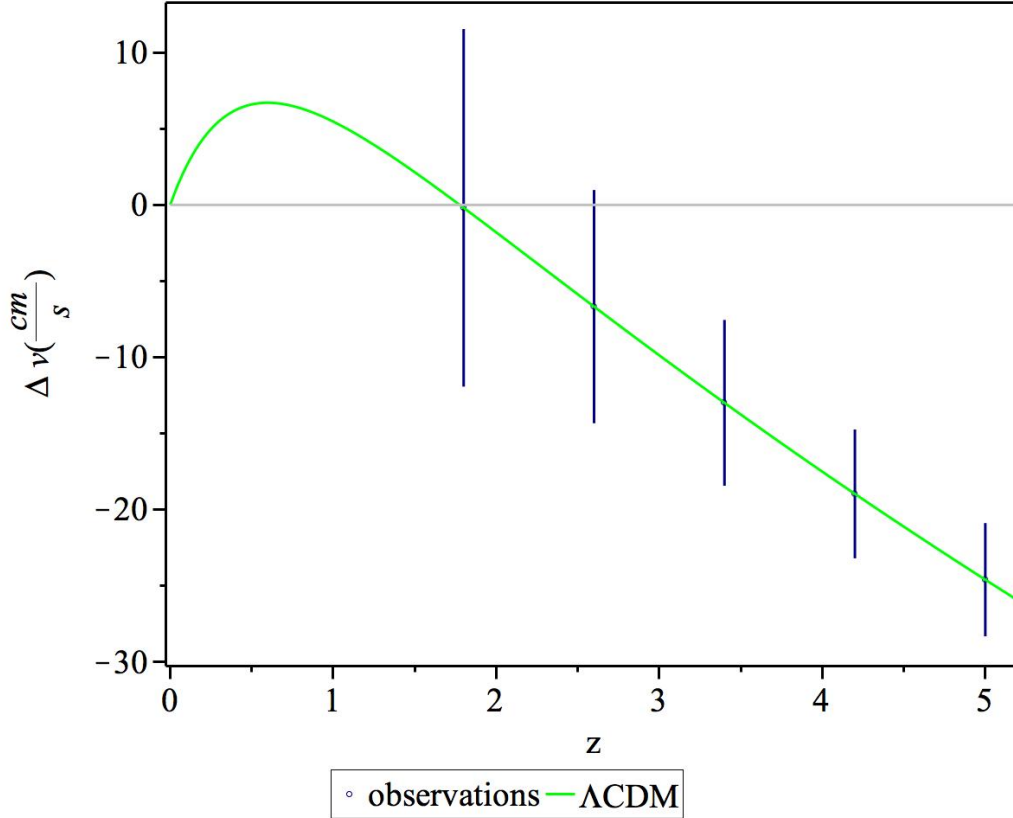


**Figure 2.4:**  $\Delta v$  vs. redshift for  $\Lambda$ CDM model (Planck Collaboration et al., 2015) and simulated observational points. Here we used  $\Delta t_0 = 30$  yr,  $N_{QSO} = 20$ ,  $S/N = 2000$ ,  $a_1 = 1.35$  for the simulated observational points and their theoretical uncertainties. The 20 quasars are considered to be distributed equally in the 5 redshift bins.

What we see from Figure 2.4 is that from  $z = 0$  to  $z \simeq 2$ , there is a shift in the velocity of the quasar; an increase and then a decrease. Then, the plot crosses the zero line at around  $z \simeq 2$ . For the  $\Lambda$ CDM model, using Planck 2013 values (Planck Collaboration et al., 2015), this happens at  $z_{\text{cross}} = 1.7760$ . This means at this redshift, no velocity shift is detected. In other words, no change in the redshift of the quasars at this redshift is detected. Again we emphasize that as this shift is not large enough to be observed by today’s telescopes, by using the word “*detection*”, we mean simulated data points. After crossing the line, the velocity shift will happen again but in a different direction. And it decreases by redshift.

### 2.1.5 Gravitational waves

Considering a small perturbation to the flat geometry metric,

$$g_{\mu\nu} = \eta_{\mu\nu} + \epsilon h_{\mu\nu} \quad (2.23)$$

in which  $\epsilon$  is very small and only up to  $O(\epsilon)$  terms can be kept. Then the Ricci tensor and Ricci scalar would become

$$\begin{aligned} R_{\mu\nu} &= \partial_\rho \tilde{\Gamma}_{\mu\nu}^\rho - \partial_\nu \tilde{\Gamma}_{\rho\mu}^\rho \\ &= \frac{1}{2} \epsilon (\partial_\rho \partial_\mu h_\nu^\rho - \square h_{\mu\nu} - \partial_\mu \partial_\nu h + \partial_\nu \partial^\rho h_{\mu\rho}) \\ R &= \epsilon (\partial_\rho \partial^\alpha h_\alpha^\rho - \square h) \end{aligned} \quad (2.24)$$

If we define a new tensor,  $\psi_{\mu\nu} = h_{\mu\nu} - 1/2 \eta_{\mu\nu} h$ , and consider the gauge condition  $\partial_\alpha \psi_\beta^\alpha = 0$ , then the vacuum solution of the Einstein field equations would result in

$$\square h = 0 \rightarrow \square h_{\mu\nu} = 0 \quad (2.25)$$

(D’Inverno, 1992). This equation is a wave equation with a solution of type  $h_{\mu\nu} = A_{\mu\nu} e^{ikx}$  that results in

$$k^2 = 0 \quad (2.26)$$

Here,  $k$  is the 4-wave vector and the above equation shows that the speed of gravitational waves is  $c$ , the same as the speed of electromagnetic waves.

As seen in the above, the gravitational waves are an interesting result of the linearized Einstein field equations. The most interesting point about observing gravitational waves is that using gravitational waves, we are able to observe sources which are undetectable using electromagnetic waves. Simply speaking, when a heavy mass moves on the space time, it perturbed the space time and makes gravitational waves. The heavier the mass is, the more the space time gets perturbed. A binary black hole merger produces gravitational waves which could only recently been detected. As the two black holes rotate, they produce gravitational waves, become more near to each other and at the end, merge and make a much more massive black hole. When gravitational waves pass between two points, the distance between these points changes. This happens because the shape of the space time changes while gravitational waves move on it (Abbott et al., 2016b,a, 2017b,c)<sup>5</sup>.

The direct observations of a binary black hole merger was done by the LIGO<sup>6</sup> team for the first time (Abbott et al., 2016b). LIGO consists of two large arms, whose lengths change slightly when gravitational waves perturb the space time. According to what the LIGO team reported, the luminosity distance of the first detected source is  $410_{-180}^{+160}$  Mpc.

<sup>5</sup>The last paper is the observation of a binary neutron star.

<sup>6</sup>Laser Interferometer Gravitational-Wave Observatory

## 2.2 $\Lambda$ CDM model challenges

Although this model shows good agreement with a lot of observations, there are some fundamental ambiguities regarding the constant  $\Lambda$  (cosmological constant). In what follows we briefly summarize some of these.

### The fine tuning problem

Considering the first equation in (2.6), at the present time which we show by the 0 indice, we have

$$H_0^2 \sim \frac{\Lambda c^2}{3} \quad (2.27)$$

So the energy density of the cosmological constant can be shown as (Coles & Lucchin, 2002)

$$\rho_\Lambda \approx \frac{\Lambda c^2}{8\pi G} \quad (2.28)$$

which results in  $\rho_\Lambda \approx 10^{-47} \text{ GeV}^4$  (Amendola & Tsujikawa, 2010). On the other hand, we can interpret the cosmological constant's energy momentum tensor as

$$T_{\mu\nu}^\Lambda = \rho_\Lambda c^2 g_{\mu\nu} \quad (2.29)$$

As we can see here, the only thing  $T_{\mu\nu}^\Lambda$  depends on is the metric and this leads us to assume it as a property of the vacuum (Hobson et al., 2006). Therefore, if we look at this energy density embedded in the vacuum, and keep in mind that GR is valid until the Planck scale, the vacuum energy density become

$$\rho_{\text{vac}} \simeq 10^{74} \text{ GeV}^4 \quad (2.30)$$

comparing the last two equations shows there is a big difference between  $\rho_\Lambda$  and  $\rho_{\text{vac}}$  - about  $10^{121}$  order (Amendola & Tsujikawa, 2010). This is called the cosmological constant's fine tuning problem : If the cosmological constant energy is coming from the vacuum energy, then what is all this big difference? If it is not the vacuum energy, then what is it?

### The coincidence problem

The other issue is that not only this value is very small but its energy density is also comparable to the value of energy density of matter. The question is although these two are totally different, matter making gravitational attraction and the cosmological constant making gravitational repulsion, why should the value of these two coincide? In other words the redshift in which the energy density of these two coincide is near 0, the present time (Amendola & Tsujikawa, 2010). Using Planck data (Planck Collaboration et al., 2015), the coincidence redshift is given by <sup>7</sup>

$$\rho_m = \rho_\Lambda \rightarrow z_c = 0.268 \quad (2.31)$$

---

<sup>7</sup>This differs when considering different values for  $\Omega_m^0$  and  $\Omega_\Lambda^0$ .

This is called the cosmological constant's coincidence problem. So in addition to the fact that  $\Lambda$  is an unknown constant to us (the same as Dark Energy), it also suffers from unsolved problems stated above.

All these questions and argues about the cosmological constant, makes one also think about alternatives. Another way to deal with this is to eliminate the cosmological constant and consider an alternative model (see e.g. (Amendola & Tsujikawa, 2010)). In the next following chapters we study some of these attempts.

## 2.3 Summary

As it was shown in this chapter, the simple Einstein-Hilbert Lagrangian cannot give a complete satisfactory explanation of our universe. In principle to explain the recent accelerated expansion of the universe, this has to be modified; either by manually putting a constant (cosmological constant) or adding higher order geometric terms (see e.g. (Amendola & Tsujikawa, 2010; Izadi et al., 2017)). The first approach is a successful one, in terms of simplicity and also observations. However, questions about its origin made people to also try the second approach. This will be more studied in Chapter 4.



# 3

## Dynamical fundamental couplings

This chapter is about the possibility of variation of fundamental constants. Unlike the constants whose values can be acquired from theory (such as  $H_0$ <sup>1</sup>), traditionally fundamental constants are “fixed rigid” values in physics (Ellis et al., 2012).

As mentioned in (Damour, 2009), General Relativity and the whole historical trend of physics lead us to the fact that the physical structures in the universe are rather “*dynamical*” than “*rigid*”. The so called constants’ of physics might then also be “*dynamical entities*” which depend on the space time being dynamical due to the energy content on it (Damour, 2009). This is more clear in the model we chose to work with in Chapter 5.

If the fundamental physical constants are actually “*constant*”, what is the reason? This question has been in people’s minds for a long time now. There is a famous statement by Paul Dirac, which is taken from “On methods in theoretical physics”, in June 1968 in Trieste, which says:

“... *It is usually assumed that the laws of nature have always been the same as they are now. There is no justification for this. The laws may be changing, and in particular quantities which are considered to be constants of nature may be varying with cosmological time...*” (Magueijo, 2003).

Since then, having doubt about the “*constancy of constants*” within the age of the universe, has lead people do several theoretical studies and also carry out observations regarding the possibility of the variation of fundamental constants (see e.g (Planck Collaboration et al., 2015; Uzan, 2004, 2011; Barrow, 2003; Barrow & Lip, 2012; Magueijo, 2003; Murphy et al., 2001a; Webb et al., 1999, 2001)). This has opened a new door to alternative cosmological models and shows the demand of studying the properties and consequences of these models.

In section 3.1, we talk about some observational constraints on the variation of fine structure

---

<sup>1</sup>present value of the Hubble parameter

constant. In chapter 5, we will use these constraints in order to put limits on the variation of speed of electromagnetic waves ( $c_{\text{EM}}$ ). In addition, in that chapter using the recent LIGO-Virgo observations (Abbott et al., 2017c), we constraint  $c_{\text{EM}}$  using the model we introduce later.

### 3.1 Dynamical fine structure constant

Fine structure constant shows the strength of electromagnetic force and is given by  $\alpha_{\text{EM}} = 1/(4\pi\epsilon_0) e^2/(\hbar c_{\text{EM}})$  (Kotuš et al., 2017),  $e$  is the electron charge,  $\hbar$  is the reduced Planck constant and  $c_{\text{EM}}$  is the speed of electromagnetic waves.

In order to find dynamics in this constant, observations sensitive to the dynamics of fine structure constant should be done in higher redshifts. The result can then be compared to the present value of  $\alpha_{\text{EM}}$  (Srianand et al., 2004).

In what follows we review some of these methods using the quasar absorption lines.

#### 3.1.1 Quasar absorption lines

Quasars are luminous objects in the center of galaxies, which are observed as point like sources. One of the interesting features of these luminous objects which are good probes of cosmology is the absorption lines in their spectra (Padmanabhan, 1993).

The possible dynamics of the fine structure constant can be achieved using the light coming from the quasars. Suppose there is a cloud on the way which this light travels through while coming to the Earth. Then the ions in the cloud make absorption lines in the spectrum of the light (Padmanabhan, 1993; Uzan, 2011). Therefore, one can say that these electromagnetic waves, contain some physical information in the redshift of the cloud (Uzan, 2011). Different methods are used to put constraints on the variation of fine structure constant. Here we briefly explain two of them:

- The *Alkali Doublet (AD)* method, is based on the fine structure doublets splitting of the Alkali atoms (Uzan, 2011). Comparing the observed separation of the doublets of the Alkali atoms with the one in the laboratory, one can constraint the dynamics of  $\alpha_{\text{EM}}$ . This separation changes due to the global redshifting of the universe and also a possible dynamic of  $\alpha_{\text{EM}}$ . In this method, the doublet separation of one ion is studied (see e.g. (Uzan, 2011; Murphy et al., 2001b)).
- In the *Many Multiplet (MM)* method, the correlation between different transitions of different atoms is used (Uzan, 2011). This method is more general than the AD method and it uses the multiplets from different kinds of atoms. In fact, unlike the AD method, in which only the wavelength separation of two doublets of an ion is studied, here they use as much doublets as possible. The different separations in these different atoms, change different from each other. The MM method then uses transition which are nearly insensitive to the dynamics of  $\alpha_{\text{EM}}$  (such as Mg II or Mg I transitions) as an anchor. The method is

basically based on comparing relative shifts between the anchor and transitions which are so sensitive to the dynamic of  $\alpha_{EM}$ , like Fe II. (Srianand et al., 2004).

Some of the observational data regarding the quasar absorption lines is given in table 3.1 and also Figure 3.1.

Method	Constraint on $\Delta\alpha/\alpha_0 (\times 10^{-5})$	Redshift	Ref.
AD <sub>1</sub>	$-0.5 \pm 1.3$	2.33 – 3.08	(Murphy et al., 2001b)
AD <sub>2</sub>	$+0.15 \pm 0.43$	1.59 – 2.92	(Chand et al., 2005)
AD <sub>3</sub>	$-3.09 \pm 8.46$	1.1862 – 1.8377	(Martínez Fiorenzano et al., 2003)
MM <sub>1</sub>	$-0.06 \pm 0.06$	0.4 – 2.3	(Chand et al., 2004)
MM <sub>2</sub>	$0.04 \pm 0.23$	1 – 2.4	(Murphy et al., 2016)

**Table 3.1:** Possible dynamics of the fine structure constant ( $\alpha_{EM}(z)/\alpha_0 - 1$ ) using the analysis of quasar absorption spectra. Considering constant  $e$  and  $\hbar$ , we relate this dynamic to the speed of electromagnetic waves; i.e.  $c_0/c_{EM} - 1$  and use this to put constraints on  $c_{EM}$  in chapter 5. The redshift range for the first AD data, is taken from (Uzan, 2011). All constraints presented here are also in agreement with a non varying fine structure constant.

As it is seen in Table 3.1, the methods stated before result in different variations of  $\alpha$  in different redshifts. All these constraints are compatible with no variations in  $\alpha$ .

Figure 3.1 shows the constraints on the possible variation of the fine structure constant, using different methods.

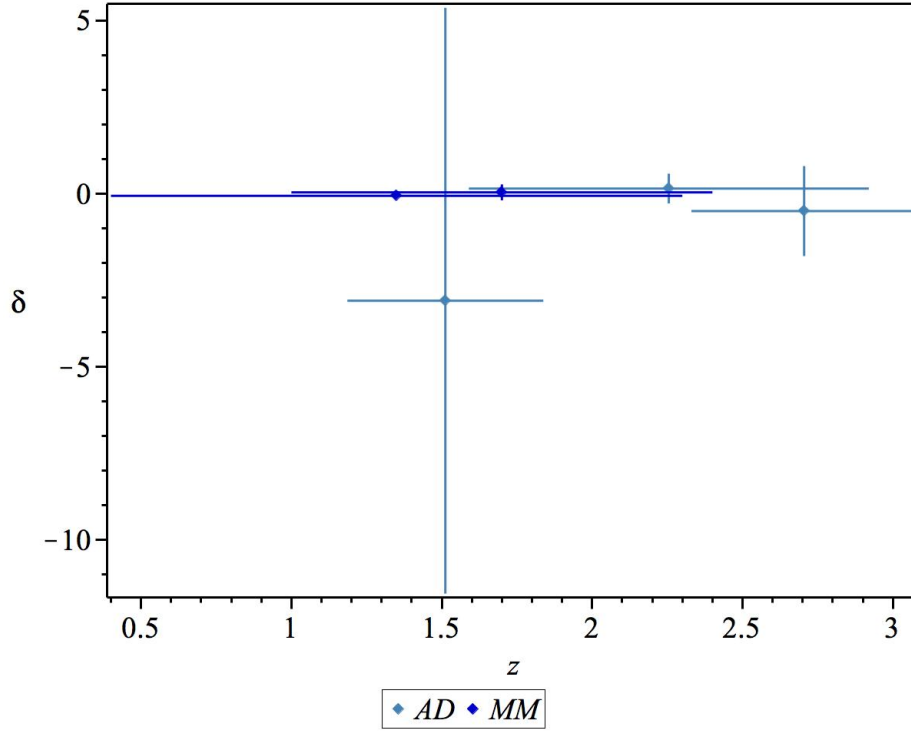


Figure 3.1:  $\delta = \alpha_{EM}(z)/\alpha_0 - 1$  vs. redshift. The data is taken from table 3.1.

### 3.2 Speed of light: different origins, different notions

In physical theories, the speed of light is not only the speed of “light” or electromagnetic waves, but it also enters different equations and plays the role of a *synthesizer* between different physical concepts. This makes the constant  $c$  to have different physical concepts and origins. For instance,  $c$  is not only the speed of electromagnetic waves, but also gravitational waves. Following the approach of G. Ellis and J. Uzan in (Ellis & Uzan, 2005), in what follows we present different notions of the speed of light.

$c_{EM}$  is the speed of electromagnetic waves. This is the speed in which we use in radars and also enters the Maxwell equations. In addition, this is the speed we have in the fine structure constant,  $\alpha_{EM}$  (Ellis & Uzan, 2005).

$c_{ST}$  is the spacetime constant (or causal structure constant). This constant enters the line element and shows the characteristics of the spacetime. This parameter is originally different from  $c_{EM}$  and it is the “universal invariant limit speed” (Ellis & Uzan, 2005). This speed enters the line element

$$ds^2 = c_{ST}^2 dt^2 - \sum_{i=1}^3 (dx^i)^2 \quad (3.1)$$

and the limit speed is given by  $ds^2 = 0$ . For measuring distances and lengths, we use the line element which means  $c_{ST}$  plays a role. Also, the proper time is given by

$$ds^2 = c_{ST}d\tau^2 \quad (3.2)$$

If these two different facets of the speed of light,  $c_{ST}$  and  $c_{EM}$ , do not coincide, one has to consider the difference between these in doing measurements. In this case instead of null geodesics, light follows timelike geodesics. Then doing measurements in non standard theories which result in the difference between these notions of the speed of light, we should first be careful which of them is involved and second how we should measure time and distance. Basically, as it is stated by G. Ellis “*the causal cone need not coincide with the light cone*” (Ellis & Uzan, 2005).

$c_{GW}$  is the speed of gravitational waves. In standard theory in a vacuum, where line element and the linearized Einstein field equations are given by

$$\begin{aligned} ds^2 &= c_{ST}^2 dt^2 - (\eta_{ij} + h_{ij}) dx^i dx^j \\ (\partial_t^2 - c_{ST}^2 \nabla^2) h_{ij} &= 0 \end{aligned} \quad (3.3)$$

then gravitational waves propagate with  $c_{ST}$ . However, again we note that if we have a non standard theory, this may not be the case and there may be a difference between these two (Ellis & Uzan, 2005). Although such attempts result in having massive gravitons which cause some problems, as it is clearly stated by G. Ellis, it is important to consider these two may differ and one should note this discrepancy in non-standard theories.

$c_E$  is called the Einstein spacetime-matter constant. This constant is used to show the coupling between matter and gravity, entering the Einstein field equations,

$$G_{\mu\nu} = \frac{8\pi G}{c_E^A} T_{\mu\nu} \quad (3.4)$$

Of course in case of GR, we have  $c_E = c_{ST}$ , but again Ellis draws our attention to the fact that in non-standard theories, this may not be the case and  $c_E$  can be different from other notions depending on the theory we use. This can happen because all facets mentioned above, have different origins (Ellis & Uzan, 2005).

Hence, when working with non-standard theories, there are some points that should be considered. First it is important to know which facets of the speed of light are involved. Second, we should know if these facets are altering and have dynamics (Ellis & Uzan, 2005; Izadi & Shojai, 2009).

### 3.3 Dynamical Speed of Light theories

Dynamical speed of light <sup>2</sup> theories have their own bright and dark sides. Among the bright sides one can mention the fact that using a dynamic speed of light, different cosmological problems such as the horizon problem and the cosmological constant problem, might become appealing (Magueijo, 2003). Additionally, one of the reasons that dynamical speed of light <sup>3</sup> theories are not as widely acceptable as other dynamical constants, is that by altering the speed of light, things get complicated; in the sense that special relativity is changed, modern physics would differ and in general the structure of physics is altered. However, as stated above these theories might be the answer to some cosmological questions which cannot be solved without proposing exotic features like Dark Energy or inflation. That being the case, it might be worth going through all the complications (Magueijo, 2003).

Discussions about the dynamics of a dimensional constant have always been a hot topic for people, both against and in favor of these theories. As clearly mentioned and explained by George Ellis in (Ellis et al., 2012), when defining systems of units using speed of light, one cannot discuss any variation of  $c$ . In other words, using natural units for determining distances,  $c$  is unity by definition <sup>4</sup>. In order to find out any change in the speed of *electromagnetic waves*, one needs to use other methods for distance measurements rather than radar and such systems of units (Ellis et al., 2012). Just to be clear on this subject: if a system of unit is based on speed of light, let's say similar to when we define light seconds or light years, then the speed of light is considered to be unity *by definition*. However, this is not the speed with which the electromagnetic waves move (Ellis et al., 2012).

All debates and questions aside, the main reason this discussion arises is that  $c$  is not dimensionless. However, even when one accepts the dynamics of a dimensionless constant, like the fine structure constant ( $\alpha = e^2/\hbar c$ ), then one has to accept that at least one of the dimensional constants involved or a combination of them alters (like  $e$ ,  $\hbar$  or  $c$ ) (Magueijo, 2003).

At the end, it is worth mentioning that in most dynamical speed of light theories, no difference between the speed of electromagnetic waves and the causal speed limit is considered. As it is mentioned in (Ellis et al., 2012), this is a “*key point*” which should be clarified in non-standard theories. The approach explained in chapter 4 and also used in chapter 5, clearly takes this difference into account.

#### 3.3.1 Cosmological questions and dynamical speed of light

As mentioned before, dynamical speed of light theories are one of the attempts for solving different cosmological problems, among which we can mention the horizon problem (Magueijo, 2003).

---

<sup>2</sup>DSL

<sup>3</sup>Also called as VSL or varying speed of light theories.

<sup>4</sup>e.g. if the speed is  $1c$ , then in  $1s$  time, one can go  $1$  light seconds. This does not mean electromagnetic waves *have to* move with constant speed, because this is just our definition of system of units.

Observing different isotherm places in the universe, which are not expected to be causally connected in the past, is an ambiguous fact. Standard Big Bang Theory consists of an inflationary period which makes an accelerated expansion during inflation and puts the whole early universe in causal contact. DSL theories on the other hand, propose a solution to this problem by suggesting a larger speed of light in earlier times in the cosmic history. Then one can put these disconnected places in each other's horizons and make them causally connected. This way, the horizon problem can be solved either by using DSL or a combination of DSL and inflation (Magueijo, 2003; Albrecht & Magueijo, 1999).

As stated above, if the comoving horizon is much larger in the earlier times compared to now, then the causally disconnected regions locate in each others' horizons. This is shown in Figure 3.2. Figure 3.2a shows that although we see different isotherm places in our causal cone, their causal cones have been disconnected in earlier times. This happens when one considers a constant speed of light or no inflation. Other than inflation, one can consider a dynamical speed of light, which as it is shown in Figure 3.2b, makes the causal cone larger in earlier times (Magueijo, 2003). The model shown in this Figure, consists of a phase transition, which happens at  $t_c$ . In this model, the speed of light changes from a larger value ( $c^-$ ) to its present value ( $c^+$ ) at this time, resulting in  $r_h \gg r$ ; hence the horizon's size at the time  $t_c$ , is much larger than the comoving radius  $r$ . In other words, the dynamics of the speed of light opens the causal cone more and enlarges  $r_h$  (Magueijo, 2003; Albrecht & Magueijo, 1999). This model is an example of many dynamical speed of light models.

### 3.3.2 A model, as an example

In  $c = c_0 a^n$  model, speed of light increases (decreases) with time for a positive (negative) value of  $n$ . This way for a negative value of  $n$ , speed of light changes from a large value in the early universe to  $c_0$  in present time. As an example, here we mention (Balcerzak & Dabrowski, 2014), which considers the redshift drift in this class of dynamical speed of light. Considering a FRW universe, one can define the redshift drift as

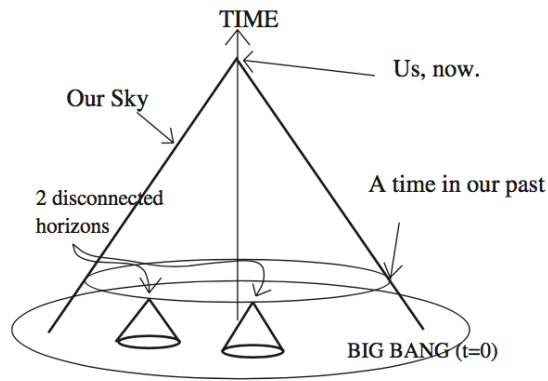
$$\Delta z = \Delta t_0 \left( H_0(1+z) - H \frac{c_0}{c} \right) \quad (3.5)$$

here,  $c = c(t)$ ,  $H$  is the Hubble parameter,  $H_0$  and  $c_0$  are the value of the Hubble parameter and the speed of light at present time. If  $c = c_0 a^n$ , then

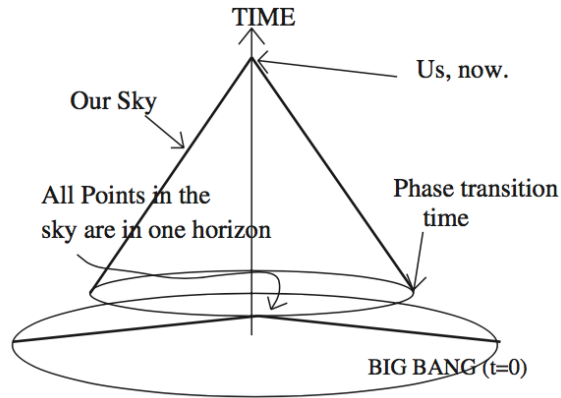
$$\Delta z = \Delta t_0 (H_0(1+z) - H(1+z)^n) \quad (3.6)$$

Here the authors use the Hubble parameter of the standard  $\Lambda$ CDM model and their main goal is to study the effect of variation of speed of light on the redshift drift predictions by the  $\Lambda$ CDM model<sup>5</sup>. Taking the Hubble parameter to be the same as in  $\Lambda$ CDM model, redshift drift is plotted in Figure 3.3 for different values of  $n$ ,  $\Lambda$ CDM model and the CDM model (Cold Dark Matter).

<sup>5</sup>Unlike our approach, which is explained in chapter 5.



(a) Conformal diagram illustrating the horizon problem. Different places in the earlier times are causally disconnected.



(b) Using a larger speed of light in the earlier times, the causal cone changes its shape and makes causal connection between all the places.

**Figure 3.2:** The horizon problem and the solution proposed by dynamical speed of light theories. The figure is taken from (Magueijo, 2003).

As stated by the authors and is also shown in Figure 3.3, considering 15 years of observations, the theoretical error bars agree with  $|n| < 0.045$  (Balcerzak & Dabrowski, 2014). In other terms, in 15 years of observations, the error bars are big enough to cover a  $\Lambda$ CDM model consisting of a varying speed of light scaling with scale factor with  $|n| < 0.045$ . It can also be seen in Figure 3.3 that a CDM model which only consists of matter in recent universe, shows a decelerating universe; which means it always has a negative redshift drift.

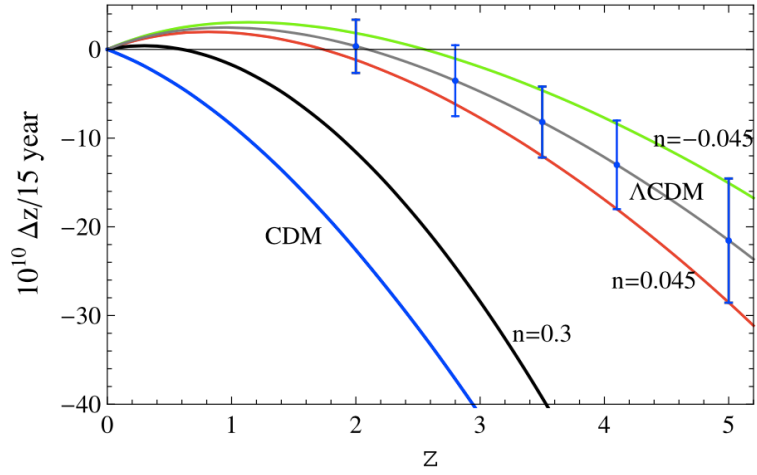


**Figure 3.3:** The redshift drift taken from reference (Balcerzak & Dabrowski, 2014). Here the authors considered 15 years observations for the theoretical error bars. These error bars show that a varying speed of light in the form of  $c_0 a^n$  is indistinguishable from the  $\Lambda$ CDM model (Balcerzak & Dabrowski, 2014).

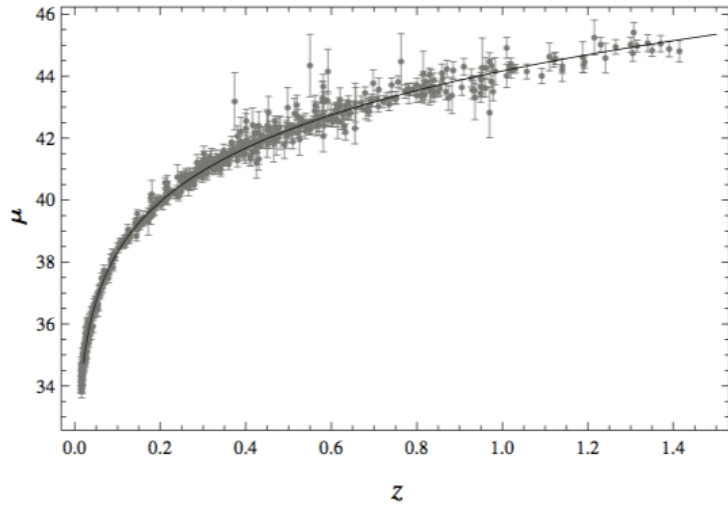


**Figure 3.4:** Distance modulus of SN Ia taken from (Zhang & Meng, 2014), shown for the observational points and the  $c_0 a^n$  model for  $n = -0.861$  and  $\mu_0 = 34.05$ . The minimum of  $\chi^2$  is 568.313 ( $\chi_r^2 = 0.983$ ) (Zhang & Meng, 2014).

This type of variation of speed of light has also been presented and used to fit with SN Ia distance modulus (Zhang & Meng, 2014). The difference between this study and the one above is that here only matter has been considered in the content of the universe. This results in  $n = -0.861$  (again a negative value of course) for the minimum value of  $\chi^2$  fitted with SN Ia luminosity distance. This is shown in Figure 3.4

Here although the cosmological constant or Dark Energy have not been assumed, the dynamics of the speed of light helps in having an acceptable luminosity distance (Zhang & Meng, 2014).

We would like to note that an acceptable model, is the one which fits with all observations. However, it is worth exploring all well motivated models and find their advantages and shortcomings.

# 4

## Extended theories of gravity

In general, there are two different classes of cosmological models, the standard model and the extended one. The most important difference between these two classes, is of course in the form of general relativity that is used. In the standard model, general relativity is supposed to be the main theory that has to accept an extra term, which in its simplest form is  $\Lambda$  (cosmological constant), or some kind of a non constant energy, called Dark Energy making a negative pressure and being responsible for the accelerated expansion of the universe. The other class of models considers a modification of the standard general relativity; in principle by putting some extra terms such as combinations of geometric terms (e.g. Ricci scalar, ...). Again these extra terms are responsible for the accelerated expansion of the universe (see e.g. (Izadi et al., 2017; Amendola & Tsujikawa, 2010)).

Apart from the indirect confirmations which state that we should put a large fraction of dark components to the energy content of the universe, there is no direct observations or data. In fact, we can only “sense” the dark components by sensing their effects on the matter (Fatibene & Francaviglia, 2012). On the other hand, we know that gravity works well in small scales like millimeters to larger ones like the astrophysical scales. Its success and precision in these scales, motivates us to expect for its effectiveness in even smaller (quantum gravity) or larger scales (Olmo, 2012).

As gravity is the most effective force in even larger scales (such as cosmological scales) and it does not work well without considering the dark components, this can be a clue to try to modify this theory (e.g. (Clifton et al., 2012; Faraoni & Capozziello, 2011; Sotiriou & Faraoni, 2010)).

In general, modified gravity theories consist of corrections to the Einstein-Hilbert Lagrangian. These corrections can be functions of scalars made of the curvature tensor such as  $R^2$  or  $R_{\mu\nu}R^{\mu\nu}$  (see e.g (Amendola & Tsujikawa, 2010; Li et al., 2007; Capozziello & de Laurentis, 2011)). This

makes a large number of modified gravity models. Therefore, studying these models in order to either falsify or at least know their characteristics better, is worth spending time.

In what follows we review the EPS framework and then choosing Palatini formalism, we study  $f(\mathcal{R})$  and  $f(\mathcal{R}^{\mu\nu}\mathcal{R}_{\mu\nu})$  models in general. Selecting a specific  $f(\mathcal{R}^{\mu\nu}\mathcal{R}_{\mu\nu})$  model and focusing on this model, we review the change made to different facets of the speed of light, by this modified model.

It is important to remember that the space time has been considered to be torsion-free in this thesis. This should be taken into account while following the math of this section, because tensors like the Ricci tensor are symmetric.

## 4.1 EPS framework

It is well explained in (Fatibene & Francaviglia, 2012) that GR deals with both physical quantities (gravitational fields) and observational protocols (measuring time and distances using a metric) using the same object : the metric. On the other hand, it is also confirmed that standard GR is just a special subset of a lot of possible gravitational theories.

It was shown by Ehlers, Pirani and Schild in 1972 that using worldlines of particles and light rays which are observable quantities, one can make the geometric structure on a manifold, known as EPS framework rather than working within a predefined geometric structure (see e.g. (Fatibene & Francaviglia, 2012; Fatibene & Garruto, 2016; Capozziello et al., 2012)). This means instead of working with a manifold which has predefined geometrical properties (for instance a metric), we get to the geometry of a manifold using physical observations: light rays and particle worldlines (Fatibene & Francaviglia, 2012; Fatibene & Garruto, 2016; Capozziello et al., 2012).

As in this framework, there is not a prior dependence between the metric and the connection, and we are interested in such frameworks, we review this point of view and its properties in this section (Fatibene & Francaviglia, 2012; Fatibene & Garruto, 2016; Capozziello et al., 2012):

- Suppose that we have a manifold called M. Our events happen on this manifold. The first observables used here, are the light rays. There are enough light rays assumed on M. This means in every neighborhood of an event, there are at least two light rays going from the event to a particle worldline nearby. Light rays make light cones on M and they make a conformal structure of metrics that is called  $\mathcal{C}$ . The representative of this structure is the metric which specifies causality and shows the worldlines of photons. Using these worldlines, one can define the conformal class of metrics ( $\mathcal{C} = [g]$ ) as

$$\tilde{g} = \phi(x)g \tag{4.1}$$

Light cones divide M into three different parts: inside, outside and on the manifold. Topologically, these parts are different from each other. There are time-like, light-like and space-like world lines given inside, on the surface and outside of the light cones. If we have a special case of  $\phi(x) = 1$ , then we recover standard GR, in which the manifold M can be described using only one metric.

- The second observables, are particle worldlines. Again, there are enough particles assumed on  $M$  to help gaining the properties of this manifold. The particle worldlines (time-like) fill the light cones made by the light rays. Choosing the ones which show freely falling particles, these worldlines make a projective structure of connections here that are shown as  $\mathcal{P}$ . The representative of this structure is the connection which enters the particles' geodesic equation.

The most general geodesic for particles is given by

$$\ddot{x}^\alpha + \Gamma_{\mu\nu}^\alpha \dot{x}^\mu \dot{x}^\nu = \lambda \dot{x}^\alpha \quad (4.2)$$

And the projective class  $\mathcal{P} = [\Gamma]$  consists of different connections which defines projectively equivalent geodesics. EPS can also be shown as  $(M, \mathcal{C}, \mathcal{P})$ .

$$\tilde{\Gamma}_{\mu\nu}^\alpha = \Gamma_{\mu\nu}^\alpha + \delta_{(\mu}^\alpha V_{\nu)} \quad (4.3)$$

in which  $V_\mu$  is a covector. By this transformation, geodesics from  $\tilde{\Gamma}_{\mu\nu}^\alpha$  and  $\Gamma_{\mu\nu}^\alpha$ , are projectively equivalent.

- The discussions above, show that according to the EPS framework, there is a fundamental difference between the causality and the equivalence principle.

As the light cones are filled with particle worldlines, light rays must be related to the particle worldlines. Similar to the particles, the light rays are also affected by gravitational fields and they get bent by the field; so one can conclude that the conformal  $\mathcal{C}$  structure belongs to the projective  $\mathcal{P}$  structure. In other words, the particle geodesics consist of the light ray geodesics too. The EPS-compatibility condition is then given by

$$\nabla g = 2Ag \quad (4.4)$$

This is equivalent to

$$\Gamma_{\mu\nu}^\alpha = \left\{ \begin{matrix} \alpha \\ \mu\nu \end{matrix} \right\} + (g^{\alpha\epsilon} g_{\mu\nu} - 2\delta_{(\mu}^\alpha \delta_{\nu)}^\epsilon) A_\epsilon \quad (4.5)$$

This shows the relation between the projective structure and the conformal structure.

In equation (4.5),  $\Gamma_{\mu\nu}^\alpha$  is the christoffel symbol of the metric  $\mathcal{G}_{\mu\nu}$ , which in general does not have to be the same as  $g_{\mu\nu}$ .

One of the main questions in such frameworks is: now that there are two metrics on  $M$  (one that makes the affine connection and the other that makes the christoffel symbols), which one should be used to do measurements? As an example, when measuring distances, which metric should be used? The first metric which has been given by the light rays and their echos <sup>1</sup> is used for measurements and the other one which is given by the movement of particles, is related to free fall. Of course there is a relation between these two which is stated in equation (4.5).

---

<sup>1</sup>The light rays from particle worldline  $P$  to particle worldline  $Q$ , are called a message. If there are messages from  $P$  to  $Q$  and vice versa, this is an echo.

- To summarize, the manifold has  $g$  as the representative of the conformal structure  $\mathcal{C}$ , which is responsible for causality and the measurements. It also has  $\Gamma$  as the representative of the projective structure  $\mathcal{P}$ , which is responsible for free fall.
- *A special case:* if a metric which belongs to  $\mathcal{C}$  also belongs to  $\mathcal{P}$ , then this metric describes light cones and explains particle free fall. In addition to this criteria, if the Lagrangian is the Einstein Hilbert Lagrangian, then the theory is standard GR. This is shown as  $(M, [g], \{g\})$ . In this special case, there is one metric which is used for making the causal cone, doing measurements on M and determining free fall. This can be achieved by putting  $A_\mu = 0$  in equation 4.5; therefore standard GR is a very special case of the general EPS framework. In principle, there can be less geometric constraints on M in EPS than GR.

The points above summarize the EPS framework (Fatibene & Francaviglia, 2012; Fatibene & Garruto, 2016; Capozziello et al., 2012). According to EPS framework, GR puts a lot of constraints on the geometry of the manifold. As stated above, there is no need to put priori constraints on the connection. Connection can be in general an affine connection which is independent of the metric. The only constraint made by EPS is the relation in equation 4.5. Extended theories of gravity are theories in which this relation is held between the connection and the metric. Among these theories, Palatini  $f(\mathcal{R})$  theories for example, are metric Weyl geometry in which the affine connection is conformally related to the metric. In Palatini and metric-affine theories for instance, the relation between the metric and the affine connection comes from the dynamics of the system; i.e. Einstein field equations (see e.g. (Capozziello et al., 2012; Fatibene & Francaviglia, 2012)).

The above points, motivates us to explore the properties of more general cases and test it on the analysis of different cosmological observations.

## 4.2 A brief review on the Palatini formalism

At first, Palatini formalism was proposed by Einstein himself. But for the Einstein-Hilbert Lagrangian, both metric and Palatini formalism result in the same field equations (Faraoni & Capozziello, 2011).

According to the points explained in section 4.1, generally there is no prior need to have a constraint on the connection to be a metric connection.

In Palatini formalism, metric and connection are considered to be independent from each other (e.g. (Li et al., 2007)).

$$\Gamma_{\mu\nu}^\alpha = \left\{ \begin{matrix} \alpha \\ \mu\nu \end{matrix} \right\} + \gamma_{\mu\nu}^\alpha \quad (4.6)$$

Therefore, the Ricci scalar ( $\mathcal{R}$ ) and the curvature tensor ( $\mathcal{R}_{\mu\nu}$ ) are made from the affine connection ( $\Gamma_{\mu\nu}^\alpha$ ), which is in principle different from the Christoffel symbol ( $\left\{ \begin{matrix} \alpha \\ \mu\nu \end{matrix} \right\}$ ). The Ricci tensor which is made of the affine connection is given as

$$\mathcal{R}_{\mu\nu} = R_{\mu\nu} + \nabla_\alpha \gamma_{\mu\nu}^\alpha - \nabla_\nu \gamma_{\alpha\mu}^\alpha + \gamma_{\mu\nu}^\alpha \gamma_{\beta\alpha}^\beta - \gamma_{\mu\beta}^\alpha \gamma_{\nu\alpha}^\beta \quad (4.7)$$

As a result, one can vary the action with respect to the affine connection and also the Christoffel symbol and unlike the metric formalism, this results in two different equations (Li et al., 2007). In what follows, we consider two different modified Lagrangians in Palatini formalism and briefly review their characteristics. According to what we reviewed in section 4.1, the movement of particles are of course related to the projective structure of the manifold  $M$ . In other words, matter is related to the connection. So it is much logical to consider the matter Lagrangian to be dependent on the metric, matter fields and also the connection. This leads us to the metric affine theories. However, this would make the problem mathematically more difficult. Therefore, we consider the matter fields to be independent of the affine connection; so we consider the Palatini formalism (Fatibene & Francaviglia, 2012).

To avoid any confusion between the metric and the Palatini formalism, the Ricci scalar is shown as  $\mathcal{R}$  and  $R$  in Palatini formalism and metric formalism respectively.

#### 4.2.1 Palatini $f(\mathcal{R})$ gravity

$f(\mathcal{R})$  models are famous for different cases such as playing the role of inflation (as Starobinsky inflation) or turning into GR plus a cosmological constant (Olmo, 2008; Sotiriou & Faraoni, 2010). Mathematically, one may claim there is an equivalence between  $f(\mathcal{R})$  models and Brans-Dicke theories. Using this equivalence, one can say these models are problematic because they do not agree with solar system tests. However, this has to be naive and can be rejected considering the fundamental difference between these two class of models. This is more explained in section 4.2.2 (Fatibene & Francaviglia, 2012).

In  $f(\mathcal{R})$ , the action is given as (e.g. (de Felice & Tsujikawa, 2010; Fatibene & Francaviglia, 2012; Sotiriou & Faraoni, 2010))

$$S = \frac{1}{2\kappa} \int d^4x \sqrt{-g} f(\mathcal{R}) + S_m(g, \psi) \quad (4.8)$$

$\psi$  is the matter field and the affine connection and the metric are considered to be independent from each other, so by varying the action with respect to the metric and the connection we get the two field equations below.

$$\begin{aligned} f' \mathcal{R}_{\mu\nu} - \frac{1}{2} g_{\mu\nu} f &= \kappa T_{\mu\nu} \\ D(\sqrt{-g} f' g^{\mu\nu}) &= 0 \end{aligned} \quad (4.9)$$

Here  $f' = \partial f / \partial \mathcal{R}$  and  $\mathcal{R} = g^{\mu\nu} \mathcal{R}_{\mu\nu}$ . The second equation above, gives the auxiliary metric ( $\mathcal{G}_{\mu\nu}$ ) which is given by

$$\mathcal{G}_{\mu\nu} = f' g_{\mu\nu}. \quad (4.10)$$

According to equation 4.10, there is a conformal factor between the new metric and the physical metric:  $\phi = f'(\mathcal{R})$ . On the other hand, taking the trace of the first equation in 4.9, we get to

$$f' \mathcal{R} - 2f = \kappa T \quad (4.11)$$

in which  $T$  is the trace of the energy momentum tensor. As stated before, if one considers the vacuum case in which  $T = 0$ , then according to equation (4.11),  $\mathcal{R}$  becomes constant and the theory will reduce to GR including a cosmological constant (Olmo, 2008; Sotiriou & Faraoni, 2010; Fatibene & Francaviglia, 2012):

$$\mathcal{R}_{\mu\nu} - \frac{1}{2}\mathcal{R}\mathcal{G}_{\mu\nu} = \Lambda\mathcal{G}_{\mu\nu} \quad (4.12)$$

As this effective cosmological constant is related to the choice of  $f(\mathcal{R})$ , by choosing a suitable form for his function one can set it to the right value which matches with observations. As there are a lot of choices for the form of  $f(\mathcal{R})$ , in principle this model can be easily fitted with observations in vacuum.

But of course for a non vacuum energy momentum tensor, this is not the case. In this case, the modified Einstein tensor is equal to an effective energy momentum tensor, which means although there is only normal matter involved,  $f(\mathcal{R})$  models result in GR plus a modified energy momentum tensor (Fatibene & Francaviglia, 2012).

If we take the conformal factor as  $\phi = f'(\mathcal{R})$ , then provided that this relation is invertible, one can get to  $\mathcal{R} = r(\phi)$ . Then one can say, in these theories the independent fields are  $(g_{\mu\nu}, \Gamma_{\mu\nu}^\alpha, \phi)$  (Fatibene & Garruto, 2016).

#### 4.2.2 The equivalence between Brans-Dicke and $f(\mathcal{R})$ theories

Sometimes by introducing an equivalence between the Brans-Dicke and  $f(\mathcal{R})$  theories, it is claimed that  $f(\mathcal{R})$  theories are inconsistent with solar system observations. However, following the EPS concepts, one can show that this is a naive conclusion (Fatibene & Francaviglia, 2012).

In Brans-Dicke theories, in addition to the metric  $g_{\mu\nu}$  which is responsible for making light cones, free fall and also distance measurements, there is a scalar field  $\phi$  which takes part in the dynamics of the system (Fatibene & Francaviglia, 2012). The Lagrangian is given by

$$\mathcal{L} = \sqrt{g}\left(\phi R - \frac{\omega}{\phi}\nabla_\mu\phi\nabla^\mu\phi - V(\phi)\right) + \mathcal{L}_m(g, \psi) \quad (4.13)$$

Here,  $\omega$  is a real parameter,  $V(\phi)$  is the potential,  $\mathcal{L}_m$  is the matter Lagrangian which is a function of the metric and the matter fields  $\psi$ .

There is a “mathematical” equivalence between (4.13) and (4.8). Introducing a new field  $\chi$ , then the action in (4.8) can be written as

$$S = \frac{1}{2\kappa} \int d^4x \sqrt{-g} \left( f(\chi) + f'(\chi)(\mathcal{R} - \chi) \right) + S_m(g, \psi) \quad (4.14)$$

knowing the fact that varying this action with respect to  $\chi$ , brings us to  $\chi = \mathcal{R}$  if  $f'' \neq 0$ , gives us the same action as (4.8).

Again, if we define another field  $\phi$  such that

$$\begin{aligned}\phi &= f'(\chi) \\ V(\phi) &= \chi\phi - f(\chi(\phi)),\end{aligned}\tag{4.15}$$

neglecting the term  $\square\phi$  and knowing the relation between the Ricci scalar in Palatini and metric formalism,

$$\mathcal{R} = R + \frac{3}{2f'^2}\partial_\mu f' \partial^\mu f' + \frac{3}{f'}\square f'\tag{4.16}$$

equation (4.14) changes to

$$S = \frac{1}{2\kappa} \int d^4x \sqrt{-g} (\phi\mathcal{R} - V(\phi)) + S_m(g, \psi).\tag{4.17}$$

We see that equations (4.13) and (4.17) are mathematically similar if  $\omega = -3/2$  (Sotiriou, 2007). Regarding the tests in solar system, Brans-Dicke theories match observations with the parameter  $\omega$  going to infinity, so at first glance, one can say this shows that Palatini  $f(\mathcal{R})$  theories are inconsistent with solar system observations; because they are equivalent to Brans-Dicke theories with  $\omega = -3/2$ . However, this is not the case (Fatibene & Francaviglia, 2012).

As it was stated before, there is a mathematical equivalence between the Lagrangian of Brans-Dicke theories and Palatini  $f(\mathcal{R})$  theories; although physically it is not the case and there are fundamental differences between these two models (Fatibene & Francaviglia, 2012). The reason is well stated in (Fatibene & Francaviglia, 2012): As in Brans-Dicke theories, there is only one metric responsible for doing both measurements and free fall, when for example we study the movement of Mercury, we are studying a geodesic made with the christofel symbols of the main metric; although in Palatini  $f(\mathcal{R})$  theories this does not apply. There the geodesics are made from projectively equivalent affine connections. This means when comparing Brans-Dicke with Palatini  $f(\mathcal{R})$  results, one is comparing two completely different geodesics. Therefore, one can reject the fact that Palatini  $f(\mathcal{R})$  theories do not match with solar system observations just by comparing them to Brans-Dicke theories (Fatibene & Francaviglia, 2012).

### 4.2.3 Palatini $f(\mathcal{R}^{\mu\nu}\mathcal{R}_{\mu\nu})$ gravity

In this section, Palatini formalism  $f(\mathcal{R}^{\mu\nu}\mathcal{R}_{\mu\nu})$  models are presented.

Apart from assuming both metric and the connection, to be different fundamental geometric objects, these models have the advantage of developing second order field equations (unlike in metric formalism) (Olmo, 2012). This makes solving these equations much easier (Li et al., 2007).

In what follows we review the  $f(\mathcal{R}^{\mu\nu}\mathcal{R}_{\mu\nu})$  model in Palatini formalism using (Li et al., 2007):

Following the steps of (Li et al., 2007) for Palatini  $f(\mathcal{R}^{\mu\nu}\mathcal{R}_{\mu\nu})$  gravity, the Lagrangian density consists of a  $f(\mathcal{R}^{\mu\nu}\mathcal{R}_{\mu\nu})$  term added to the Einstein-Hilbert Lagrangian.

$$\mathcal{L} = \frac{1}{2\kappa} (\mathcal{R} + f(\mathcal{R}_{\mu\nu}\mathcal{R}^{\mu\nu})) + \mathcal{L}_m\tag{4.18}$$

in which  $\mathcal{L}_m$  is the matter term,  $\kappa = 8\pi G/c^4$  and the  $\mathcal{R}_{\mu\nu}(= \mathcal{R}_{\mu\nu}(\Gamma_{\beta\gamma}^\alpha))$  tensor is the Ricci tensor made of the affine connection. Unlike metric formalism, here there are two different variations of the action; one with respect to  $g_{\mu\nu}$  and another with respect to  $\Gamma_{\mu\nu}^\alpha$ . Varying the action with respect to  $g_{\mu\nu}$  leads to the modified Einstein field equations below,

$$\mathcal{R}_{\mu\nu} + 2F\mathcal{R}_\mu^\alpha\mathcal{R}_{\nu\alpha} - \frac{1}{2}g_{\mu\nu}[\mathcal{R} + f(\mathcal{R}^{\mu\nu}\mathcal{R}_{\mu\nu})] = \kappa T_{\mu\nu} \quad (4.19)$$

with  $T_{\mu\nu}$  as the energy momentum tensor of the matter and  $F = \partial f(\mathcal{R}^{\mu\nu}\mathcal{R}_{\mu\nu})/\partial(\mathcal{R}^{\mu\nu}\mathcal{R}_{\mu\nu})$ . This equation can also be written as the standard Einstein tensor which equals a combination of two energy momentum tensors:

$$R_{\mu\nu} - \frac{1}{2}g_{\mu\nu}R = \kappa T_{\mu\nu}^f + \kappa T_{\mu\nu}^{eff} \quad (4.20)$$

Here  $R_{\mu\nu} = R_{\mu\nu}(g)$  and  $T_{\mu\nu}^f$  is the energy-momentum tensor of the fluid consisting matter<sup>2</sup> and radiation and also

$$\kappa T_{\mu\nu}^{eff} = \frac{1}{2}g_{\mu\nu}(f + \delta R) - \delta R_{\mu\nu} - 2F\mathcal{R}_\mu^\alpha\mathcal{R}_{\alpha\nu} \quad (4.21)$$

which is an effective energy momentum tensor, resulting from geometric terms added to the Einstein-Hilbert Lagrangian. Additionally,

$$\begin{aligned} \delta R_{\mu\nu} &= \nabla_\alpha\gamma_{\mu\nu}^\alpha - \nabla_\nu\gamma_{\alpha\mu}^\alpha + \gamma_{\mu\nu}^\alpha\gamma_{\beta\alpha}^\beta - \gamma_{\mu\beta}^\alpha\gamma_{\nu\alpha}^\beta \\ \delta R &= g^{\mu\nu}\delta R_{\mu\nu} \end{aligned} \quad (4.22)$$

On the other hand, varying the action with respect to  $\Gamma_{\mu\nu}^\alpha$  results in a new metric which satisfies the relations below,

$$\begin{aligned} D_e[\sqrt{-g}(g^{\mu\nu} + 2Fg^{\mu\alpha}\mathcal{R}_{\alpha\beta})g^{\nu\beta}] &= 0 \\ \Rightarrow \sqrt{-\mathcal{G}}\mathcal{G}^{\mu\nu} &= \sqrt{-g}g^{\mu\alpha}(\delta_\alpha^\nu + 2F\mathcal{R}_\alpha^\nu) \end{aligned} \quad (4.23)$$

This new metric,  $\mathcal{G}^{\mu\nu}$ , is the one which makes the affine connection (Li et al., 2007).

### Solving equations using 3 + 1 decomposition

In order to solve the modified Einstein equations shown in (4.19), the 3 + 1 decomposition method is briefly mention from (Li et al., 2007). In this method, one divides the space time to splits which are perpendicular to the 4-velocity. Then the energy momentum tensor and the Ricci tensor are decomposed as

$$T_{\mu\nu} = \rho u_\mu u_\nu + 2q_{(\mu}u_{\nu)} - ph_{\mu\nu} + \pi_{\mu\nu}, \quad (4.24)$$

---

<sup>2</sup>Baryonic matter and Cold Dark Matter

$$\mathcal{R}_{\mu\nu} = \Delta u_\mu u_\nu + \Xi h_{\mu\nu} + 2u_{(\mu} \gamma_{\nu)} + \Sigma_{\mu\nu}. \quad (4.25)$$

Here  $u^\mu = dx^\mu/(d\tau)$  is the 4-velocity and it is normalized as  $u^\mu u_\mu = 1$ ,  $h_{\mu\nu} = g_{\mu\nu} - u_\mu u_\nu$  is the projection tensor  $u^\mu$ ,  $\pi_{\mu\nu} = h_\mu^\alpha h_\nu^\beta T_{\alpha\beta}$  is the projected symmetric anisotropic pressure which is trace free,  $\rho = T_{\mu\nu} u^\mu u^\nu$  is the density,  $q_\mu = h_\mu^\alpha u^\beta T_{\beta\alpha}$  which is the relativistic momentum density, and  $p = -1/3 h^{\mu\nu} T_{\mu\nu}$  is the isotropic pressure.

Using equations (4.24) and (4.25) for the energy momentum tensor and also the Ricci tensor, together with the modified Einstein field equation (4.19), the results are four equations which can be solved for the four unknown coefficients  $\Delta, \Xi, \Upsilon_\mu$  and  $\Sigma_{\mu\nu}$ . Of course here one should know the form of  $f(\mathcal{R}^{\mu\nu}\mathcal{R}_{\mu\nu})$  function and also  $\rho^f, p^f, q_\mu$  and  $\pi_{\mu\nu}$ .

$$\Delta + 2F\Delta^2 - \frac{1}{2}(\Delta + 3\Xi + f) = \kappa\rho^f c^2 \quad (4.26)$$

$$\Xi + 2F\Xi^2 - \frac{1}{2}(\Delta + 3\Xi + f) = -\kappa p^f \quad (4.27)$$

$$[1 + 2F(\Delta + \Xi)]\Upsilon_\mu = \kappa q_\mu^f \quad (4.28)$$

$$(1 + 4F\Xi)\Sigma_{\mu\nu} = \kappa\pi_{\mu\nu}^f \quad (4.29)$$

In addition to the above,  $\mathcal{R}^{\mu\nu}\mathcal{R}_{\mu\nu} = \Delta^2 + 3\Xi^2$ . The upper indices “ $f$ ” show the parameter relates to the combination of the fluid matter and radiation.  $\Upsilon_\mu$  and  $\Sigma_{\mu\nu}$  vanish except in the first order perturbation.

In addition, the relations between the new metric and  $g_{\mu\nu}$  are

$$\mathcal{G}_{\mu\nu} = \lambda g_{\mu\nu} + \xi_{\mu\nu} \quad (4.30)$$

$$\mathcal{G}^{\mu\nu} = \frac{1}{\lambda} g^{\mu\nu} + \zeta^{\mu\nu} \quad (4.31)$$

where  $\xi_{\mu\nu}, \zeta^{\mu\nu}, \lambda$  and  $\omega$  are given in the following equations:

$$\xi_{\mu\nu} = \lambda(\omega - 1)u_\mu u_\nu - 4\sqrt{\omega}F u_{(\mu} \Upsilon_{\nu)} - \frac{2F}{\sqrt{\omega}}\Sigma_{\mu\nu} \quad (4.32)$$

$$\zeta^{\mu\nu} = \frac{1}{\lambda}\left(\frac{1}{\omega} - 1\right)u^\mu u^\nu + \frac{1}{\lambda^2}\frac{2F}{\sqrt{\omega}}[2u^{(\mu}\Upsilon^{\nu)} + \Sigma^{\mu\nu}] \quad (4.33)$$

$$\lambda = \sqrt{(1 + 2F\Delta)(1 + 2F\Xi)} \quad (4.34)$$

$$\omega = \frac{(1 + 2F\Xi)}{(1 + 2F\Delta)} \quad (4.35)$$

Furthermore, the Hubble parameter is given by solving the Einstein equations. According to the fact that we have a modification of these equations here (equation (4.19)), we will have a modified Hubble parameter as well. The linearised Friedmann equation is shown as

$$\frac{1}{3}\theta^2 = \kappa\rho^{\text{tot}}c^4 \quad (4.36)$$

in which  $\theta = 3H$ ,  $H = \dot{a}/a$  is the Hubble parameter and the total density is given by

$$\kappa\rho^{\text{tot}}c^2 = \kappa\rho^f c^2 + \frac{1}{2}f - 2F\Delta^2 + \frac{1}{2}\delta R - \delta R_{\mu\nu}u^\mu u^\nu \quad (4.37)$$

The last two equations result in

$$\left(H + \frac{\dot{\lambda}}{2\lambda}\right)^2 = \frac{c^2}{6}(\Delta - 3\omega\Xi) \quad (4.38)$$

To simplify the above equation for different cosmological eras, we make use of the fact that  $\lambda = \lambda(\rho^f)$ ; hence

$$\begin{aligned} \dot{\lambda} &= \frac{\partial\lambda}{\partial\rho^f}\dot{\rho}^f \\ &= -s\frac{\partial\lambda}{\partial\rho^f}\rho^f H \\ s &= \begin{cases} 3 & \text{matter dominated era} \\ 4 & \text{radiation dominated era} \end{cases} \end{aligned} \quad (4.39)$$

Using the above equation, the modified Hubble parameter is

$$H^2 = \frac{\frac{c^2}{6}(\Delta - 3\omega\Xi)}{\left(1 - \frac{s\frac{\partial\lambda}{\partial\rho^f}\rho^f}{2\lambda}\right)^2} \quad (4.40)$$

in which  $\Delta$ ,  $\Xi$ ,  $\lambda$  and  $\omega$  are given in equations (4.26), (4.27), (4.34) and (4.35) and again  $s = 3, 4$  for matter and radiation dominated eras, respectively. Accordingly, for each cosmological era, one can get to a different modification of the Hubble parameter (Li et al., 2007).

### 4.3 Different local frames in Palatini formalism

As stated earlier, in Palatini formalism the metric and affine structures of the spacetime are treated to be independent from each other (see e.g. (Li et al., 2007; Izadi & Shojai, 2009; Izadi et al., 2017)). This brings us to two different local frames (Izadi & Shojai, 2009):

In the first local frame <sup>3</sup>, the metric is Minkowskian and as a consequence the christoffel symbols vanish. Using equation (4.6), the affine connection is  $\Gamma_{\mu\nu}^{\alpha} = \gamma_{\mu\nu}^{\alpha}$ . Then the geodesic equation has the form

$$\frac{d^2 x^{\alpha}}{ds^2} = 0 \quad (4.41)$$

The second local frame <sup>4</sup>, is the one in which the affine connection being responsible for the particle worldlines, vanishes. Its outcome is that the geodesics of this independent connection gets the form below

$$\begin{aligned} \frac{d^2 x^{\alpha}}{ds^2} + \left\{ \begin{array}{c} \alpha \\ \mu\nu \end{array} \right\} \frac{dx^{\mu}}{ds} \frac{dx^{\nu}}{ds} &= 0 \\ \frac{d^2 x^{\alpha}}{ds^2} - \gamma_{\mu\nu}^{\alpha} \frac{dx^{\mu}}{ds} \frac{dx^{\nu}}{ds} &= 0 \end{aligned} \quad (4.42)$$

The extra sentence ( $-\gamma_{\mu\nu}^{\alpha} dx^{\mu}/(ds) dx^{\nu}/(ds)$ ) is related to the variation of  $c_C$  (clock synchronization speed of light) (Izadi & Shojai (2009)).

The second frame, is an important one for us in this thesis. The reason will be explained in the next section.

### 4.4 Different facets of the speed of light in the local frame ( $\Gamma LF$ )

As explained in (Izadi et al., 2017), considering modifications to the standard gravitational model, the origin and role of some of the fundamental constants become more important than in the standard theory. Among the fundamental constants, it was shown that the speed of light is required to need more attention than before (Izadi & Shojai, 2009).

Here we consider Ricci squared gravity and show the form of different facets of the speed of light as it is done in (Izadi & Shojai, 2009). Except from the speed of electromagnetic waves ( $c_{EM}$ ), the forms of all the other facets are the same as given in (Izadi & Shojai, 2009).

#### 4.4.1 The spacetime matter constant

This constant enters Einstein field equations and couples geometry with matter. Considering  $c_E = c_0$  as (Izadi & Shojai, 2009), helps in the simplification of the field equations. This way,

---

<sup>3</sup>which we call the *CLF* here

<sup>4</sup>which we show by *GLF* here

one can write the equations as before.

#### 4.4.2 Causal structure constant in the FRW spacetime

The meaning and role of the causal structure constant has been explained in section 3.2. In principle, this facet of light enters the line element and is used to do distance measurements. It is responsible to synthesize space and time (Ellis & Uzan, 2005). Particularly, it can be shown that the causal structure constant ( $c_{ST}$ ) associated to the frames with a locally vanishing christoffel symbols (CLF), is different from the causal structure constant in a frame in which the affine connection vanishes ( $\Gamma$ LF)(Izadi et al., 2017). In this part, we follow (Izadi & Shojai, 2009) and check the form of  $c_{ST}$  considering modified gravity  $f(R^{\mu\nu}R_{\mu\nu})$  model in Palatini formalism in different local frames.

As in CLF, the space time metric is Minkowskian, one can easily see that  $c_{ST} = c_0$ . However, this is not the case in the other local frame;  $\Gamma$ LF. For the flat FRW spacetime, the line element is as below

$$ds^2 = c_0^2 dt^2 - a^2(t)(dr^2 - r^2 d\Omega^2) \quad (4.43)$$

( $d\Omega^2 = d\theta^2 + d\phi^2$  and  $k = 0$ ). Using (4.30), this line element results in

$$\begin{aligned} \mathcal{G}_{00} &= \lambda\omega \\ \mathcal{G}_{ii} &= \lambda g_{ii} \\ \Rightarrow \mathcal{G}_{\mu\nu} &= \text{diag}(\lambda\omega, -\lambda a^2(t), -\lambda r^2 a^2(t), -\lambda r^2 \sin^2 \theta a^2(t)) \end{aligned} \quad (4.44)$$

As this metric is the one making the affine connection, in the  $\Gamma$ LF, it should be locally Minkoswkian (Izadi & Shojai, 2009), i.e.

$$\begin{aligned} \mathcal{G}^{\mu\nu} &= \tilde{e}_\alpha^\mu \tilde{e}_\beta^\nu \eta^{\alpha\beta} \\ \Rightarrow \tilde{e}_\alpha^\mu &= \text{diag}\left(\frac{1}{\sqrt{\lambda\omega}}, \frac{1}{\sqrt{\lambda}a(t)}, \frac{1}{\sqrt{\lambda}ra(t)}, \frac{1}{\sqrt{\lambda}r \sin \theta a(t)}\right) \end{aligned} \quad (4.45)$$

Finally, the spacetime metric in this frame is given by

$$\begin{aligned} \tilde{g}_{\mu\nu} &= \tilde{e}_\mu^\alpha \tilde{e}_\nu^\beta g_{\alpha\beta} \\ &= \text{diag}\left(\frac{1}{\lambda\omega}, \frac{-1}{\lambda}, \frac{-1}{\lambda}, \frac{-1}{\lambda}\right) \end{aligned} \quad (4.46)$$

So in this frame in which  $\Gamma_{\mu\nu}^\alpha = 0$ , the line element is

$$ds^2 = \frac{1}{\lambda} \left( \frac{1}{\omega} c_0^2 dt^2 - a^2(t)(dr^2 - r^2 d\Omega^2) \right) \quad (4.47)$$

Assuming a null radial ray to find  $c_{ST}$ , one gets to

$$c_{ST} = \frac{c_0}{\sqrt{\omega}} \quad (4.48)$$

$c_{ST}$  is the spacetime causal structure constant,  $c_0$  is the value of this parameter at  $z = 0$  and  $\omega$  is given in equation (4.35) (Izadi & Shojai, 2009). Therefore, in principle, by knowing the form of the modified Lagrangian and solving the modified Einstein field equations, one can calculate the form of the causal structure constant in the  $\Gamma$ LF (Izadi & Shojai, 2009).

As it is obvious from equation (4.48),  $\omega < 1$  ( $\omega > 1$ ) results in  $c_{ST} > c_0$  ( $c_{ST} < c_0$ ). Also, if  $\omega = 1$  which can be a result of having no correction term to the Lagrangian, then one recovers the causal structure constant in the standard theory. In addition, if  $\omega$  has dynamics,  $c_{ST}$  gets dynamics as well.

#### 4.4.3 Speed of electromagnetic waves in FRW spacetime

As it was stated earlier, one can consider different features for the speed of light. There is no prior good reason to consider all these different features to be the same. For instance, the speed of the electromagnetic waves can in principle be different from the speed with which the gravitational waves travel. This is an interesting fact that is still under study and of course needs more theoretical and observational consideration and work; e.g. this is also studied using recent LIGO-Virgo results (Abbott et al., 2017a). In this section the form and the possible variation of the speed of electromagnetic waves ( $c_{EM}$ ) in the preferred local frame in which  $\Gamma_{\mu\nu}^\alpha = 0$  is reviewed. We repeat the steps done in (Izadi & Shojai, 2009), however at the end we correct their result.

In the CLF in which the christoffel symbols vanish, considering  $A_\nu = \epsilon_\nu e^{ik \cdot x}$ , the Lorentz gauge results in

$$\nabla \cdot A = \partial_\mu A^\mu = 0 \rightarrow \epsilon^\mu A_\mu = 0 \quad (4.49)$$

Then the field equations will be

$$\begin{aligned} \nabla_\mu F^{\nu\mu} &= \partial_\mu F^{\nu\mu} - \gamma_{\mu\alpha}^\nu F^{\nu\alpha} = 0 \\ \epsilon^\nu k^2 &= 0 \\ k^2 &= 0 \end{aligned} \quad (4.50)$$

which means that in this frame the speed of electromagnetic waves is constant.

On the other hand in the  $\Gamma$ LF, again if  $A^\mu$  is the electromagnetic vector potential, the Lorentz gauge is

$$\nabla \cdot A = \partial_\mu A^\mu + \left\{ \begin{matrix} \mu \\ \mu\nu \end{matrix} \right\} A^\nu = 0 \quad (4.51)$$

Then as in this frame  $\Gamma_{\mu\nu}^\alpha = 0$ , we have

$$\partial_\mu A^\mu - \gamma_{\mu\nu}^\mu A^\nu = 0 \quad (4.52)$$

Considering  $A_\nu = \epsilon_\nu e^{ik \cdot x}$ , Lorentz gauge results in

$$k_\mu \epsilon^\mu + i \gamma_{\mu\nu}^\mu \epsilon^\nu = 0 \quad (4.53)$$

On the other hand, the electromagnetic tensor is given by  $F_{\nu\mu} = \partial_\mu A_\nu - \partial_\nu A_\mu$ , and the field equations are thus given by

$$\nabla_\mu F^{\nu\mu} = 0 \quad (4.54)$$

in which

$$F^{\mu\nu} = \tilde{g}^{\mu\alpha} \tilde{g}^{\nu\beta} (\partial_\alpha A_\beta - \partial_\beta A_\alpha) \quad (4.55)$$

Finally, we come to

$$\epsilon^\nu (-ik^2 + \gamma_{\mu\sigma}^\mu k^\sigma) + (\epsilon_\beta k_\alpha - \epsilon_\alpha k_\beta) \partial_\mu (\tilde{g}^{\nu\alpha} \tilde{g}^{\mu\beta}) = 0 \quad (4.56)$$

$\tilde{g}_{\mu\nu}$  is given in equation (4.46). Keeping in mind that as  $\omega$  and  $\lambda$  are just functions of time, the only non-zero element of  $\gamma_{\mu\sigma}^\mu$  is,

$$\begin{aligned} \gamma_{\mu 0}^\mu &= q(t) \\ &= \frac{2}{\lambda c_{ST}} \frac{\partial \lambda}{\partial t} + \frac{1}{2\omega c_{ST}} \frac{\partial \omega}{\partial t} \end{aligned} \quad (4.57)$$

which proceeds to

$$\epsilon^\nu (-ik^2 + \gamma_{\mu 0}^\mu k^0) + (\epsilon_\beta k_\alpha - \epsilon_\alpha k_\beta) \partial_\mu (\tilde{g}^{\nu\alpha} \tilde{g}^{\mu\beta}) = 0 \quad (4.58)$$

For the time derivatives, we use

$$\begin{aligned} \frac{\partial}{\partial t} &= \frac{\partial \rho}{\partial a} \dot{a} \frac{\partial}{\partial \rho} \\ &= \begin{cases} -3\rho H \frac{\partial}{\partial \rho}, & \text{matter dominated era} \\ -4\rho H \frac{\partial}{\partial \rho}, & \text{radiation dominated era} \end{cases} \end{aligned} \quad (4.59)$$

- Taking  $\nu = 0$  component, then knowing the fact that the metrics are diagonal, equation (4.58) turns into

$$\epsilon^0 (-ik^2 + qk^0) = 0 \quad (4.60)$$

On the other hand, having  $k^\mu = |\vec{k}|(c_0/c_{EM}, 1, 0, 0)$  as the wave 4-vector, in which  $\vec{k}$  is the wave vector and  $k^2 = k^\mu k^\nu \tilde{g}_{\mu\nu} = (|\vec{k}|)^2 1/\lambda [(c_0/c_{EM})^2 1/\omega - 1]$ , equation (4.60) turns into

$$|\vec{k}| \frac{1}{\lambda} \left( \left( \frac{c_0}{c_{EM}} \right)^2 \frac{1}{\omega} - 1 \right) + iq \left( \frac{c_0}{c_{EM}} \right) = 0 \quad (4.61)$$

Taking this equation into account,  $c_{EM}$  can in principle be different from  $c_0$ . Solving equation (4.61), results in a complex term for  $c_0/c_{EM}$  and as a result the magnitude of  $c_{EM}$  can be written as

$$\frac{c_{EM}}{c_0} = \frac{1}{\sqrt{\omega}} \quad (4.62)$$

For each cosmological era, first we solve equations (4.27) and (4.26) for  $\Xi$  and  $\Delta$ , then using equations (4.35) and (4.34),  $\omega$  and  $\lambda$  are calculated. Finally using equation (4.62),  $c_{EM}$  is calculated. This form of the  $c_{EM}$ , is different from what is derived in (Izadi & Shojai, 2009). The limit  $\omega = \lambda = 1$  which is followed by  $F = 0$ , results in the standard value for the  $c_{EM}$ . By doing so, one can conclude that the form of  $c_{EM}$  is in principle the same as  $c_{ST}$ . However, in chapter 5, we will study if observations could put different constraints on these two distinct facets of the speed of light (compare equations (4.62) and (4.48)).

From now on, when we mention speed of electromagnetic waves, we mean  $c_{EM}$  given in equation (4.62) and it can in principle fit different compared to the causal structure constant which appears in the line element. In other words, in Palatini  $f(\mathcal{R}^{\mu\nu}\mathcal{R}_{\mu\nu})$  theories in the  $\Gamma$ LF, photons “may” move with a speed independent from the causal structure constant, which is used for distance measurements.

#### 4.4.4 Speed of the gravitational waves

Basically, the standard theory considers the gravitational waves as the ripples of the space time. This assumption makes the gravitational waves to move with the same value of causal structure constant. Additionally, in GR this speed is the same as the one with which the electromagnetic waves travel. But this “may” not be true in non standard theories; meaning that the speed of gravitational waves may not only be different from  $c_{EM}$  and  $c_{ST}$ , but it can also become either variable or constant.

In order to get the speed of gravitational waves,  $c_{GW}$ , the linearized modified Einstein field equations is used. Beginning with the linearization of the metric  $g_{\mu\nu} = \eta_{\mu\nu} + \epsilon h_{\mu\nu}$ , in which  $\epsilon$  is small, the affine connection, Ricci tensor and Ricci scalar are given as

$$\begin{aligned} \Gamma_{\mu\nu}^{\alpha} &= \epsilon \tilde{\Gamma}_{\mu\nu}^{\alpha} \\ \mathcal{R}_{\mu\nu} &= \partial_{\alpha} \Gamma_{\mu\nu}^{\alpha} - \partial_{\nu} \Gamma_{\alpha\mu}^{\alpha} \\ \mathcal{R} &= \eta^{\mu\nu} (\partial_{\alpha} \Gamma_{\mu\nu}^{\alpha} - \partial_{\nu} \Gamma_{\alpha\mu}^{\alpha}) \end{aligned} \quad (4.63)$$

Here  $\tilde{\Gamma}_{\mu\nu}^{\alpha} = \Gamma_{\mu\nu}^{\alpha}(h)$ . Using equation (4.63) together with (4.19) in vacuum,

$$\partial_{\alpha} \tilde{\Gamma}_{\mu\nu}^{\alpha} - \partial_{\nu} \tilde{\Gamma}_{\mu\alpha}^{\alpha} - \frac{1}{2} \eta_{\mu\nu} \eta^{\alpha\beta} (\partial_{\gamma} \tilde{\Gamma}_{\alpha\beta}^{\gamma} - \partial_{\beta} \tilde{\Gamma}_{\alpha\gamma}^{\gamma}) = 0 \quad (4.64)$$

Again introducing the new tensor  $\psi_{\mu\nu} = h_{\mu\nu} - 1/2 \eta_{\mu\nu} h$ , and considering the gauge condition  $\partial_{\alpha} \psi_{\beta}^{\alpha} = 0$ , results in  $\square h_{\mu\nu} = 0$ . Finally, this equation results in  $k^2 = 0$ . This shows that the

speed of gravitational waves is constant (see also (Izadi & Shojai, 2009) for a different approach with the same result).

This is an interesting result that the speed of gravitational waves is different from the causal structure constant. Although we expect that the facet coming from the line element be the same as  $c_{\text{GW}}$ , this is not the case in this model.

## 4.5 Summary

In this chapter, the  $f(\mathcal{R}^{\mu\nu}\mathcal{R}_{\mu\nu})$  model in Palatini formalism was reviewed. Assuming that speed of light can have different facets, considering this model in a frame in which  $\Gamma_{\mu\nu}^\alpha = 0$ , not only these different facets become variable, but they also may become different from each other (Izadi & Shojai, 2009). All the results are given in table

$c_i$	possible variation
$c_{\text{E}}$	$c_0$
$c_{\text{ST}}$	$c_0/\sqrt{\omega(z)}$
$c_{\text{EM}}$	$c_0/\sqrt{\omega(z)}$
$c_{\text{GW}}$	$c_0$

**Table 4.1:** Different facets of the speed of light considering  $\mathcal{L} = \mathcal{R} + F\mathcal{R}^{\mu\nu}\mathcal{R}_{\mu\nu}$ . These facets are written in the local frame in which the affine parameter vanishes. Here the functions  $\lambda(z)$ ,  $\omega(z)$  and  $q(z)$  are given in equations (4.34), (4.35) and (4.57) respectively and  $z$  means redshift.

As it is seen in Table 4.1, in the discussed Palatini models  $c_{\text{ST}}$  and  $c_{\text{EM}}$  can have possible variations. In principle, we do not expect them to be completely the same and we will fit them separately in chapter 5. Here  $c_0$  is the usual constant value (page 1) which is called “*the speed of light*” in standard theories.

Although the causal structure constant can become variable in this model (see equation (4.48)) and it is in principle a function of the density, the speed of gravitational waves does not vary. This is one of the main differences between this of extended theory with the standard GR : The so called “*speed*” which is present in the line element and is used for distance measurements, is different from the speed with which gravitational waves move. In GR these waves are considered as the ripples of the space time; which makes the connection between them and the causal structure constant. But this is not the same in this model which considers a more general geometry than in GR. In fact, considering a difference between the christoffel symbols and the affine connection makes a whole different structure for the space time and one of the results of doing so is that  $c_{\text{GW}}$  is not the same as the causal structure constant anymore in the  $\Gamma$ LF frame.

In the next chapter, we see if these variations can be helpful in describing some of the cosmological observations without using the cosmological constant. We will study how to put limitations on the model parameters for different facets of the speed of light mentioned in Table 4.1. At the end, these different facets will be compared with each other by their values and variations.

# 5

## A detailed investigation of the $f(\mathcal{R}^{\mu\nu}\mathcal{R}_{\mu\nu})$ model in the local frame, $\Gamma$ LF

In a very fundamental work, George Ellis has discussed different origins of the constant “ $c$ ” has in physical equations (Ellis & Uzan, 2005).

As discussed in chapter 4, Palatini formalism gives a more generic geometric structure for a manifold compared to the metric formalism. In that chapter, it was reviewed that different notions of the speed of light can in principle have dynamics within the age of the universe. This was a result of rewriting equations in a local frame with a vanishing affine connection.

Finally, in this chapter, we gather these results and explore if distinct observations can put constraints on different facets of the speed of light. Motivated by some cosmological questions regarding the cosmological constant, we will investigate if this model can help in eliminating this constant. Taking a modified  $f(\mathcal{R}^{\mu\nu}\mathcal{R}_{\mu\nu})$  gravity model in Palatini formalism, we obtain the form of different facets of the speed of light and search for any change in different conditions. At the end, we compare these different notions in terms of their values and dynamics with redshift. We compare the modified model with this model. Being interested in looking for the possibility of eliminating the cosmological constant, we consider the energy contents of the universe in the new model to be only matter in the recent universe.

When considering a difference between the speed of electromagnetic waves and the causal structure constant, one cannot rely on techniques which use radar for measurements and there has to be some alternations (Ellis & Uzan, 2005; Izadi & Shojai, 2013). Interpreting observations in frames which show a varying  $c_{EM}$  is not our main concern at the moment and needs studying more observational techniques. Thus we overcome this problem to some extent by accepting  $\Lambda$ CDM model as the most successful model and trying to see if the modified model can follow and mimic

$\Lambda$ CDM model. In other words, we shift the question “ How to use observational data to fit the model? ” to “ How good can the model mimic  $\Lambda$ CDM model? ”

In the model used in this thesis, the best way to do observations in such models is to use the gravitational waves. This is a result of having a constant speed for the gravitational waves.

Before starting this chapter, the following points are worth mentioning:

- The value of all the constants used here, are given in page 1.
- We consider a flat universe,  $K = 0$ .
- As one of our goals is to investigate the possibility of replacing the cosmological constant with the modified model presented here, we consider  $\Lambda = 0$  in all cosmological eras for this model; e.g. for the present time we assume a matter dominated era with  $\Omega_m^0 = 1$ . This is unlike some models which only consider the effect of dynamical speed of light on the standard model (e.g. (Balcerzak & Dabrowski, 2014)).
- Regarding the modified model, everything is written in the  $\Gamma$ LF frame explained in 4.4. The main reason is that as mentioned in chapter 4, both the causal structure constant and the speed of electromagnetic waves have dynamics in this frame and our goal is to analyze this result.

We proceed as follows:

We solve the modified Einstein field equations while adding a  $F\mathcal{R}_{\mu\nu}\mathcal{R}^{\mu\nu}$  term to the Einstein-Hilbert Lagrangian in Palatini formalism, for a purely matter dominated universe. Afterwards, we focus on how these special conditions<sup>1</sup>, affect different facets of the speed of light. First, we investigate if a dynamical causal structure constant can play the role of Dark Energy at least to some extent; which means if it gives the recent accelerated expansion of the universe. Second, we focus on possible dynamics of the speed of the electromagnetic waves. Then we use the fact that this approach gives rise to a constant speed of the gravitational waves and study the advantage of distance measurements using  $c_{\text{GW}}$  in this approach. At the end, we compare all these different facets of the speed of light and their dynamics and see if the approach presented in this thesis would really show differences between them.

## 5.1 Approach and model ( $\mathcal{L} = \mathcal{R} + F\mathcal{R}^{\mu\nu}\mathcal{R}_{\mu\nu}$ )

Here, we take  $\mathcal{L} = \mathcal{R} + F\mathcal{R}^{\mu\nu}\mathcal{R}_{\mu\nu}$  and proceed by determining the form of different facets of the speed of light in our preferred frame, in which the affine connection vanishes (we called this frame  $\Gamma$ LF).

Here  $F$  has the dimension of  $L^2$ . In order to simplify our free parameter, which should be fitted with the observation, we assume  $F = \gamma\Gamma$ , in which  $\Gamma = 2.743 \times 10^5 \text{ Mpc}^2$  (Izadi et al., 2017).

---

<sup>1</sup>whose motivations have been mentioned in chapter 4

Comparing with  $\Lambda$ CDM model,  $F\mathcal{R}^{\mu\nu}\mathcal{R}_{\mu\nu}$  must be comparable with  $\mathcal{R}$ . Having a small curvature at the present time and also adding the Ricci squared ( $\mathcal{R}_{\mu\nu}$ ), leads to a big  $F$ . When choosing a small value for  $\gamma$ ,  $F\mathcal{R}^{\mu\nu}\mathcal{R}_{\mu\nu}$  becomes small and compared to  $\mathcal{R}$ , it is not a very big correction; e.g. for  $\gamma = 10^{-2}$ ,  $F\mathcal{R}_{\mu\nu}\mathcal{R}^{\mu\nu}/\mathcal{R}|_{z=0} \sim 10^{-4}$ ; while in standard  $\Lambda$ CDM model  $\Lambda/R|_{z=0} \sim 10^{-1}$ . Here,  $\mathcal{R}$  and  $R$  are the Ricci scalar in Palatini and metric formalism, respectively.

To sum up,

$$F = 2.743 \times 10^5 \gamma (\text{Mpc})^2. \quad (5.1)$$

Using this model ( $F\mathcal{R}^{\mu\nu}\mathcal{R}_{\mu\nu}$ ), equations (4.26) and (4.27) become as follows

$$\Delta + 3F\Delta^2 - 3\Xi - 3F\Xi^2 = 2\kappa\rho c_0^2 \quad (5.2)$$

$$-\Xi + F\Xi^2 - \Delta - F\Delta^2 = -2\kappa p. \quad (5.3)$$

By solving equations (5.2) and (5.3), and assuming  $\rho = \rho_m^0(1+z)^3$  and  $p = 0$ , we get

$$\Delta = \frac{1}{2}\kappa\rho c_0^2, \Xi = -\frac{1}{2}\kappa\rho c_0^2. \quad (5.4)$$

Then following section 4.2.3,

$$\begin{aligned} \omega &= \frac{(1 + 2F\Xi)}{(1 + 2F\Delta)} \\ &= \frac{-F\kappa\rho c_0^2 + 1}{F\kappa\rho c_0^2 + 1} \end{aligned} \quad (5.5)$$

$$\begin{aligned} \lambda &= \sqrt{(1 + 2F\Delta)(1 + 2F\Xi)} \\ &= \sqrt{(-F\kappa\rho c_0^2 + 1)(F\kappa\rho c_0^2 + 1)}. \end{aligned} \quad (5.6)$$

As mentioned in page 40, the Hubble parameter is then given by

$$H = \frac{\sqrt{\frac{c_0^2}{6}(\Delta - 3\omega\Xi)}}{\left(1 - \frac{s}{2\lambda} \frac{\partial \lambda}{\partial \rho^f} \rho^f\right)}, \quad (5.7)$$

in which  $\rho^f$  is the fluid's density and for the matter dominated era,  $s = 3$ . It is worth mentioning that in the redshift range that we consider, we can neglect radiation. So the only component in the energy content of the universe in this model is matter. However, to study higher redshifts and specially early universe, one has to consider radiation as well and resolve equations (5.2) and (5.3) to get new functions for  $\omega$  and  $\lambda$ .

As shown before, in this model, the parameters  $\Delta$  and  $\Xi$  are given by solving equation (5.2) and (5.3). The key to remember, is that the dynamic of different facets comes from the redshift dependence of the right hand side of equations (5.2) and (5.3); i.e. the fluid's density and pressure. This means for vacuum solution ( $\rho = P = 0$ ) we do not see any dynamics in any of the facets mentioned before. This implies that in local area, all the facets remain the unchanged value  $c_0$ . So we conclude that the solar system observations remain unchanged in this model, meaning that  $c = c_0$  for all facets. Also, local constraints on the dynamics of  $c$ , such as the ones made by Oklo mine, do not count for this model.

We take  $c = c_0$  for all local and vacuum solutions and emphasis that we study the dynamics of the speed of light non-locally.

For checking the consistency of this model with observational data, the  $\chi^2$  minimization test is used,

$$\chi^2 = \sum_i \frac{(f_{\text{obs}}^i - f^i)^2}{(\Delta f_{\text{obs}}^i)^2}, \quad (5.8)$$

where  $f_{\text{obs}}^i$  are the observational points,  $f^i$  are the theoretical points given by each model and  $\Delta f_{\text{obs}}^i$  are the observational uncertainties. If  $f^i$  are functions of a parameter, let's say  $\gamma$ , then the best fit of the model is given when a  $\gamma$  value minimizes  $\chi^2$ . The reduced  $\chi^2$  is given by

$$\chi_r^2 = \frac{\chi^2}{N - n}. \quad (5.9)$$

$N$  is the number of data points and  $n$  is the degree of freedom. The two models which will be compared with each other in this chapter are :

*$\Lambda$ CDM model* : The concordance or the  $\Lambda$ CDM model, is the standard cosmological model which considers  $H_0 = 65.1 \text{ kms}^{-1} \text{ Mpc}^{-1}$ ,  $\Omega_m^0 = 0.3289$  (Planck Collaboration et al., 2015)<sup>2</sup> (given in table in page 1).

*Modified model* : If we consider a correction  $F\mathcal{R}^{\mu\nu}\mathcal{R}_{\mu\nu}$  to the Lagrangian in the Palatini formalism, going to the affine connection vanishing local frame ( $\Gamma$ LF), different facets of the speed of light show dynamics in time. in this model we assume a matter dominated universe for the present time,  $\Omega_m^0 = 1$ .

Before going further, we mention that we have used union 2 data (Suzuki & et. al., 2012) in order to compare the modified and  $\Lambda$ CDM model with each other. However, we are aware of the fact that in this data set,  $h = 0.7$  is assumed ( $H_0 = 100 h$ ). Therefore, we know that the best fit would be if we consider the same value for the Hubble constant in modified and  $\Lambda$ CDM model. Nevertheless, just for the sake of comparison, we still report the  $\chi^2$  for both models.

## 5.2 Fitting the model parameter, $\gamma$

Starting to fit the causal structure constant  $c_{\text{ST}}$ , in this section we try to find a  $\gamma$  value which matches the most with different relevant observations. The observations we look for, are the

---

<sup>2</sup>In this work, the Planck collaboration assumed a possibility of dynamics of fundamental constants.

ones which deal with distance and length measurements. All these observations are explained and studied more in chapter 2 and in what follows we use them to fit our model.

### 5.2.1 Observable Hubble Data and different models

Different models result in different functions for  $H$  which should be tested with observational data. Here we test the models with OHD (Observable Hubble Data). Using equation (5.7) together with (5.4), results in  $H^{\text{mod}}(z)$ . We use this Hubble parameter in our modified model. In Figure 5.1, Hubble parameter is given for the  $\Lambda$ CDM model and also different values of  $F$  for the modified model. The OHD data are taken from (Farooq & Ratra, 2013) (selected data from measurements of differential age method).

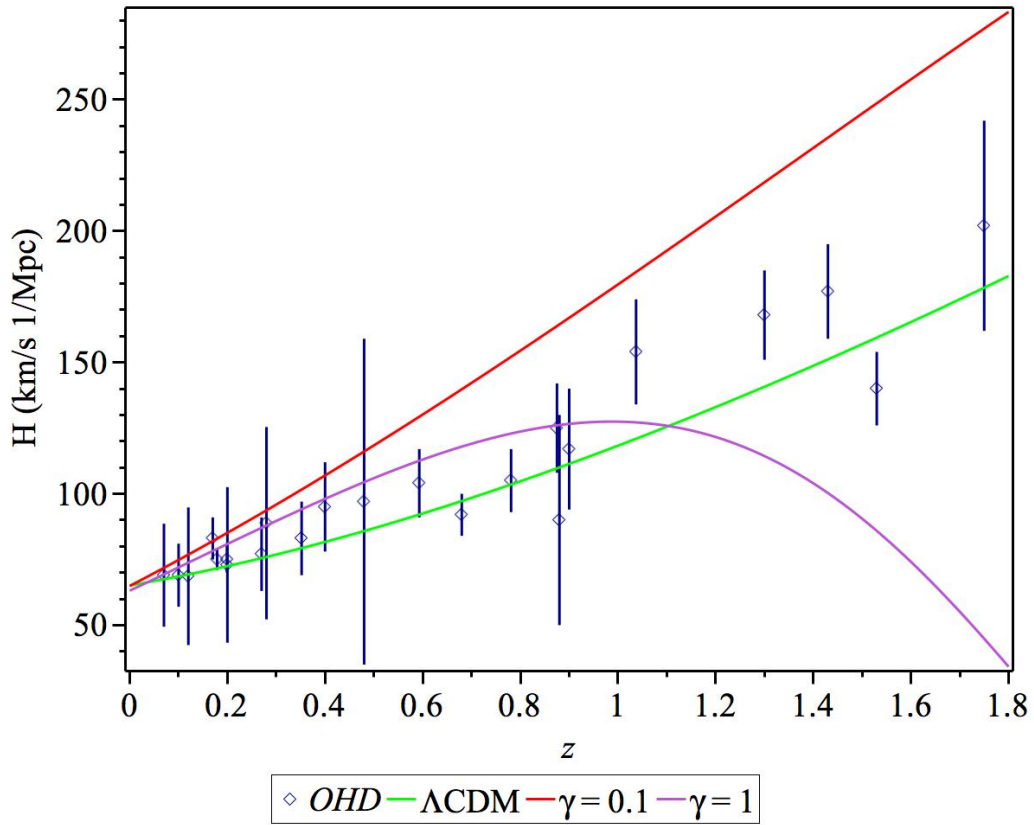


**Figure 5.1:** The Hubble parameter for OHD (Observable Hubble Data),  $\Lambda$ CDM model and the model presented in page 48 which is plotted for two different  $\gamma$  values as an example. The smaller (larger)  $\gamma$  is the smaller (larger) the correction to the Lagrangian is. Also, a smaller (larger)  $\gamma$  results in smaller (larger) dynamics in  $c_{ST}$ . This is shown in Figure 5.3. As shown here, non of the values for  $\gamma$  here, results in an acceptable trend for the Hubble parameter, similar to the  $\Lambda$ CDM model. The OHD data points are taken from (Farooq & Ratra, 2013).

It is obvious from this figure that in this redshift range, non of the constant values of  $\gamma$  used here are helpful. Clearly, the larger the redshift is, the bigger the difference gets. We try to fix this

problem by fitting the  $\gamma$  parameter using the SN Ia data later in this chapter . For this reason, we need to modify the SN Ia luminosity distance/ SN distance modulus regarding the change of  $c_{ST}$  in the modified model.

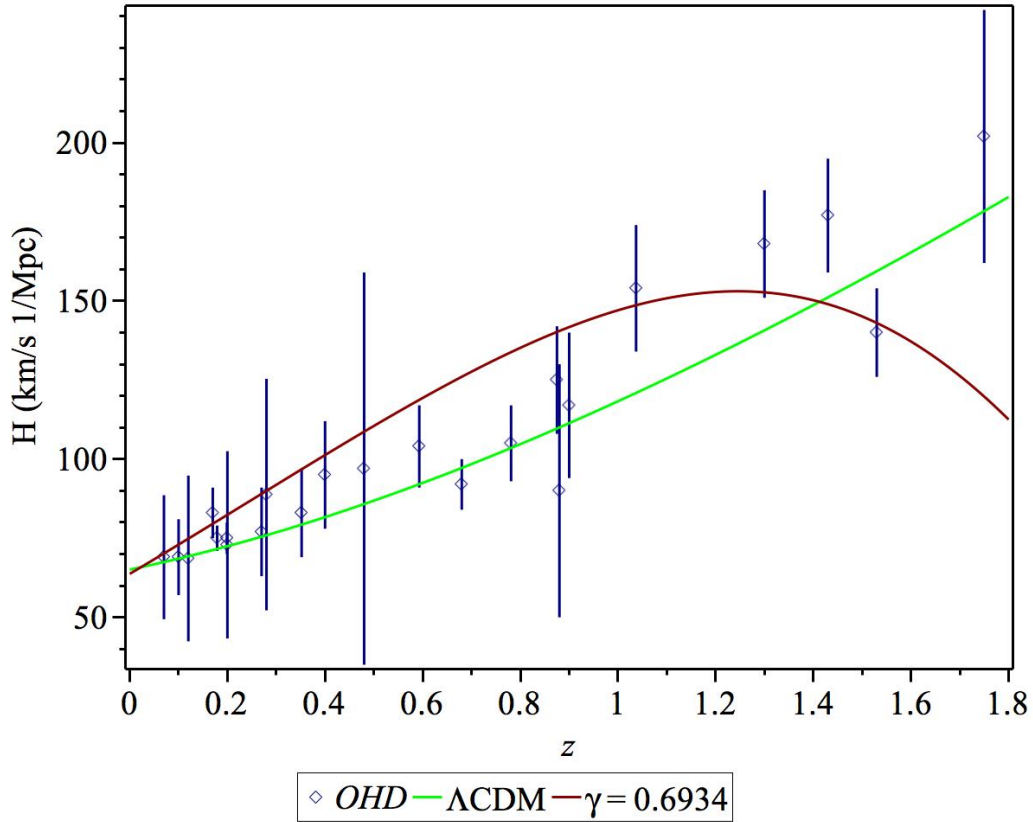
But before that, we do some statistical studies on the aforementioned models.

Using Planck results ( $63.2 < H_0 \text{ (km/s Mpc}^{-1}\text{)} < 66.8$ ) (Planck Collaboration et al., 2015), the Hubble parameter in equation (5.7) results in  $0 < \gamma < 0.9553$  for  $H_0$ .

On the other hand, using the  $\chi^2$  minimization test, we get to :

$\chi^2_{\Lambda\text{CDM}} = 16.0498$  for the  $\Lambda\text{CDM}$  model ( $\chi^2_r = 0.6978$ ). Here we have  $H_0 = 65.1 \text{ km s}^{-1} \text{ Mpc}^{-1}$ .

Then for the Hubble parameter of the modified model,  $\chi^2_{\text{min}} = 42.6014$  ( $\chi^2_r = 1.9364$ ) for  $\gamma = 0.6934 \pm 0.0498$ . This value of  $\gamma$  results in  $H_0 = 63.7384 \text{ km s}^{-1} \text{ Mpc}^{-1}$  which is in the range of the allowed region given by Planck. This Hubble parameter is shown in Figure 5.2.



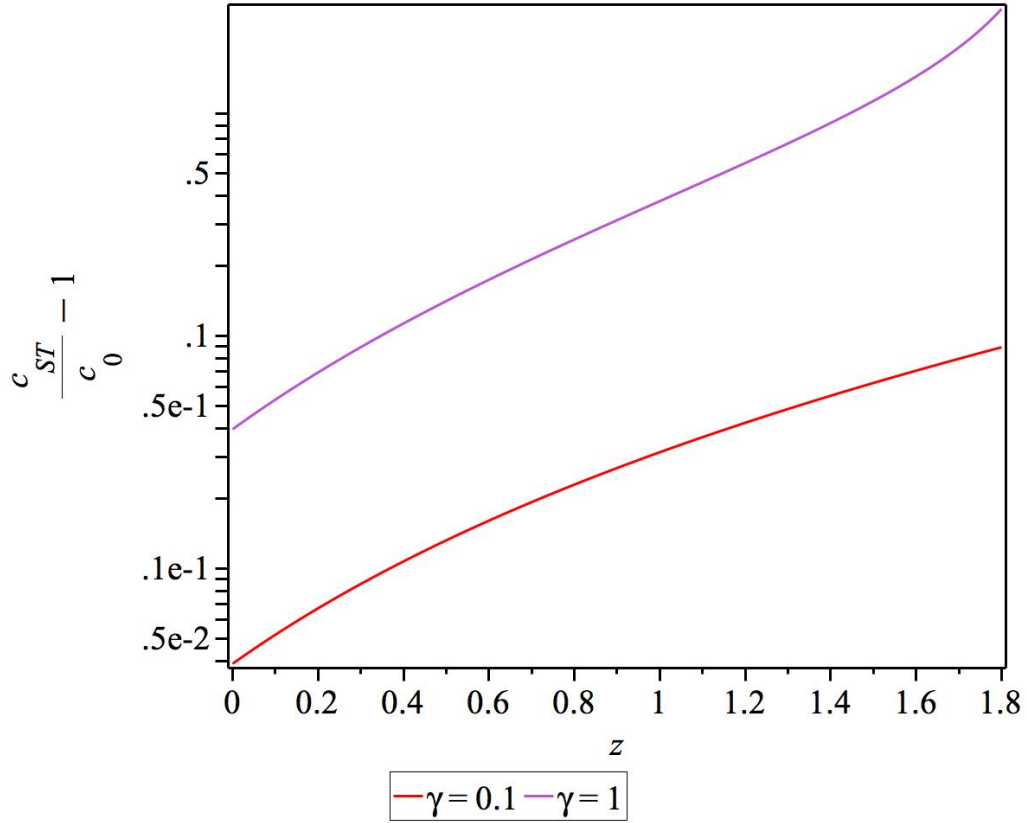
**Figure 5.2:** The Hubble parameter for OHD (Observable Hubble Data),  $\Lambda\text{CDM}$  model and the model with  $\gamma = 0.6934$ , which makes  $\chi^2_{\text{min}}$ . As it is shown here, this value cannot make an acceptable evolution for the Hubble parameter.

Figure 5.2 shows that this constant value for  $\gamma$ , does not make a reasonable trend for the Hubble parameter of the modified model. Although it makes a suitable value for  $H_0$ , it results in a bend in the curve in higher redshifts.

Additionally, we should mention that as we are only using matter in this model, putting  $\gamma = 0$ , results in the Hubble parameter of the Einstein de-Sitter model which is not consistent with OHD of course. Also, the larger  $\gamma$  gets, the more its trend gets different from what we expect. This means that after a while, the Hubble parameter starts to decrease, which is not acceptable. Obviously from this plot, one concludes that although this value for  $\gamma$  minimizes  $\chi^2$ , it does not give an acceptable Hubble parameter.

### 5.2.2 The causal structure constant ( $c_{ST}$ )

Although we have seen that no value for  $\gamma$  can help in getting a correct form for the Hubble parameter, we continue studying how different values of  $\gamma$  would help in fitting the model with other observations; such as the SN Ia distance modulus or the redshift drift. Our goal is to find the best way to fit our model parameter for the causal structure constant.



**Figure 5.3:** The relative change of casual structure constant ( $c_{ST}$ ) compared to  $c_0$  for two different values of  $\gamma$ . Here we considered  $\gamma$  to be constant. For  $\gamma = 0.1, 1$ , we have  $c_{ST}/c_0(z = 0) - 1 = 0.004, 0.04$  respectively. This facet of light increases with redshift, meaning that it has been larger in the past. In addition, the larger (smaller) the model parameter,  $\gamma$  is, the larger (smaller) the relative difference between  $c_{ST}$  and  $c_0$  in each redshift gets.

Until now, we have only seen the form of  $c_{ST}$  in our approach (equation (4.48)). The solution set in (5.4) together with a positive  $\gamma$ , results in  $c_{ST} \geq c_0$  which is increasing with redshift. Here we see how much this facet is varying, and also how it affects different cosmological observations regarding the distances and lengths. Using (4.48) and (5.5), figure 5.3 shows  $c_{ST}$  for two different  $\gamma$  values.

As it is clear in Figure 5.3, for the same redshift range, the larger the value of  $\gamma$  is, the larger  $c_{ST}$  is. As an example, for  $\gamma = 0.6934$  which made  $\chi_{\min}^2$  for the Hubble parameter,  $c_{ST}/c_0(z = 0) - 1 = 0.0273$ . Also, taking  $\gamma = 0$ , results in  $c_{ST} = c_0$  for all redshifts. For a positive non zero  $\gamma$ ,  $c_{ST}$  increases with redshift.

As stated before, here  $c_{ST}$  (and also  $c_{EM}$  which we study in section 5.4) has become a dynamical constant depending on the space time structure which is in principle coming from the energy content on it.

### 5.2.3 Studying the effect of a varying $c_{ST}$ on SN Ia luminosity distance

Dynamics of  $c_{ST}$ , has for sure an impact on different observational data. In fact, by varying the  $c_{ST}$ , one gets a larger distance compared to the standard theory. This can help in explaining observations which show larger distances than expected in the standard cosmology.

The SN Ia luminosity distance is larger than the value predicted by a universe without Dark Energy (Amendola & Tsujikawa, 2010). This leads us to consider a large amount of the energy content of the universe to be Dark Energy (See Table in page 1). As the luminosity distance of SN Ia is an important cosmological measurement which is used to prove the recent expansion of the universe and the existence of Dark Energy, we study the effect of a varying  $c_{ST}$  on this observation.

To start with the standard equations for the luminosity distance we have (Amendola & Tsujikawa, 2010)

$$d_L^2 = \frac{L_s}{4\pi\mathcal{F}}. \quad (5.10)$$

Here,  $L_s$  is the absolute luminosity and  $\mathcal{F}$  is the observed flux which is given by

$$\mathcal{F} = \frac{L_o}{4\pi(a_0 f(\chi))^2}, \quad (5.11)$$

in which  $L_o$  is the observed luminosity and  $f(\chi)$  is given by

$$\begin{aligned} f(\chi) &= \frac{1}{\sqrt{-K}} \sinh(\sqrt{-K}\chi) \\ &= \begin{cases} \sin \chi & \text{for } K = +1 \\ \chi & \text{for } K = 0 \\ \sinh \chi & \text{for } K = -1 \end{cases} \end{aligned} \quad (5.12)$$

$K$  shows the curvature of the universe which can be  $+1$ ,  $0$ ,  $-1$  for a closed, flat or open universe<sup>3</sup>. Also,

$$\chi = \int_0^z c \frac{dz}{H}. \quad (5.13)$$

Putting  $a_0 = 1$ , equation (5.10) can then be written as

$$d_L = f(\chi) \sqrt{\frac{L_s}{L_o}}. \quad (5.14)$$

On the other hand, assuming  $L$  as the luminosity of light which has been emitted in an time interval  $\Delta t$  with energy  $\Delta E$ , we have  $L = \Delta E / (\Delta t)$  which results in

$$\begin{aligned} d_L &= f(\chi)(1+z) \\ &= \chi(1+z) \\ &= (1+z) \int_0^z c \frac{dz}{H}. \end{aligned} \quad (5.15)$$

$H$  is the Hubble parameter which is set according to the model we choose. For instance, for the  $\Lambda$ CDM model in present time, we ignore radiation and take  $H = H_0 \sqrt{\Omega_m^0 (1+z)^3 + \Omega_\Lambda^0}$ .

On the other hand as discussed earlier in this section, if we consider different origins and facets for the speed of light, then depending on the model and formalism that we chose, what we usually call “the speed of light ” (causal structure constant) can get dynamics.

After putting  $c_{ST}$  instead of a constant  $c$  in the line element as the causal structure constant, equation (5.13) together with (5.15) results in

$$d_L = (1+z) \int_0^z c_{ST} \frac{dz}{H}. \quad (5.16)$$

Using union II data (Suzuki & et. al., 2012), we study this change here. Figure 5.4 shows the distance modulus for different models and also union II data. From the observational point of view, luminosity distance is written in parsec<sup>4</sup> as

$$d_L = 10^{1+\mu/5} \text{pc}, \quad (5.17)$$

in which  $\mu = m - M$  is the distance modulus,  $m$  is the apparent magnitude, and  $M$  is the absolute magnitude.

---

<sup>3</sup>Here in this thesis, we consider a flat universe; so  $K = 0$ .

<sup>4</sup> $1\text{pc} = 3.0857 \times 10^{16} \text{m}$ .

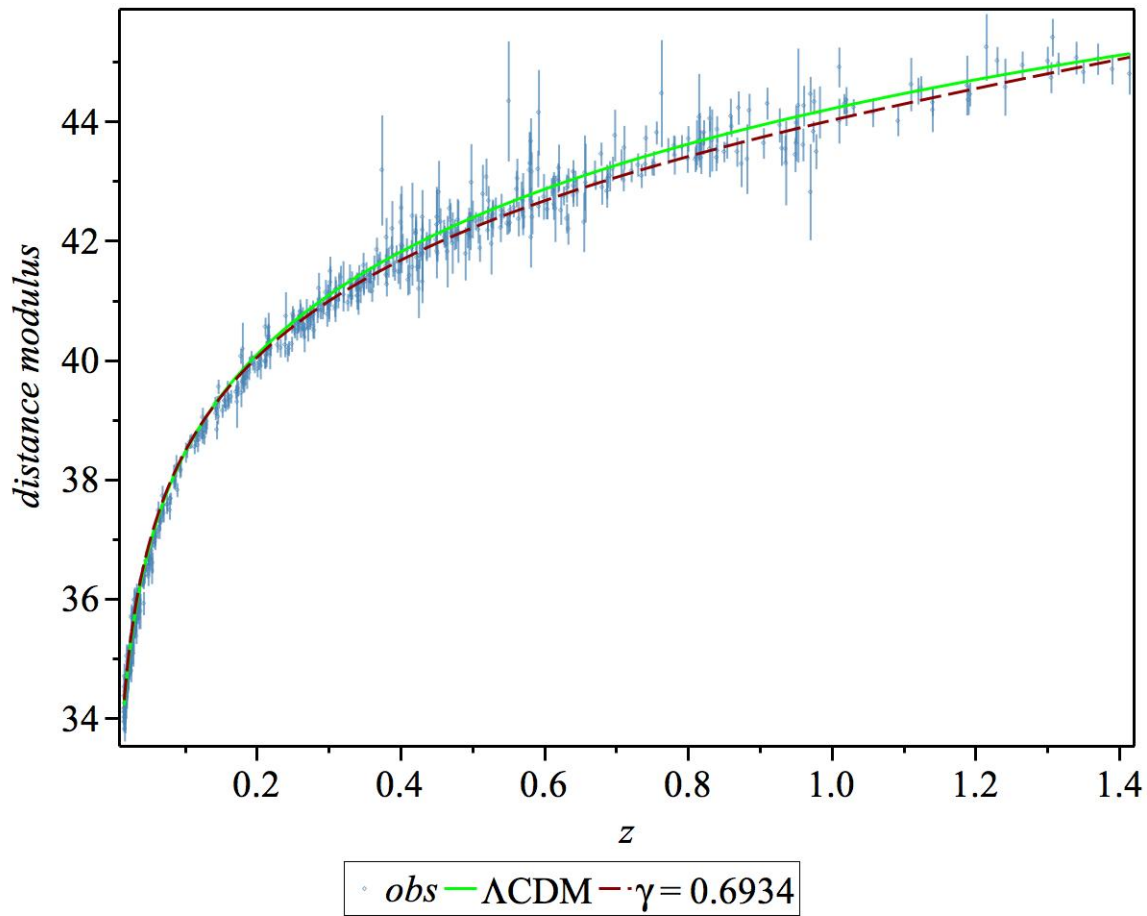


**Figure 5.4:** The distance modulus for the  $\Lambda$ CDM model, the the modified model with  $\gamma = 0.6934$  and also Union II data (Suzuki & et. al., 2012). As shown here, despite having an unacceptable trend for the Hubble parameter, the distance modulus of the the modified model has an acceptable trend similar to the  $\Lambda$ CDM model.

Figure 5.4 shows the distance modulus for  $\gamma = 0.6934$  which makes  $\chi^2_{\min}$  for Hubble parameter compared to OHD. The larger the redshift, the larger the distance modulus. Although this  $\gamma$  does not minimize  $\chi^2$  of SN distance modulus of the model compared to union II data, it shows a reasonable trend and follows the  $\Lambda$ CDM model's trend. However, here we remind that as shown in Figure 5.2, this does not make an acceptable trend for the Hubble parameter.

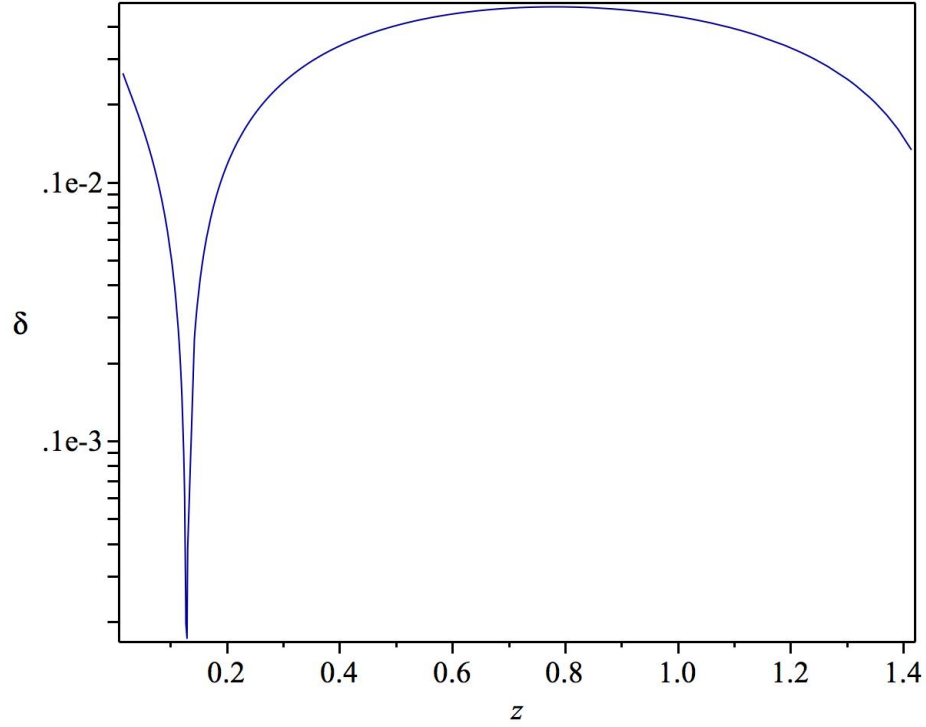


**Figure 5.5:**  $\delta = |1 - \mu_{\text{model}}/\mu_{\Lambda\text{CDM}}|$  with  $\gamma = 0.6934$ . The relative difference increases with redshift and then the two functions of distance modulus coincide, which makes a minimum in the relative difference. Afterwards, an increase and then a decrease is seen.

In Figure 5.5, we see the relative difference between the distance modulus of the  $\Lambda\text{CDM}$  model and the modified model for  $\gamma = 0.6934$ . The relative difference is mostly of the order of  $10^{-3}$ . The distance modulus of the modified model crosses the  $\Lambda\text{CDM}$  model at about  $z \sim 0.1$ , this is why we see a minimum in this figure. The relative difference then shows an increase and again a decrease, which are all of the order of  $10^{-3}$  as shown in this figure.

Let us calculate  $\chi_{\text{min}}^2$  for the the modified model compared to this data :  
 $\chi^2 = 936.8010$  for the  $\Lambda\text{CDM}$  model ( $\chi_r^2 = 1.6152$ ).  
 $\chi_{\text{min}}^2 = 955.4651$  with  $\gamma = 0.5126^{+0.0280}_{-0.0282}$  for the VSL model ( $\chi_r^2 = 1.6502$ ). The value  $\gamma = 0.5126$  makes  $H_0 = 64.1025 \text{ km s}^{-1} \text{ Mpc}^{-1}$  and  $c_{ST}/c_0(z=0) - 1 = 0.0201$ .

Figure 5.6 shows the distance modulus of the  $\Lambda\text{CDM}$  model and also the modified model for its best choice of  $\gamma$  which makes  $\chi_{\text{min}}^2$  for the distance modulus.

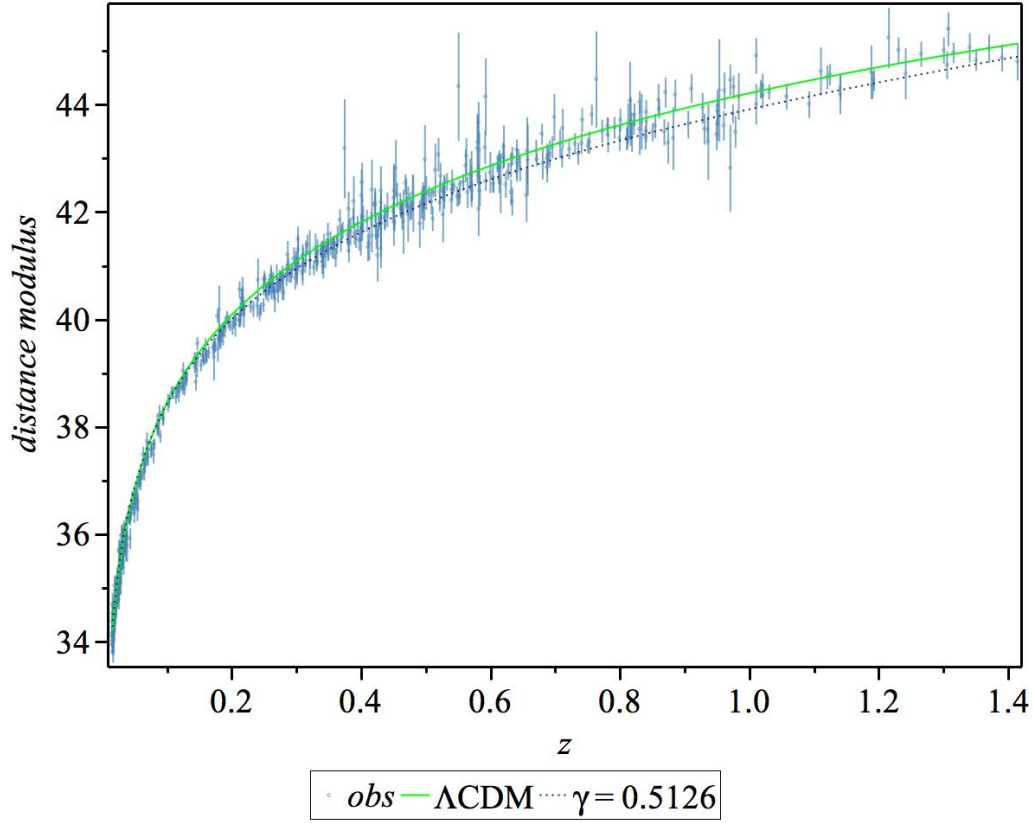


**Figure 5.6:** SN distance modulus for observations,  $\Lambda$ CDM model and the modified model with the best choice of  $\gamma$  which makes  $\chi^2_{\min}$  (Izadi et al., 2017). For the observational data, we used (Suzuki & et. al., 2012). Again, despite the Hubble parameter, here an acceptable trend for the distance modulus of the the modified model is seen.

Obviously from the Figure 5.6, VSL model has similar trend and form compared to the  $\Lambda$ CDM model. Compared to the  $\gamma$  value used in Figure 5.4, here in Figure 5.6 we used a smaller value. This makes the distance modulus smaller in this figure. Also, compared to the observational data (union II (Suzuki & et. al., 2012)), this value for  $\gamma$  makes a smaller  $\chi^2$  in total. Again this Figure shows that in larger redshift, a constant  $\gamma$  does not show a completely similar value to  $\Lambda$ CDM model.

The relative difference of the distance modulus for  $\Lambda$ CDM model and the modified model is shown in Figure 5.7. It is clearly not that different from Figure 5.5. This shows that a small difference in the value of  $\gamma$ , does not make much change in the distance modulus. Again the relative difference is mostly of the order of  $10^{-3}$ .

Here we conclude that in contrast to the Hubble parameter, we are able to find a value for  $\gamma$  which to some extent agrees with observational data of SN Ia. Of course regarding the distance modulus, it does not match with  $\Lambda$ CDM model completely but at least it follows it and shows similar trend.

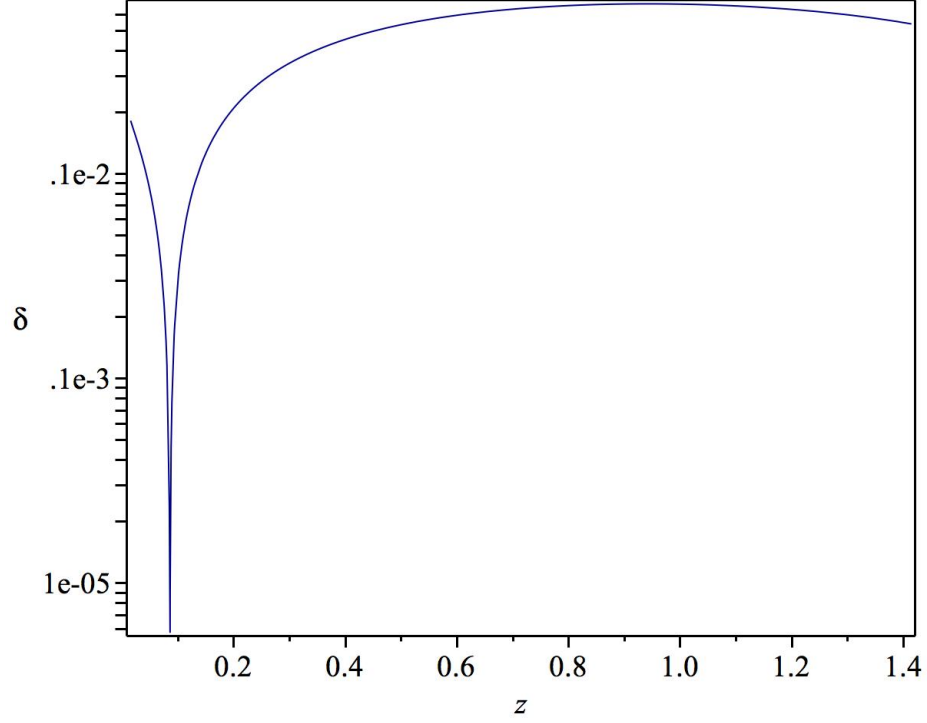


**Figure 5.7:**  $\delta = |1 - \mu_{\text{model}}/\mu_{\Lambda\text{CDM}}|$  with  $\gamma = 0.5126$ . Again similar to Figure 5.5, the relative difference increases with redshift and then the two functions of distance modulus coincide, which makes a minimum in the relative difference. Afterwards, and increase and then a decrease is seen.

#### 5.2.4 The redshift drift

Following the steps in section 2.1.4, we rederive redshift drift for a modified model in which speed of light has dynamics. Again, the redshift of the source varies by

$$\begin{aligned}
 \Delta z &= z(t_0 + \Delta t_0) - z(t_0) & (5.18) \\
 &\simeq \frac{a_0}{a} \left( H_0 \Delta t_0 - H^{\text{mod}} \Delta t \right) \\
 &= (1 + z) \Delta t_0 \left( H_0 - H^{\text{mod}} \frac{\Delta t}{\Delta t_0} \right).
 \end{aligned}$$

Here  $H^{\text{mod}}$  is given in equation (5.7). Now we have to go back to the definition of redshift. As we know, if the causal structure constant is dynamic (similar to (Balcerzak & Dabrowski, 2014)), then

$$\begin{aligned}
 \int_t^{t_0} \frac{c(t) dt}{a(t)} &= \int_{t+\Delta t}^{t_0+\Delta t_0} \frac{c(t) dt}{a(t)} & (5.19) \\
 \rightarrow \frac{c(t)\Delta t}{a(t)} &= \frac{c_0\Delta t_0}{a_0},
 \end{aligned}$$

in which  $c_0 = c(t_0)$  and  $a_0 = a(t_0)$ . Using this equation together with equation (5.18),

$$\begin{aligned}\Delta z &= (1+z)\Delta t_0 \left( H_0 - H^{\text{mod}} \frac{c_0}{c} \frac{a}{a_0} \right) \\ &= \Delta t_0 \left( H_0(1+z) - H^{\text{mod}} \frac{c_0}{c} \right).\end{aligned}\tag{5.20}$$

Figure 5.8, shows the redshift drift for the  $\Lambda$ CDM model and also the the modified model for  $\gamma = 0.5126$  which makes  $\chi^2_{min}$  for SN distance modulus and  $\gamma = 0.3$ .

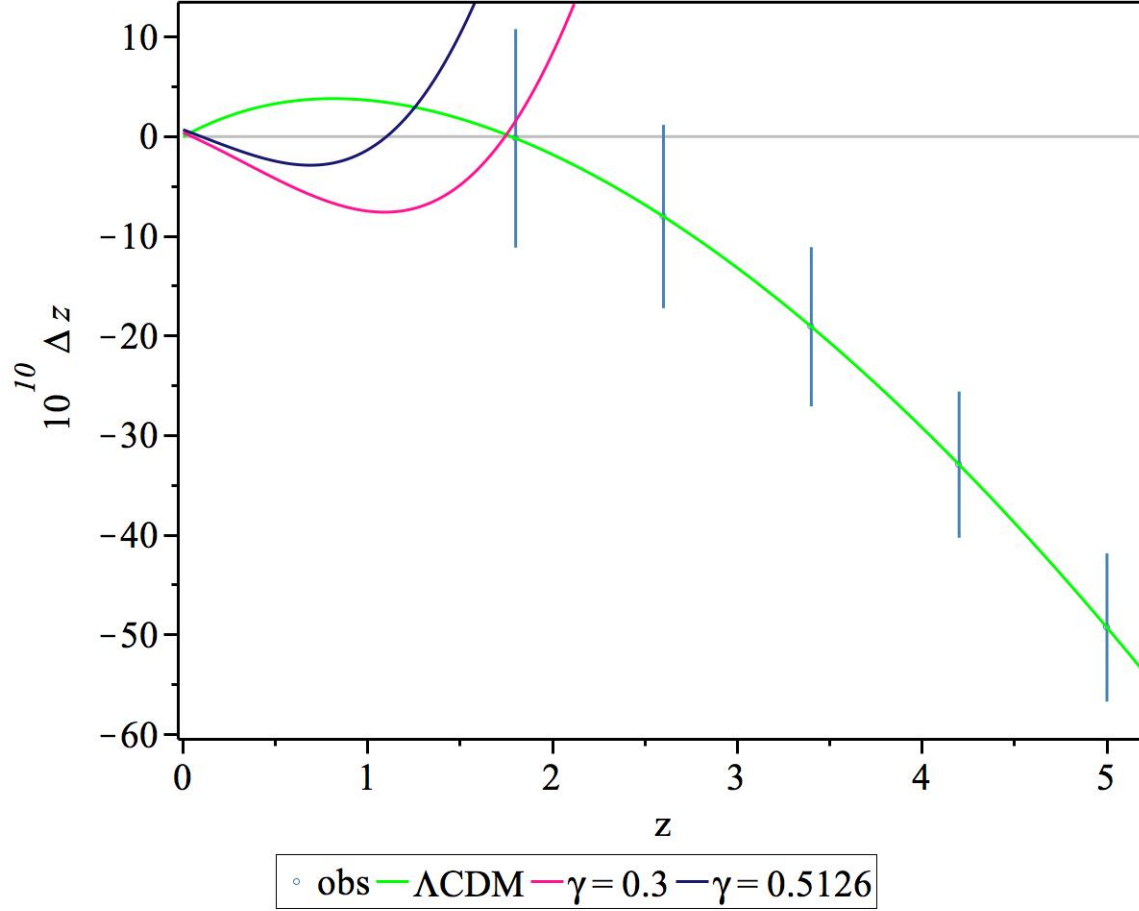


**Figure 5.8:** Redshift drift ( $10^{10} \Delta z$ ) for  $\Lambda$ CDM model, the modified model and simulated observational points. The error bars are taken from (Liske et al., 2008a). We used  $\Delta t_0 = 30$  yr,  $N_{\text{QSO}} = 20$  and  $S/N = 2000$ . As it is seen here, non of the values of  $\gamma$  can be acceptable. Again this plot leads us to exclude the the modified model in the form it has been presented so far, because it does not follow the  $\Lambda$ CDM model and the simulated data points.

Figure (5.8) shows  $\Delta z$  as a function of  $z$  for  $\gamma = 0.3$  and  $\gamma = 0.5126$ . Obviously, the redshift drift in this model can be fitted in a way that it crosses the zero line at  $z \simeq 2$ . It also shows a

non zero value for the redshift drift in smaller redshifts. However, the sign of this shift is different than what is expected in  $\Lambda$ CDM model. This means that if we convert this shift to the shift of the apparent velocity of the source, we would see a change in the velocity, but in another direction from what is expected in  $\Lambda$ CDM model.

The other difference happens in  $z > 2$  and which is not only the shift of the redshift gets so much higher than the expected values in  $\Lambda$ CDM model, but it also has definitely a different sign. Again if we convert this to the change in the apparent velocity of the source, which is a quasar here, the change in the velocity is much higher than what expected from the  $\Lambda$ CDM model and also the direction changes.

So we can conclude that Figure (5.8) again guides us to look for another fit for the model parameter. In this model, the dynamics of  $c_{ST}$  depends on both redshift and  $\gamma$ . In the next section, we look for a redshift dependent  $\gamma$  which comes from fitting the model with SN Ia luminosity distance and redshift drift. The reason is mentioned in this section; there are several problems with this constant  $\gamma$  which is as an example shown in Figure 5.8. First, obviously it does not follow  $\Lambda$ CDM model. So if we agree that we are looking for a model which similar to  $\Lambda$ CDM model, our method up to here does not work. Also, although redshift drift is supposed to be positive at first and then get negative, this behaves vice versa.

To conclude, current studies seem to validate the view that although a constant model parameter,  $\gamma$ , works well with the SN Ia luminosity distance, it is not a suitable one and we should look for another choice of model parameter. This will be done in the next section. A key thing to remember here is that what we have done so far was fitting  $c_{ST}$  with relevant observation. Here we emphasis that this may not be the case for other facets of the speed of light.

Our next step is to fit the model parameter using SN luminosity distance (distance modulus) and redshift drift. Comparing with the standard SN distance modulus and redshift drift, if we set  $c_0/c_{ST} H^{\text{mod}} \rightarrow H^{\Lambda\text{CDM}}$  then this function matches the  $\Lambda$ CDM model. We will proceed using this idea in the following sections and examine the results.

### 5.3 A new fit for the model parameter

As stated earlier, we are going to find a model parameter  $\gamma$  which fits well with all observations we have studied here regarding distance measuring.

Obviously from equation (5.16), in order for the model to follow the  $\Lambda$ CDM model, we have

$$\frac{c_{ST}}{H} = \frac{c_0}{H_{\text{con}}}, \quad (5.21)$$

in which  $c_{ST}$  is the causal structure constant ( $c_{ST} = c_0/\sqrt{\omega}$ ),  $\omega$  is given in equation (5.5),  $c_0$  is the constant speed of light we consider in standard theory,  $H_{\text{con}}$  is the Hubble parameter of the  $\Lambda$ CDM model (concordance model) and  $H$  is given in equation (4.38). Equation 5.21 shows how we approach dealing with the distance measurements. The theoretical assumption behind this is as follows: The fraction  $c_{ST}/H$  has the dimension of length; meaning that fitting this fraction

with the standard one, helps in getting the distances as large as they should be. This leads to a differential equation for  $d\gamma(z)/dz$  which after solving, gives us  $\gamma(z)$ :

$$\begin{aligned} \frac{d\gamma(z)}{dz} &= f(z) \\ \rightarrow \gamma &= \gamma(z). \end{aligned} \quad (5.22)$$

Both ratios  $c_{ST}/H$  and  $c_0/H_{\text{con}}$  have length dimension. This means in equation (5.21), we are actually fitting the model parameter  $\gamma$ , matching the lengths in the modified model with the standard model. This match is of course useful to get to a correct value for  $c_{ST}$  in each redshift, because this facet of light matches the concept of length measurements and distances. Again we remind that this may not be the case for other facets of the speed of light and they are going to be studied in following sections.

Solving equation (5.22), doing a rational interpolation<sup>5</sup> and fitting the  $\gamma(z)$  function in the range  $0 < z < 5$ , this function can be written as below

$$\gamma(z) = \frac{\sum_{i=0}^5 a_i (1+z)^i}{\sum_{i=0}^5 b_i (1+z)^i}. \quad (5.23)$$

Figure 5.9 shows the  $\gamma(z)$  given in equation (5.23).

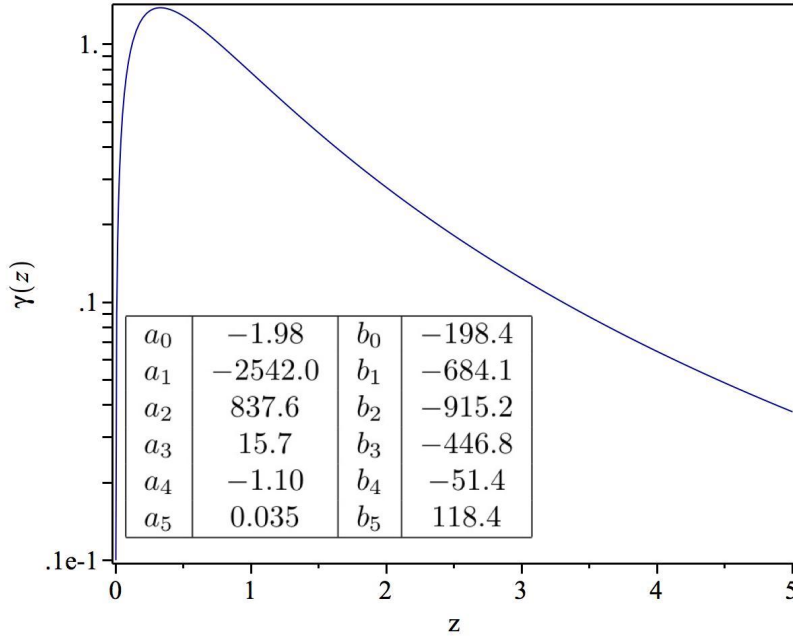


**Figure 5.9:**  $\gamma(z)$  from the equation (5.23) vs. redshift. This  $\gamma(z)$  is another attempt to fit the the modified model with different observations regarding the causal structure constant. The function shows an increase and then it decreases for the redshift range we studied.

<sup>5</sup>Solving the equation (5.22) numerically, we need to fit the result with a function. We use the rational interpolation for the range  $0 < z < 5$  and get to a rational function for  $\gamma(z)$ . as the initial condition, we put  $\gamma(0) = 0.01$ .

The plot in Figure 5.9 shows the  $\gamma(z)$  given in the equation (5.23). This function increases with redshift upto a certain point and then decreases. It can be concluded that assuming a matter dominated era for the present universe, the correction made to the Lagrangian,  $\mathcal{L} = \mathcal{R} + F\mathcal{R}^{\mu\nu}\mathcal{R}_{\mu\nu}$ , is more effective in recent era, because of its larger value. After affecting in recent era and playing the role of the cosmological constant or Dark Energy, it will decrease with redshift. The fitted function starts at  $z = 0$ ,  $\gamma = 0.01$  which results in  $c_{ST}/c_0(z = 0) - 1 = 0.0004$  and  $H_0 = 65.0748 \text{ km s}^{-1} \text{ Mpc}^{-1}$ . The maximum happens at  $z = 0.3290$ ,  $\gamma = 1.3872$  with  $c_{ST}/c_0(z = 0.3290) - 1 = 0.1355$ . The the function decreases again and at  $z = 5$  makes  $\gamma = 0.0376$  and  $c_{ST}/c_0(z = 5) - 1 = 0.3862$ . As we have solved the differential equation (5.22) numerically and fitted it with a function up to  $z = 5$ , we do not report any further values for  $\gamma(z)$  here. Figure 5.10 shows how  $c_{ST}$  changes with this  $\gamma(z)$ . Using the  $\gamma(z)$  ( $F\mathcal{R}^{\mu\nu}\mathcal{R}_{\mu\nu}|_{z=0} \sim 10^{-4}$  which shows this is a much smaller value compared to the cosmological constant in  $z = 0$ ).

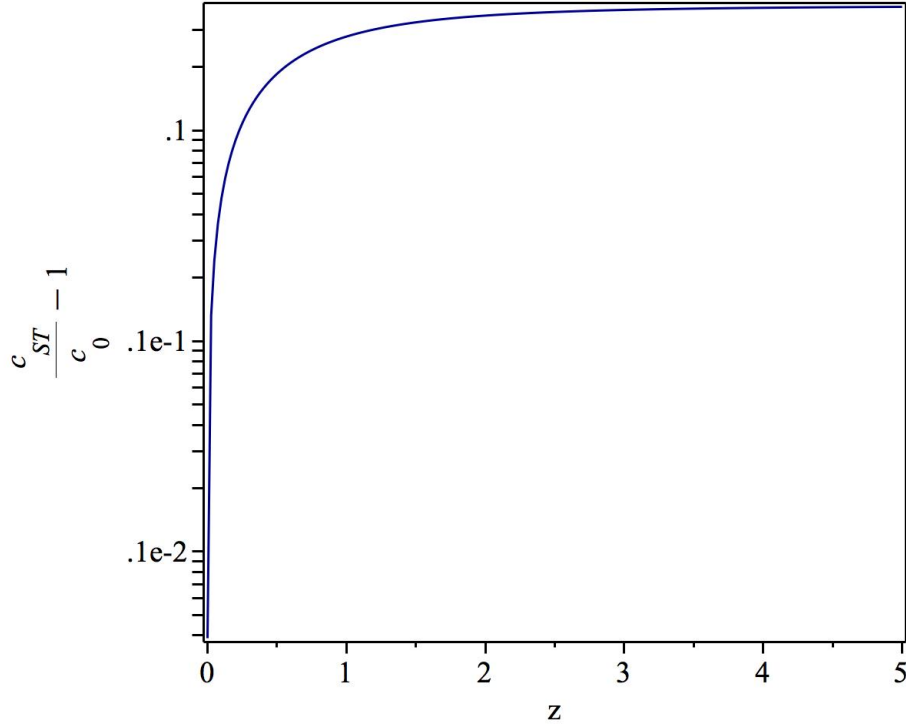


**Figure 5.10:**  $c_{ST}/c_0 - 1$ , plotted vs. redshift using  $\gamma(z)$  from the equation (5.23). Using the  $\gamma(z)$  which is given to fit the the modified model with observations regarding the causal structure constant, the relative difference between  $c_{ST}$  and  $c_0$  will increase as seen in this plot.

Although,  $\gamma(z)$  increases with redshift at first and then continues decreasing with redshift, as shown in Figure 5.10,  $c_{ST}$  always increases with  $z$ . Another key to remember is that the most change is seen in lower  $z$  and as  $z$  increases the growth of  $c_{ST}$  decreases. This shows that in lower  $z$ ,  $c_{ST}$  is experiencing a sudden decrease.

As stated earlier, the fit for  $\gamma(z)$  results in  $c_{ST}/c_0(z=0) - 1 = 0.0004$ . This means even at very small redshifts, there is a difference between  $c_{ST}$  and  $c_0$  of the order of  $10^{-4}$ . As mentioned before, this facet of speed of light ( $c_{ST}$ ) is related to distance measurements; therefore, it does not reject the general premise that the speed of electromagnetic waves,  $c_{EM}$ , is  $c_0$  at the present time. For the current value of  $c_{EM}$  see section 5.4.

In following sections, we check this fit with different observations. We also look for any observational difference between the results of this model and the  $\Lambda$ CDM model.

### 5.3.1 The Hubble parameter with $\gamma(z)$

Using the fit in (5.23), here we study the Hubble function given in (5.7) which we use for our the modified model. As the model parameter is changed, compared to Figures 5.1 and 5.2, we expect a change in this parameter too.

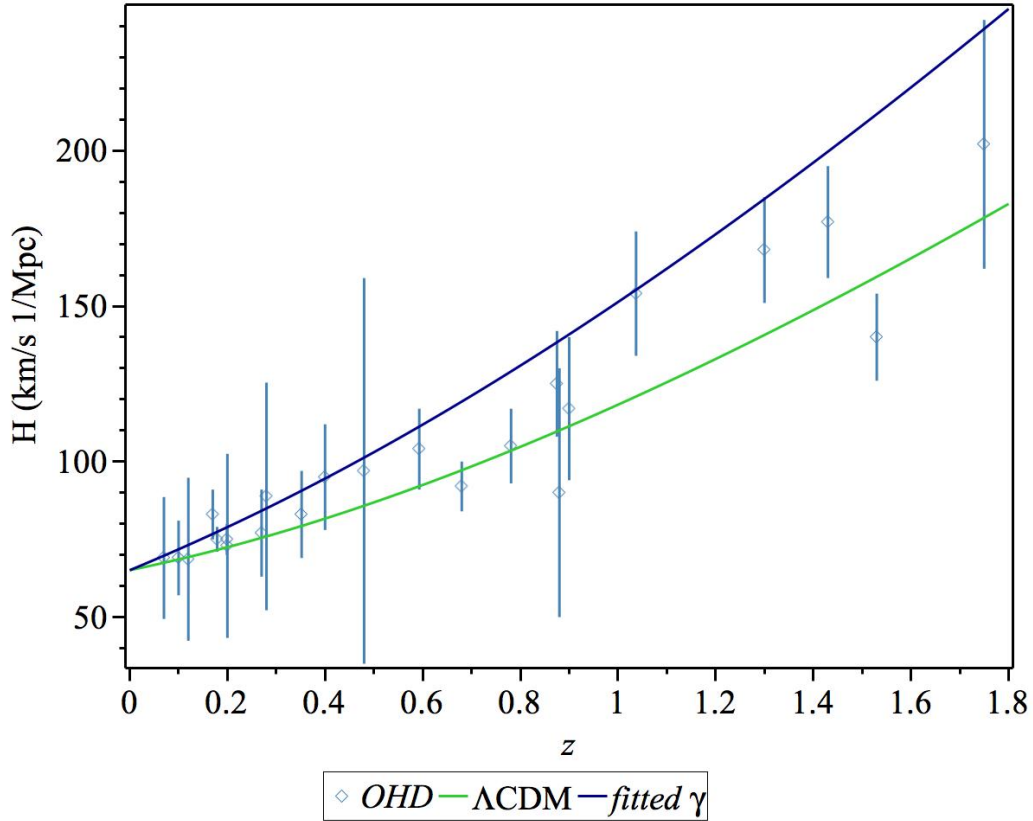


**Figure 5.11:** This plot shows the Hubble function for the  $\Lambda$ CDM model and also the modified model using the fit (5.23) which function gives  $H_0 = 65.0748 \text{ km s}^{-1} \text{ Mpc}^{-1}$ . For the observational data we used (Farooq & Ratra, 2013) (selected data from measurements of differential age method). These data points have been given in the redshift range  $0.070 < z < 1.750$ . Here one can see that the  $\gamma(z)$  function given in equation (5.23), results in an acceptable trend for the Hubble parameter.

Figure 5.11 shows that although the fitted  $\gamma(z)$  does not make Hubble parameter to be completely similar to  $\Lambda$ CDM model, it gets a similar trend and also, it is still following OHD. It is also way smaller than what is expected in the model with only matter, the Einstein de-Sitter model. Although we have not considered any Dark Energy here and we considered a matter dominated universe, this difference is made by the correction we put in the Lagrangian,  $\mathcal{L} = \mathcal{R} + F\mathcal{R}^{\mu\nu}\mathcal{R}_{\mu\nu}$ . This makes  $H_0 = 65.0748 \text{ km s}^{-1} \text{ Mpc}^{-1}$ , which is still in the Planck limits for the value of Hubble constant.

The  $\chi^2$  minimization test results in :  
 $\chi^2 = 51.0307$  ( $\chi_r^2 = 2.2187$ ) with  $\gamma(z)$  given in (5.23) for the Hubble function given in (5.7). Comparing with the values given in page 52, it is larger than what we see in the  $\Lambda$ CDM model,  $\chi_{\Lambda\text{CDM}}^2 = 16.0498$  ( $\chi_r^2 = 0.6978$ ). However, compared to the model presented with constant  $\gamma$ , it has an acceptable trend, meaning that it increases with redshift. This grows the support for a non constant  $\gamma$ . We study the effect of this new fit more in the following sections.

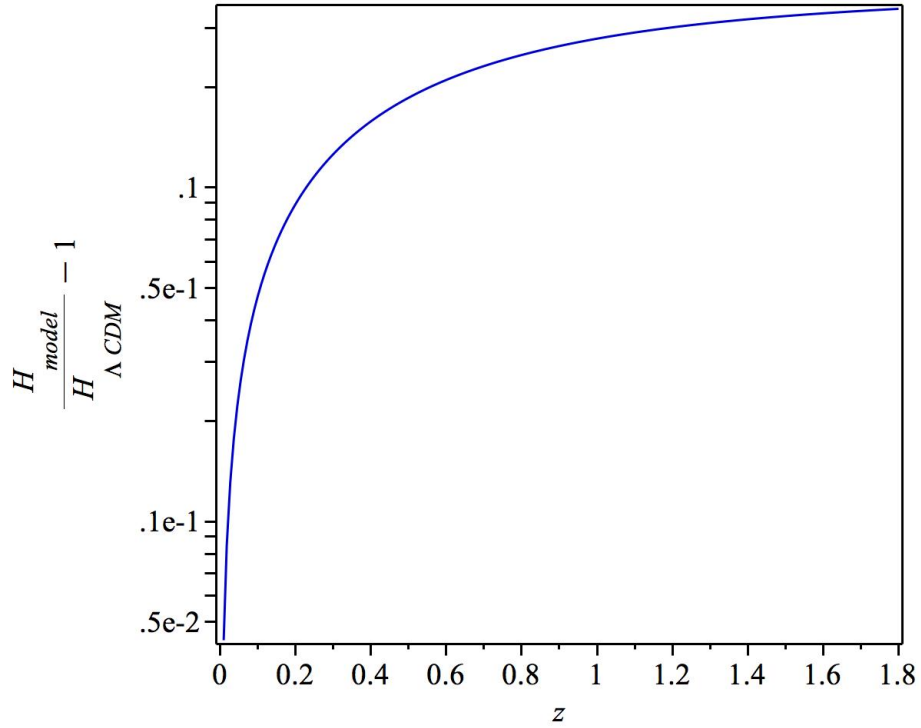


**Figure 5.12:** Here  $H_{\text{model}}(z)/(H_{\Lambda\text{CDM}}(z)) - 1$  is plotted vs. redshift, in which the  $H_{\text{model}}(z)$  is plotted for the  $\gamma(z)$  function given in (5.23). As seen in the plot, the relative difference increases with redshift. As the observational data given in (Farooq & Ratra, 2013) (selected data from measurements of differential age method) are in the redshift range  $0.070 < z < 1.750$ , we plot the relative difference in this redshift range.

The relative difference of  $\Lambda$ CDM model and modified model for the  $\gamma(z)$  is given in Figure 5.12. This relative difference increases with the redshift.

### 5.3.2 The distance modulus of SN Ia with $\gamma(z)$

In page 61, we fitted the function  $c_{ST}/H$  which has the dimension of length, with  $c_0/H_{\Lambda\text{CDM}}$ . This fit which is taken from equation (5.22), can be used to get the correct distance. Finally, using equation (5.17), the distance modulus is shown in Figure 5.13.

This Figure, clearly shows that compared to a constant  $\gamma$ , using the fitted  $\gamma(z)$ , makes the distance modulus of the modified model more similar to the standard model. Of course as we fitted the model parameter using equation (5.22), we expected this good agreement. The distance modulus increases with redshift and of course has similar trend compared to the  $\Lambda\text{CDM}$  model.

For this function,  $\chi^2 = 940.5452$  ( $\chi_r^2 = 1.6216$ ); which is of course in good agreement with the  $\Lambda\text{CDM}$  model, with  $\chi^2 = 936.8010$  ( $\chi_r^2 = 1.6152$ ).

The relative difference between these two models is plotted in Figure 5.14.

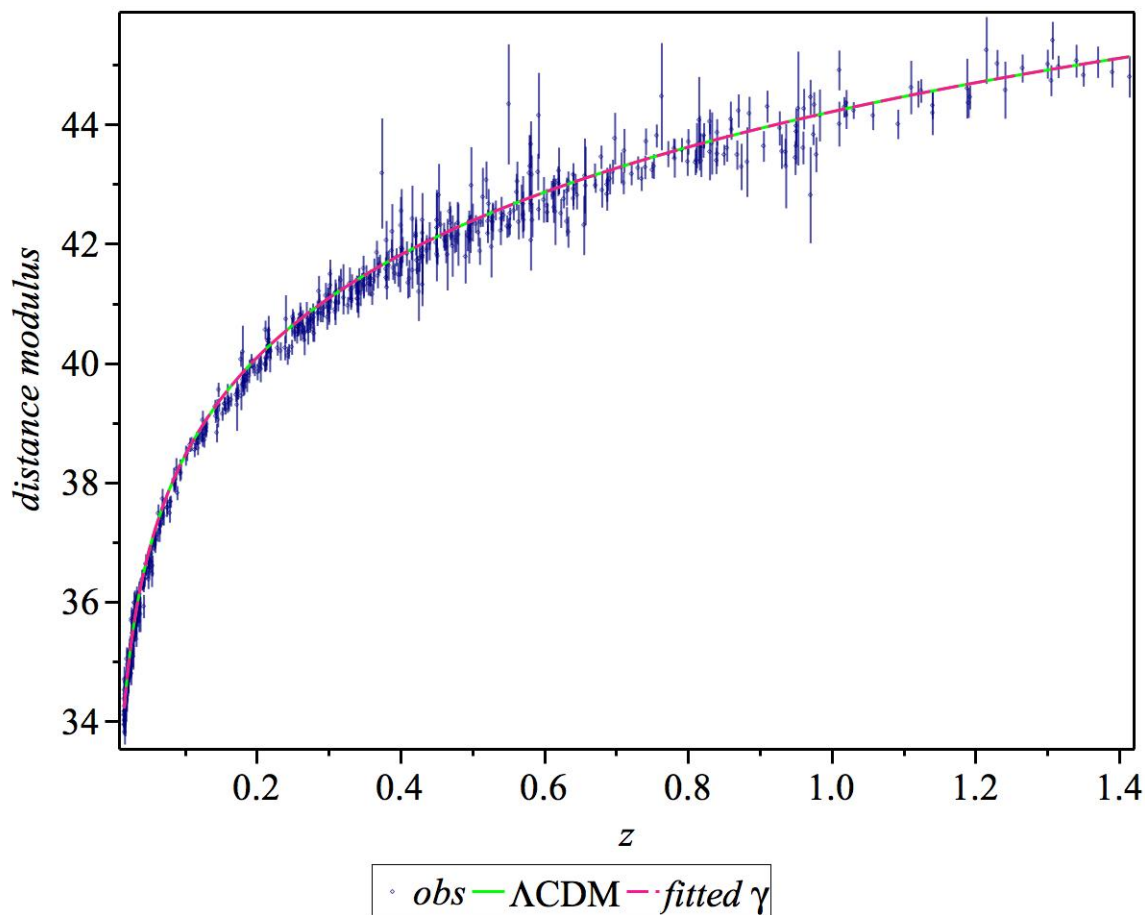


**Figure 5.13:** SN distance modulus for the model parameter (5.23). Observational points are taken from (Suzuki & et. al., 2012). As it was expected and also it can be seen from this plot, the the modified model is in good agreement with the  $\Lambda\text{CDM}$  model.

As it is illustrated in Figure 5.13, the relative difference between the distance modulus of the

modified model and  $\Lambda$ CDM model is decreasing with redshift. This is unlike what is seen in for instance Figure 5.5 for a constant  $\gamma$ . This shows the more the redshift increases, the less difference between the two models we have and they agree with each other better in terms of the distance modulus.

As it is shown in Figure 5.14, using  $\gamma(z)$  from equation (5.22) the difference between the distance modulus of the model and the  $\Lambda$ CDM model is smaller than when using a constant  $\gamma$ .

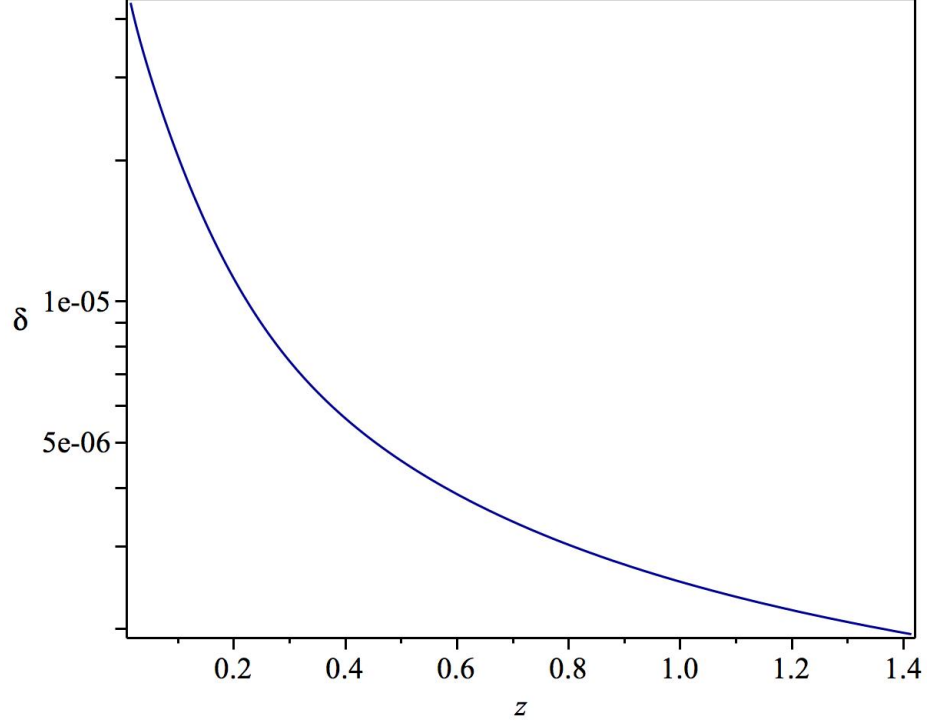


**Figure 5.14:** Here  $|1 - \mu_{\text{model}}/\mu_{\Lambda\text{CDM}}|$  is plotted for the fitted  $\gamma(z)$  solving equation (5.21). The relative difference between the distance modulus of the the modified model and the  $\Lambda$ CDM model decreases with redshift. Again, this shows that using the fitted  $\gamma(z)$ , the the modified model is in good agreement with the  $\Lambda$ CDM model.

### 5.3.3 The redshift drift with $\gamma(z)$

As stated in section 5.2.4, a constant  $\gamma$  cannot make an acceptable redshift drift function. This is clearly shown in Figure 5.8. Therefore, again using the  $\gamma(z)$  from equation (5.23), we plot the modified redshift drift of equation (5.20) in Figure 5.15.

Obviously, the fit for the model parameter  $\gamma(z)$ , works for the redshift drift as well. Because as stated before, if  $c_0/c_{ST} H^{\text{mod}} \rightarrow H^{\Lambda\text{CDM}}$  then the modified redshift drift follows the  $\Lambda$ CDM model. Again we used an observation time of  $\Delta t_0 = 30$  yr, for 20 quasars in total and signal to noise ratio of  $S/N = 2000$  for the simulated observational points and their uncertainties.

In Figure 5.15, redshift drift is plotted for both model : the modified model and the  $\Lambda$ CDM model.

As redshift drift has a very small value, the difference is not seen easily. As an example, the plot is zoomed in for  $1.01 < z < 1.06$ , which shows a difference between the two models. The relative difference is more clear and is shown in Figure 5.16.

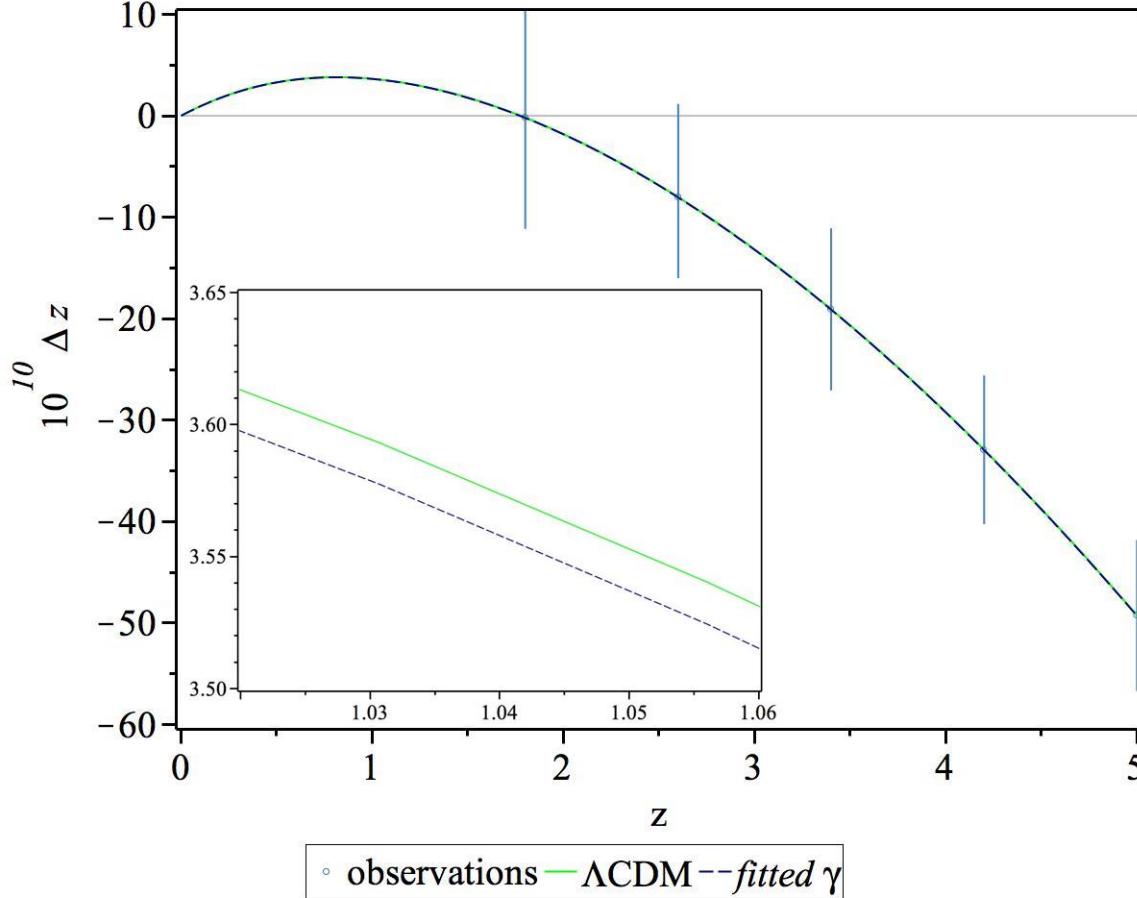


**Figure 5.15:** Comparing redshift drift for the modified model and the  $\Lambda$ CDM model, using the  $\gamma$  value (5.23). The error bars are the simulated errors from equation (2.22) taken from (Liske et al., 2008a). We considered  $\Delta t_0 = 30$  yr, for 20 quasars in total and  $S/N = 2000$ . One can see that again similar to the distance modulus, the  $\gamma(z)$  function results in an acceptable function for the redshift drift. The relative difference can be seen in Figure 5.16.

Figure 5.16 shows the relative difference between  $\Delta z_{\Lambda\text{CDM}}$  and  $\Delta z_{\text{model}}$ . The peaks seen here are due to the fact that  $\Delta z_{\Lambda\text{CDM}}$  vanishes at  $z = 0$  and  $z = 1.7760$ . This difference is mostly of the order of  $10^{-3}$  in this redshift range. This small difference shows that observationally we are not going to be able to distinguish between the  $\Lambda$ CDM model and the modified model used easily.

Here we note that a redshift drift crossing the  $\Delta z = 0$  line is a characteristic of models which have accelerated expansion. Unlike these models, models which only consider matter in their energy content, do not show this crossing feature. However, the model studied in this chapter

crosses this line although we only consider matter. This is in expense of considering a difference between different facets of the speed of light and also adding the geometric term  $F\mathcal{R}^{\mu\nu}\mathcal{R}_{\mu\nu}$  to the Lagrangian.

There are some differences between the  $\Lambda$ CDM model and this model:

The redshift drift of the  $\Lambda$ CDM model crosses the zero line at  $z = 1.7760$ . But this happens for the modified model at  $z = 1.7731$ . This is one of the characteristics of this model which can in principle be treated as an observational difference between this model and the  $\Lambda$ CDM model. However, similar to what we explained above, this observationally not easily achievable. After observing redshift drift, we can find the exact zero crossing redshift and then an acceptable redshift range for this zero crossing can be given.

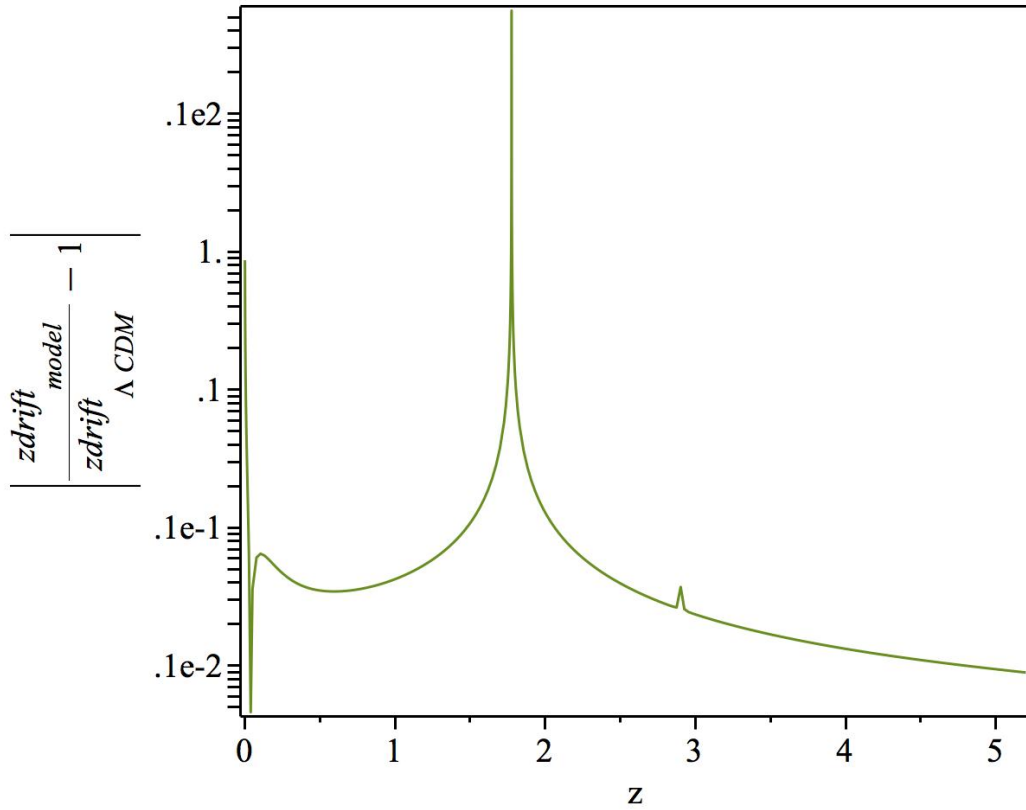


**Figure 5.16:** Here  $|\Delta z_{model}/(\Delta z_{\Lambda CDM}) - 1|$  is plotted vs. redshift. As expected and shown in Figure 5.15, the difference between the two redshift drifts is small (mostly of the order of  $10^{-3}$ ). For  $\Delta z_{model}$ ,  $\gamma(z)$  is used from equation (5.23). Both redshift drifts are plotted in Figure 5.15. The two peaks in this plot are the result of vanishing redshift drift.

The two redshifts,  $z = 0$  and  $z_{cross}$  are the two important redshifts of the redshift drift in future observations, which make  $z_{drift} = 0$ . On the other hand, there are more interesting differences between this model and the  $\Lambda$ CDM model regarding the change in the apparent velocity of the source. Following the steps in page 14, we know that considering two points  $p$  and  $p'$  with an

infinitesimal distance of  $\Delta l$  from each other, it takes

$$\Delta t = \frac{\Delta l}{c_{ST}} \quad (5.24)$$

for a signal from  $p'$  to arrive at  $p$ . And this results in

$$\Delta v = \frac{c_{ST} \Delta z}{1 + z} \quad (5.25)$$

which is the change in the apparent velocity of the source, when considering a difference between  $c_{ST}$  and  $c_0$ . Using this equation, here we plot  $\Delta v$  for different models in Figure 5.17.

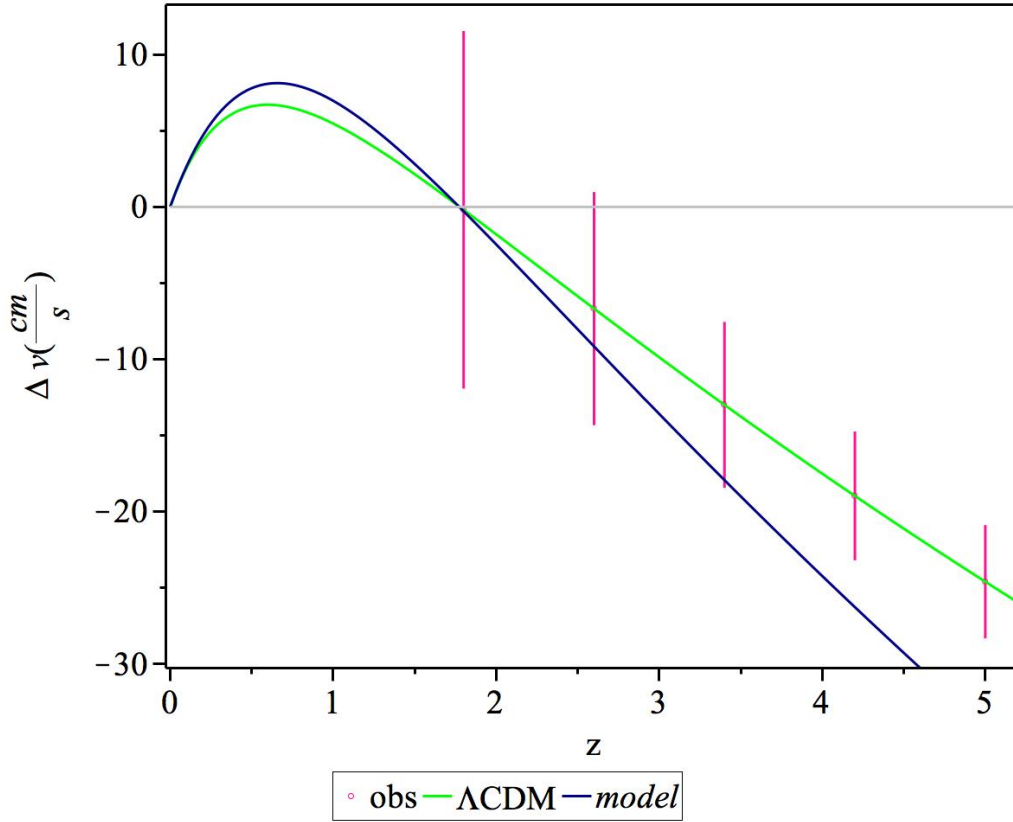


**Figure 5.17:**  $\Delta v$  vs.  $z$  for simulated data points,  $\Lambda$ CDM model and the modified model (5.25). The redshift drift of the the modified model has similar trend compared to the  $\Lambda$ CDM model, meaning that it shows an increase and then a decrease. However, in higher redshifts there is a difference between the the modified model and the  $\Lambda$ CDM model which does not match with the simulated observational points.

Figure 5.17, shows that there are clear differences between this model and the  $\Lambda$ CDM model for the change in the apparent velocity.

- Unlike the  $\Lambda$ CDM model, at  $z = 0$ , the shift of the velocity does not vanish and it gets the value  $\Delta v_{\text{model}} = 0.0002$ . Of course this difference can only be observed by non ground based observations which would also be able to detect the shift in redshifts smaller than 2.
- As stated before, the zero crossing redshift is different from  $\Lambda$ CDM model as well; for  $\Lambda$ CDM model it happens at  $z = 1.7760$  and for the modified model at  $z = 1.7731$ .
- For the  $\Lambda$ CDM model, the maximum happens at  $z = 0.5981$  which  $\Delta v = 6.7089 \text{ cm s}^{-1}$ , but this is  $z = 0.6568$  for the modified model and it makes  $\Delta v = 8.1297 \text{ cm s}^{-1}$ .
- Obviously, the  $\Delta v$  made by the modified model, does not go through the last two error bars predicted by equation (2.22) to the standard  $\Delta v$ . So when taking the error bars from this equation, there is a difference between the two models in higher redshifts.

The differences between the models which are stated above, are theoretically observable. However in practice, these can only be observed is we have suitable observational conditions.

## 5.4 Dynamics of the speed of electromagnetic waves

Until here, we studied possible dynamics of the causal structure constant and its effect on some of the related observations. In this section, we will focus on the speed of electromagnetic waves. The form of speed of electromagnetic waves ( $c_{EM}$ ) in the affine connection vanishing frame is given in the equation (4.62) (it is different from what is derived in (Izadi & Shojai, 2009)). As it can be seen, using this model,  $c_{EM}$  depends on the choice of  $\gamma$  and  $\omega$  which depend on the redshift. As stated before, we only focus the dynamics of different facets of the speed of light. Therefore, in order to fit our model with observations regarding the possible dynamics of the fine structure constant, we only consider the dynamics of  $c_{EM}$ ; i.e.  $\alpha_{EM}(z)/\alpha_0 - 1 = c_0/c_{EM}(z) - 1$ . Using the model explained in page 48, we plot  $c_{EM}$  for different random  $\gamma$  values to see the dependence of  $c_{EM}$  on both redshift and  $\gamma$ .

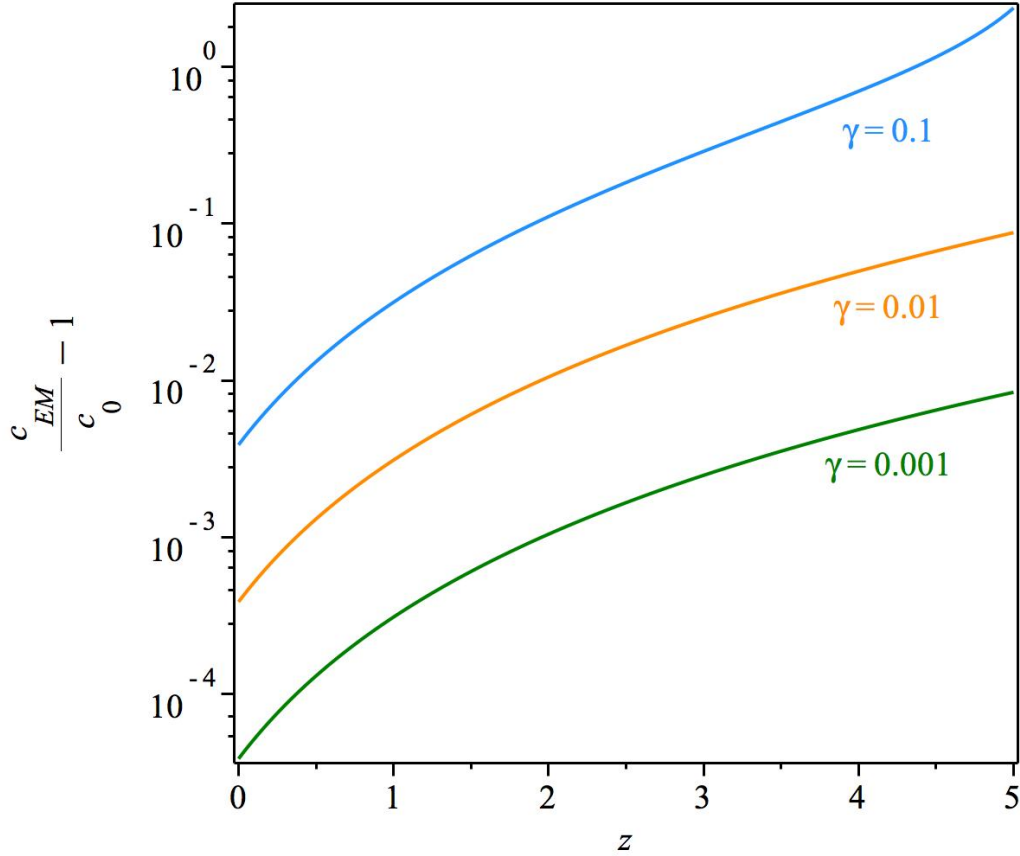


**Figure 5.18:**  $c_{EM}/c_0(z) - 1$  vs. redshift for different random values of  $\gamma$ . As one can see in the plot, the larger (smaller) the  $\gamma$  is, the larger (smaller) the relative difference is. The best value of  $\gamma$  regarding to  $c_{EM}$ , can be given using observational constraints.

Figure 5.18 shows  $c_{EM}$  for different values of  $\gamma$ . Obviously, for a constant value of  $\gamma$ ,  $c_{EM}$  increases with redshift. The larger  $\gamma$  is, the larger  $c_{EM}$  gets for each redshift. In the next sections we fit  $c_{EM}$  with different related observations.

It is worth mentioning that for the observational constraints, we only use the limit  $\alpha/\alpha_0 - 1 < 0$  which results in  $c_{EM} \geq c_0$ . This is because we are interested in an increasing  $c_{EM}$  with redshift for the the modified model.

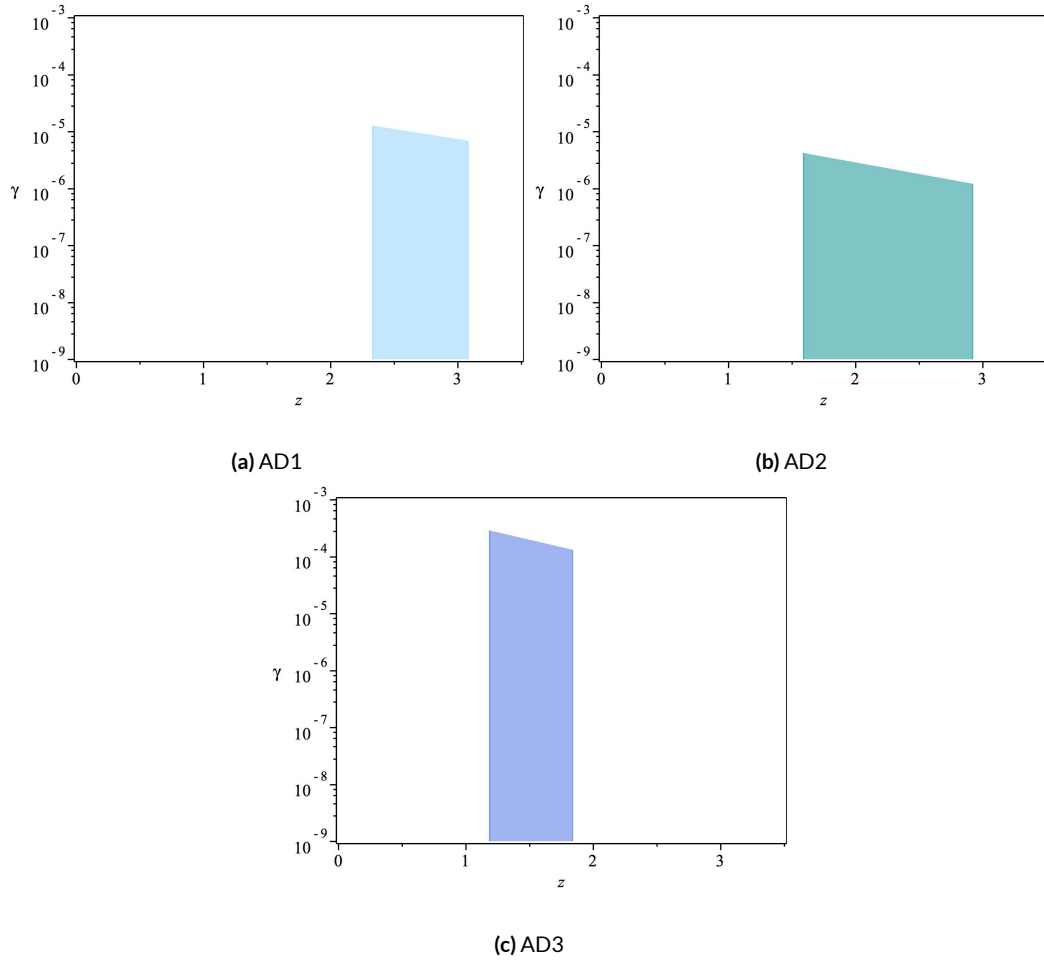
#### 5.4.1 The quasar absorption lines and $c_{EM}$

In order to fit the model parameter for the speed of electromagnetic waves in this model, we use equation (4.62). This is in principle, the same as  $c_{ST}$ . However, we do not prejudge the fittings and use constraints coming from the quasar absorption lines to fit  $c_{EM}$ .

In table 5.1, the model parameter  $\gamma$  is fitted with constraints coming from the quasar absorption lines given in table 3.1. These results are also shown in Figure 5.21.

Method	Redshift range	$\Delta\alpha/\alpha_0 (\times 10^{-5})$ , Ref.	$\gamma (\times 10^{-6})$
AD <sub>1</sub>	2.33 – 3.08	$-0.5 \pm 1.3$ , (Murphy et al., 2001b)	$0 < \gamma < 6.83$
AD <sub>2</sub>	1.59 – 2.92	$+0.15 \pm 0.43$ , (Chand et al., 2005)	$0 < \gamma < 1.20$
AD <sub>3</sub>	1.1862 – 1.8377	$-3.09 \pm 8.46$ , (Martínez Fiorenzano et al., 2003)	$0 < \gamma < 130.25$
MM <sub>1</sub>	0.4 – 2.3	$-0.06 \pm 0.06$ , (Chand et al., 2004)	$0 < \gamma < 0.86$
MM <sub>2</sub>	1 – 2.4	$0.04 \pm 0.23$ , (Murphy et al., 2016)	$0 < \gamma < 1.25$

**Table 5.1:**  $\gamma$  fits using the quasar absorption lines data given in table 3.1. Here  $\Delta\alpha/\alpha_0 = c_0/c_{EM} - 1$ . Different observational constraints result in different limits for the value of  $\gamma$ . All constraints presented here are also compatible with non-dynamical fine structure constant and  $c_{EM}$  respectively.



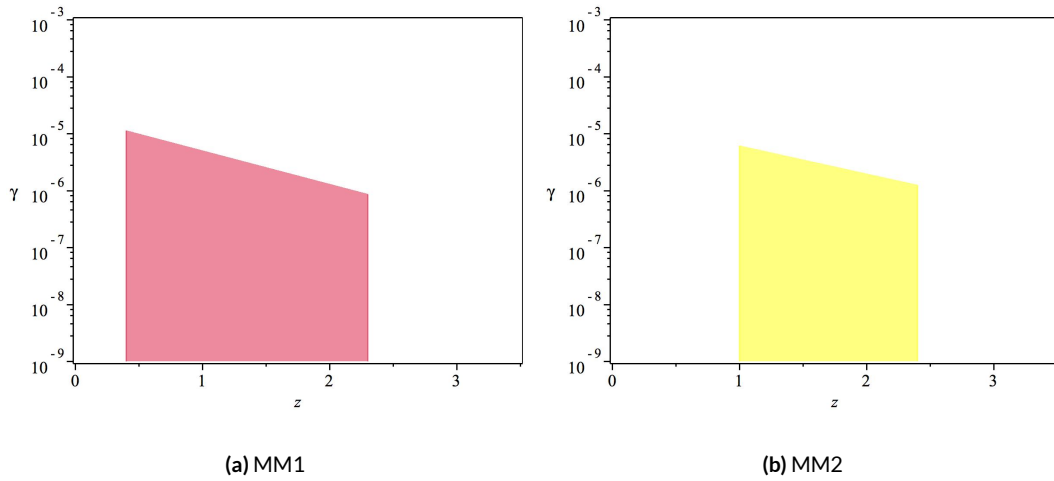
**Figure 5.19:**  $\gamma$  vs. redshift for the Alkali Doublet method, given in Table 5.1. In these fittings  $\gamma$  has been considered to be constant. All constraints here are also compatible with non-dynamical  $c_{EM}$ .

Table 5.1 shows different possible dynamics of  $c_{EM}$  for different methods. Also, we have calculated the allowed  $\gamma$  range for each test. As it is clear in this table, the redshift dependence of

$c_{EM}$ , results in different ranges for the model parameter,  $\gamma$ , in each redshift limit. This means for each redshift, there are unique maximum and minimum ranges for  $\gamma$ . In the “ $\gamma$ ” column, we reported the maximum and minimum range which can be used for all the redshift range. We do not consider negative values for  $\gamma$ , as in our model only positive  $\gamma$  values result in  $c_{EM}/c_0 \geq 1$  for  $z \geq 0$ .

According to Table 5.1, we conclude that one can find one range for  $\gamma$  to fit  $c_{EM}$  with all these data. This is the main reason we do not look for any other fit for the model parameter (unlike what we had to do for  $c_{ST}$ ). This table is also shown in Figures 5.19 and 5.20.

Figure 5.19 shows the  $\gamma$  fitting with AD method. The constraints coming from the AD method in Table 5.1, are consistent with no dynamics in  $c_{EM}$ .



**Figure 5.20:**  $\gamma$  vs. redshift for the Many Multiplet method, given in Table 5.1. In these fittings  $\gamma$  has been considered to be constant. All constraints here are also compatible with non dynamical  $c_{EM}$ .

Figure 5.19 shows the  $\gamma$  fitting with MM method. The constraints coming from the MM1 and MM2 in Table 5.1, are consistent with non dynamical  $c_{EM}$ .

As a constant  $\gamma$ , is valid for these observations, unlike what we did for the causal structure constant, we do not go further and consider a redshift dependent  $\gamma$ . All plots from Figures 5.19 and 5.20 are shown in Figure 5.21 together to show the overlap of the possible  $\gamma$  values in each redshift.

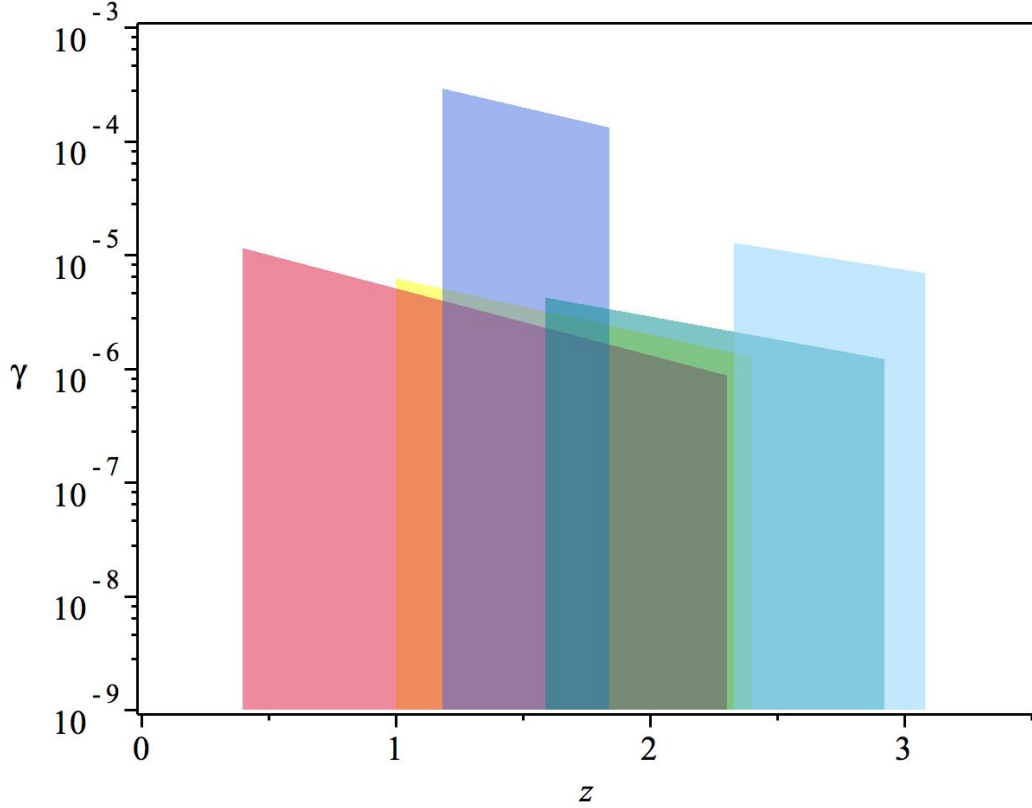


**Figure 5.21:** The model parameter  $\gamma$  vs. redshift for data in Table 5.1. This plot shows all plots in Figures 5.19 and 5.20 together. As it can be seen here, all these ranges overlap, so one can choose a single value to be consistent with all these constraints.

Obviously from Figure 5.21, one can choose one value for the model parameter  $\gamma$  in the shown redshift range and still confirm the quasar absorption lines observations; eg.  $\gamma = 7 \times 10^{-7}$ .

### 5.4.2 Comparing the dynamics of $c_{ST}$ and $c_{EM}$

The model we study in this thesis, which was presented in chapter 4, develops the claim that there are fundamental differences between different notions of the speed of light. We will check this claim in this section numerically.

As it is expressed in the last section, the presented data suggests that in order to show the value of  $c_{EM}$ ,  $\gamma$  can be a constant value and in principle does not have to have dynamics. Choosing a relevant value for  $\gamma$ , here we study the difference between the values of  $c_{ST}$  and  $c_{EM}$ . We have already fitted their values with different observations and it is interesting to see how different they are in a framework which considers a deep difference between them.

Figure 5.22 compares these two different facets of the speed of light,  $c_{ST}$  and  $c_{EM}$ .

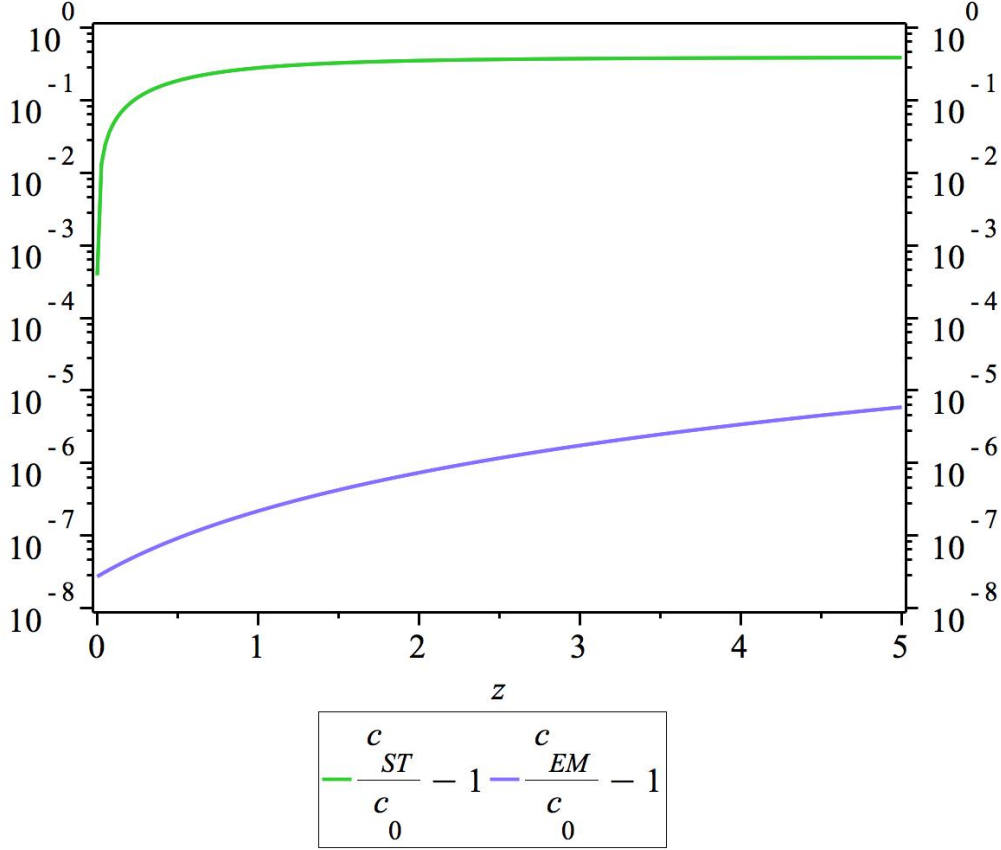


**Figure 5.22:**  $c_{ST}/c_0 - 1$  and  $c_{EM}/c_0 - 1$  vs. redshift. For  $c_{ST}$ , we used  $\gamma(z)$  from equation (5.23) which is in agreement with causal structure constant related observations that we have studied before. For  $c_{EM}$ , we used  $\gamma = 7 \times 10^{-7}$  which agrees with the constraints coming from quasar absorption lines. This is only one choice and as it is shown in Figure 5.21, there can be a lot of other choices (also  $\gamma = 0$ ). Using the values mentioned above for the model parameter, one can see that  $c_{ST}$  is larger than  $c_{EM}$ .

In Figure 5.22, we used  $\gamma(z)$  from equation (5.22) for  $c_{ST}$  and  $\gamma = 7 \times 10^{-7}$  for  $c_{EM}$ . This value of  $\gamma$  is acceptable in this redshift range according to the fitting in Figure 5.21. Smaller (larger) values of  $\gamma$  lead to smaller (larger) values for  $c_{EM}$  in each redshift.

There are several interesting features shown in this Figure.

First, obviously after fitting the two facets  $c_{ST}$  and  $c_{EM}$  with observations, this model results in two completely different values and dynamics. Although we have taken these two facets to be potentially different from each other, at the end after fitting with observations, they could have been similar. But as we see here, this is not the case and the difference is of several orders of magnitude.

In addition, we always have  $c_{ST} > c_{EM}$ . As the speed of gravitational waves is constant in this model, one can conclude that in general  $c_{ST} > c_{EM} \geq c_{GW}$  in each redshift; meaning that the causal structure constant is the limiting speed in this model.

## 5.5 Speed of gravitational waves

We start this section with repeating these questions: In standard  $\Lambda$ CDM model there is no difference between the speed of gravitational waves and electromagnetic waves. But do these two facets of the speed of light really coincide? If not, what are the consequences of this non equality?

Typically, the measuring tool in cosmological observations is light. However, using gravitational waves, we can broaden our knowledge about the universe and observe sources which are not electromagnetically detectable.

On the other hand, in the model presented and fitted here, unlike the speed of electromagnetic waves, the speed of gravitational waves is constant over redshift (or time). This constancy can make a good tool out of these waves in order to measure distances, as there is no need to do fitting for these waves in this model.

The observations of gravitational waves done by the LIGO team, are still quit new. These fascinating observations, opened a new door to us to see the unseen parts of the universe. In short terms, by detecting gravitational waves and measuring their altitude and frequency, the chirp mass is measured and then the so called luminosity distance of the source is determined. From this distance, the redshift of the source is also calculated. Let us call the distance measured by gravitational waves,  $r_g$ ,

$$r_g = (1 + z) \int_0^z c_{GW} \frac{dz}{H_{\Lambda\text{CDM}}} \quad (5.26)$$

in which  $c_{GW} = c_0$  and  $H_{\Lambda\text{CDM}}$  is the Hubble parameter of the  $\Lambda$ CDM model. However, in a non standard model such as the one we discussed here, the luminosity distance is dealing with  $c_{ST}$ , which comes from the line element. Moreover as  $c_{ST}$  is varying here, we need to use the luminosity distance from equation (5.16),

$$d_L = (1 + z) \int_0^z c_{ST} \frac{dz}{H}. \quad (5.27)$$

Here  $c_{ST}$  is the causal structure constant and  $H$  is given in (5.7). Although the model is fitted by the  $\Lambda$ CDM model, this makes a difference between the distance measured by the gravitational waves and the usual luminosity distance coming from  $c_{ST}$ . This difference can be in principle used to study the validity of the  $\gamma$  fitted for the  $c_{ST}$  or in general the validity of this model.

Again we emphasis here that in standard theory both these facets coincide. And the price of excluding the cosmological constant from the theory and adding geometric correction, is to modify distances and measurements.

Figure 5.23 shows the difference between  $r_g$  and  $d_L$  given in equations (5.26) and (5.27) as a function of redshift.

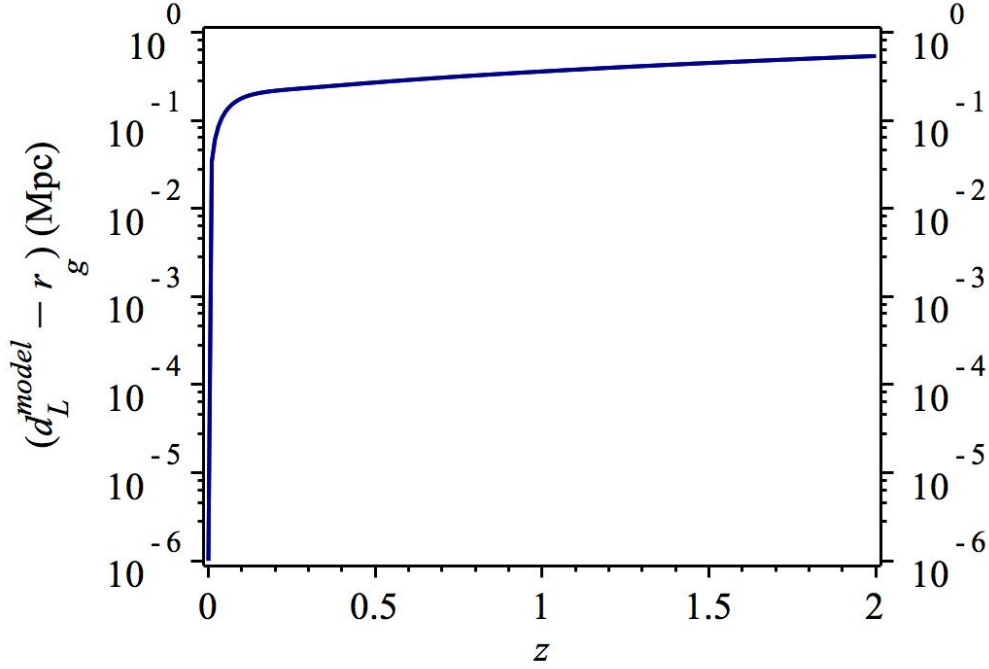


**Figure 5.23:**  $(d_L^{\text{model}} - r_g)$  (Mpc) as a function of  $z$ . As it is clear in this plot, the difference is small in  $z \simeq 0$  and it is increasing with redshift.

The difference between the distance measured by gravitational waves ( $r_g$ ) and the luminosity distance for the fitted model is shown in Figure 5.23. Of course for both models the distance vanishes at  $z = 0$ . As it is clear in this figure, this difference is increasing with redshift. It shows that by the fitting we did in equation (5.22), the model gives a slightly larger distance compared to  $\Lambda$ CDM model. Let us study this difference in detail for the first LIGO observation of the black hole merger and see if it is detectable.

For this detection (the so called GW150914 event), they determined that the luminosity distance of the black hole merger is  $410_{-180}^{+160}$  Mpc, which we call  $r_g$ , meaning the distance calculated with gravitational waves. Using the values of (Planck Collaboration et al., 2015), we determine that the redshift of this merger determined from  $r_g$ , is  $z = 0.08_{-0.04}^{+0.03}$ . But using the modified model presented before, we know that the luminosity distance is related to space time measurements and it consists of  $c_{\text{ST}}$  which is not constant (equation (5.16)). Using the redshift ranges which we got from  $r_g$ , the luminosity distance in the  $\mathcal{L} = \mathcal{R} + F^{\mu\nu}\mathcal{R}_{\mu\nu}$  model within an affine vanishing frame, gets  $d_L = 410.17_{-180.08}^{+160.00}$  Mpc. Therefore, we can conclude that within today's precision reported by LIGO, the difference is not detectable. However, in principle this is an observational difference which should be detectable if the observation's precision increases. Basically, if the difference is not within the detection, either the fit has to change or the model is ruled out.

We have done this calculations for all three LIGO and also the recent LIGO-Virgo observations. The results can be seen in Table 5.2.

Event	Reported distance (Mpc)	Predicted redshift	Model's predicted distance (Mpc)
GW150914 (Abbott et al., 2016b)	$410^{+160}_{-180}$	$0.08^{+0.03}_{-0.04}$	$410.17^{+160.00}_{-180.08}$
GW151226 (Abbott et al., 2016a)	$440^{+180}_{-190}$	$0.09^{+0.03}_{-0.04}$	$440.17^{+180.02}_{-190.05}$
GW170104 (Abbott et al., 2017b)	$880^{+450}_{-390}$	$0.17^{+0.08}_{-0.07}$	$880.21^{+450.02}_{-390.03}$
GW170817 (Abbott et al., 2017c)	$40^{+8}_{-14}$	$0.0086^{+0.0103}_{-0.0030}$	$40.03^{+8.00}_{-14.01}$

**Table 5.2:** Comparing the distances reported by LIGO and by the model studied in this chapter. The reported luminosity distance is the one reported by LIGO which is derived using the properties of the gravitational waves. Using this luminosity distance and considering the  $\Lambda$ CDM model, we gain the redshift of the source. The modified luminosity distance of the model, gives us the distance given by the model.

As it is clear here, for a larger redshift, the difference between the standard and the modified model increases. However, with today's precision, this difference is of no interest or importance.

Table 5.2 shows different observations of gravitational waves done by LIGO and Virgo. Taking the distance from the properties of the gravitational waves that LIGO received, the redshift of the source is calculated and then the luminosity distance is determined. Among all the events shown in Table 5.2, the GW170817 event is different in two aspects. First, this event is the nearest one to us; which means it happened in a much smaller redshift. This results in a smaller difference between the standard model and the modified one, that is practically harder to detect. Second, it involves an electromagnetic counterpart; which means it can be used to constrain the speed of electromagnetic waves with respect to  $c_{GW}$  in this redshift. This will be explored more in the next section.

The difference between  $c_{ST}$  and  $c_{GW}$  is one of the interesting features of this model. Although in standard theory, one considers the gravitational waves to move with the causal structure constant, in this model there is a difference between these two. In standard theory, we know gravitational waves as the ripples of the space time, which move with the same speed as  $c_{ST}$ . But here the speed of the causal structure becomes different than the speed with which these ripples move. By using the model discussed in this thesis, the degeneracy between these two concepts is broken. This difference increases with redshift and can be seen in Figure 5.24.

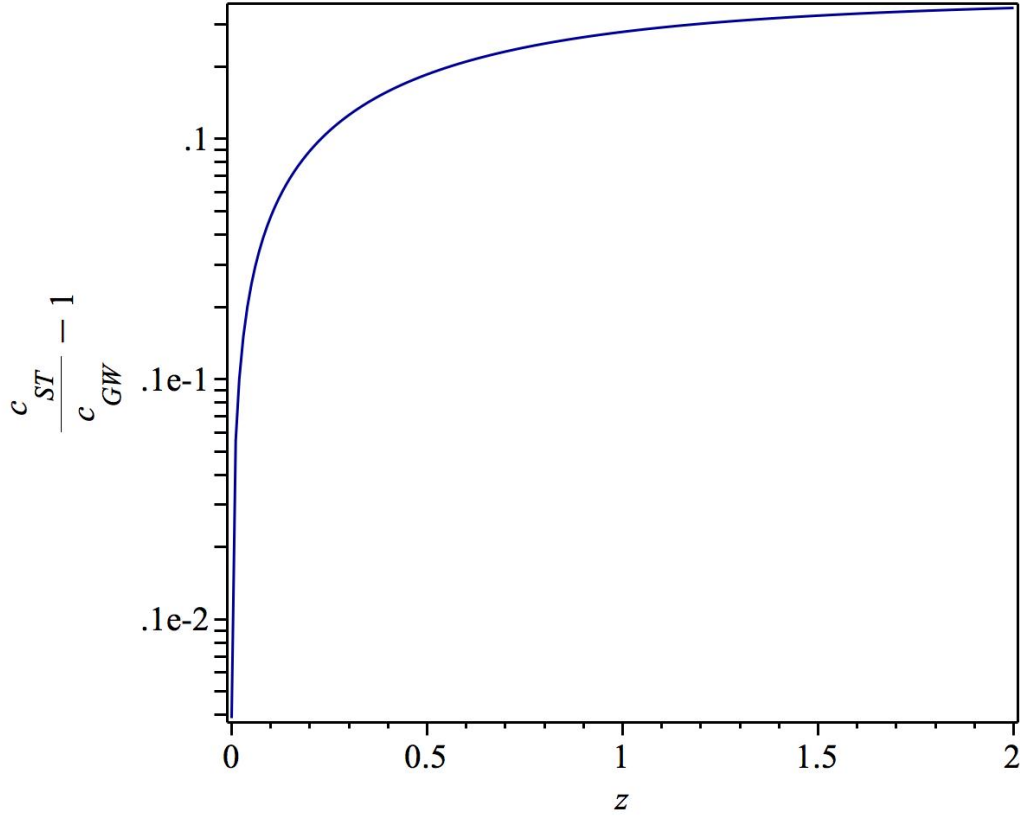


**Figure 5.24:**  $c_{ST}/c_{GW} - 1$  as a function of  $z$ , which is increasing with redshift. According to what stated earlier in section 4.4.4,  $c_{GW}$  is constant in this model. Using the fit in (5.22),  $c_{ST}/c_{GW}|_{z=0} - 1 = 3.88 \times 10^{-4}$ . Here we have plotted the relative change if this facet of the speed of light to the causal structure constant.

Clearly, the difference between  $c_{ST}$  and  $c_{GW}$  increases with redshift; this means when going back in time considering this model in Palatini formalism, there is a much noticeable difference between these two facets of the speed of light. The speed of gravitational waves on the other hand, has always been constant. Thus, it does not need to be fit with any observations and can be a good tool for measuring distances.

### 5.5.1 Constraints on $c_{EM}$ using gravitational wave observations

As stated before, the model presented in this chapter does not result in a dynamical speed of gravitational waves,  $c_{GW}$ . However, it shows a possibility to have a difference between  $c_{GW}$  and  $c_{EM}$ . Here we present some recent attempts to put constraints on these two.

Obviously, the speed of electromagnetic waves, cannot be constrained using only gravitational wave observations unless there is an electromagnetic counter part observed. Fortunately, the fourth GW event mentioned in Table 5.2, has an electromagnetic coalescence (Abbott et al., 2017c). A time delay of  $+1.74 \pm 0.05$  seconds has been reported (Abbott et al., 2017a) which

can in principle be used to put constraints on the difference between the speed of electromagnetic waves and gravitational waves <sup>6</sup>. Then assuming that in our model  $c_{GW} = c_0$ ,

$$\begin{aligned} \frac{\Delta c}{c_{EM}} &= \frac{c_{GW}}{c_{EM}} - 1 \\ &= \frac{\Delta t c_0}{D} \end{aligned} \quad (5.28)$$

in which  $D$  is the distance the waves had to travel,  $\Delta c = c_0 - c_{EM}$  and  $\Delta t = t_{EM} - t_{GW}$  is the time difference between the arrival of electromagnetic and gravitational waves <sup>7</sup>. Following the steps in (Abbott et al., 2017a), which considers the distance ( $D = 26$  Mpc), for the upper limit we consider both waves emitted at the same time. For the lower limit, we consider the electromagnetic waves to be emitted 10 s before the gravitational waves (again as the bound similar to (Abbott et al., 2017a)). This way we get to

$$-3.1053 \times 10^{-15} \leq \frac{\Delta c}{c_{EM}} \leq +6.6888 \times 10^{-16}, \quad (5.29)$$

which is also compatible with no difference between  $c_{EM}$  and  $c_{GW}$ . Using this bound and also knowing the redshift of the source given in Table 5.2, we can put constraints on the model parameter,  $\gamma$ , related the speed of electromagnetic waves. Fitting the model, while knowing that  $c_{GW} \leq c_{EM}$ , we get to  $0 \leq \gamma \leq 7.8682 \times 10^{-14}$  which holds for  $z = 0.0056$ .

---

<sup>6</sup>A likely explanation for this time delay is related to the production of the Gamma rays.

<sup>7</sup>Equation 5.28 is different from the one in (Abbott et al., 2017a) used to constraint these two facets of the speed of light ( $\Delta c/c_{EM} = \Delta t c_{EM}/D$ ).

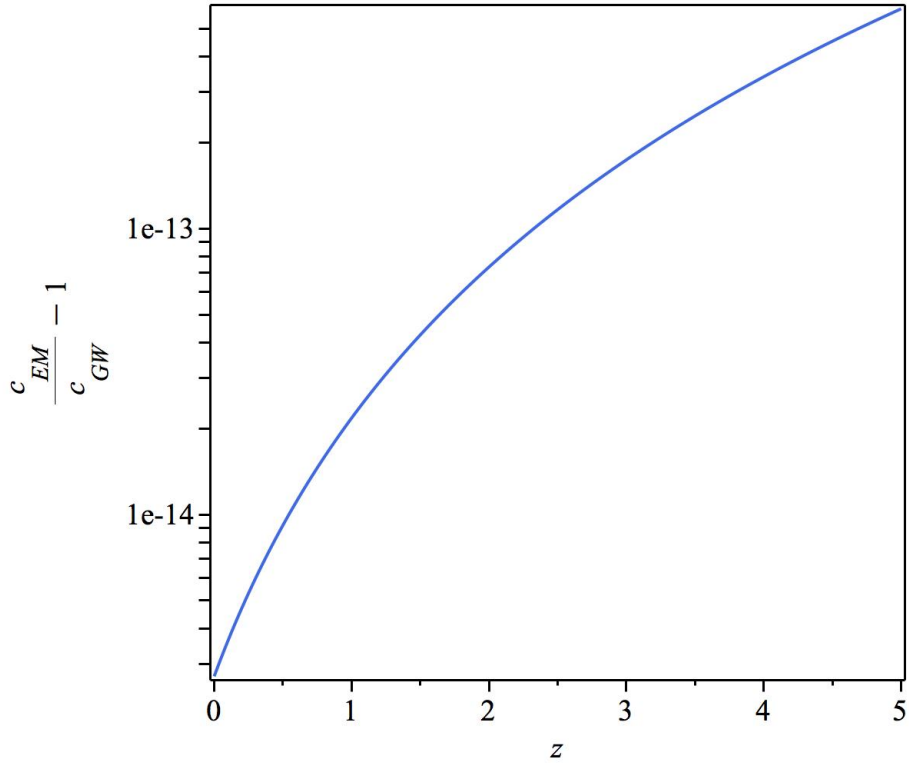


**Figure 5.25:**  $c_{EM}/c_{GW} - 1$  as a function of  $z$  for  $\gamma = 7 \times 10^{-14}$  in  $c_{EM}$ . As shown before,  $c_{GW}$  is constant in this model. Smaller (larger) values of  $\gamma$ , result in smaller (larger) dynamics of course.

Figure 5.25 show the relative change of  $c_{EM}$  for  $\gamma = 7 \times 10^{-14}$ . This  $\gamma$  value has been set by fitting  $c_{EM}$  using the fourth LIGO event. Smaller values of  $\gamma$  would of course result in smaller relative difference, which is compatible with observations.

All results for the fitting of  $c_{EM}$  are gathered in Figure 5.26. Obviously, if we want to choose a non varying model parameter  $\gamma$  for the model,  $\gamma = 0$  agrees with observations, which is compatible with a non varying  $c_{EM}$  in this redshift range.

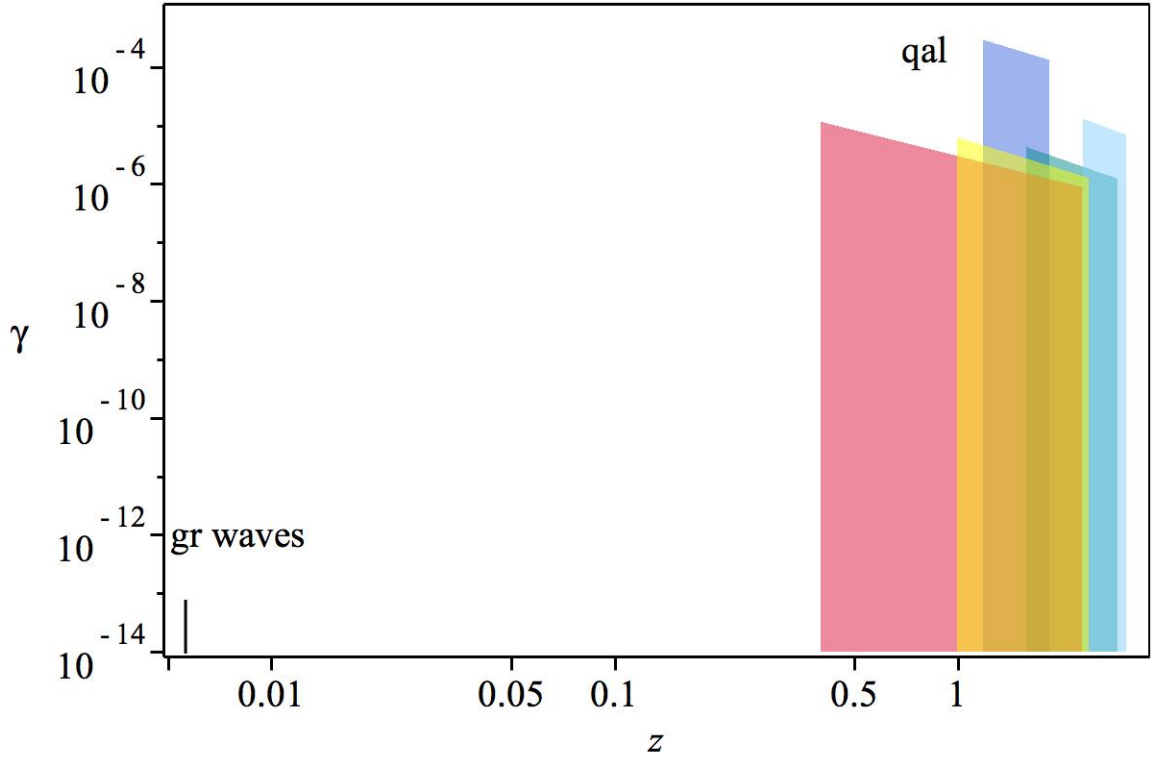


**Figure 5.26:**  $\gamma$  vs. redshift for quasar absorption lines data and LIGO-Virgo results. The line on the left hand side shows the result from the LIGO-Virgo observations at  $z = 0.0056$  and the colored bars on the right hand side show the result from the quasar absorption lines.

## 5.6 Summary

In this chapter, we investigated observational constraints on different facets of the speed of light. It was shown that assuming a Palatini geometry in an affine connection vanishing frame, the correction  $F\mathcal{R}^{\mu\nu}\mathcal{R}_{\mu\nu}$  generates an obvious difference between the values of  $c_{ST}$ ,  $c_{EM}$  and  $c_{GW}$ . The causal structure constant ( $c_{ST}$ ), which carries the concept of causality and is related to the expansion of the universe and length measurements, gets the largest value in each redshift. Light on the other hand, travels with  $c_{EM}$  which can possibly differ from  $c_0$ . However, all observations used here also agree with non dynamical  $c_{EM}$ . Finally, gravitational waves travel with constant speed,  $c_0$ . Current results of this thesis validates the view that difference facets of the speed of light can in principle be different from each other. All these different values and dynamics show that the model parameter has to be different for each facet. This is also shown in Table 5.3.

Related facet	Observations	Model parameter	redshift range	section
$c_{ST}$	SN Ia redshift drift	varying	0 – 1.414	5.3.2
		varying	0 – 5	5.3.3
$c_{EM}$	quasar absorption lines LIGO-Virgo	eg. $7 \times 10^{-7}$	0.4 – 3.08	5.4.1
		eg. $\sim 10^{-14}$	0.0086	5.5.1
$c_{GW}$	LIGO	0	0.0086	5.5
		0	0.08	
		0	0.09	
		0	0.17	

**Table 5.3:** Possible dynamics of different facets of the speed of light, given by different observations. As it is summarized here, we need different dynamics for each facet of the speed of light. For the model parameter column for  $c_{EM}$ , we chose one value for  $\gamma$  from the allowed limit.

Table 5.3 shows three different notions of the speed of light and observations which can put constraints on their dynamics.

According to observations,  $c_{ST}$  must be varying with the use of a dynamical model parameter (equation (5.22)). This makes  $(c_{ST}/c_0)|_{z=0} - 1 = 3.8818 \times 10^{-4}$  and  $H_0 = 65.0748 \text{ km s}^{-1} \text{ Mpc}^{-1}$ .

For  $c_{EM}$ , according to data resulting from the quasar absorption lines observations, we chose  $\gamma = 7 \times 10^{-7}$  as a suitable value in  $0.4 < z < 3.08$ . Also, according to LIGO-Virgo observations,  $\gamma$  can be chosen as  $0 \leq \gamma \leq 7.8682 \times 10^{-14}$  in  $z = 0.0056$ .

$c_{GW}$  on the other hand, is constant which agrees with this model and also with observations.

Figure 5.27 summarizes all results for the model parameter regarding the causal structure constant and the speed of electromagnetic waves.

Figure 5.27 shows the model parameter in terms of redshift for  $c_{EM}$  and  $c_{ST}$ . As it is shown here, there is a possible range for  $\gamma$  of  $c_{EM}$  in this redshift range; which is of orders of magnitude different from the  $\gamma(z)$  which should be taken for  $c_{ST}$ .

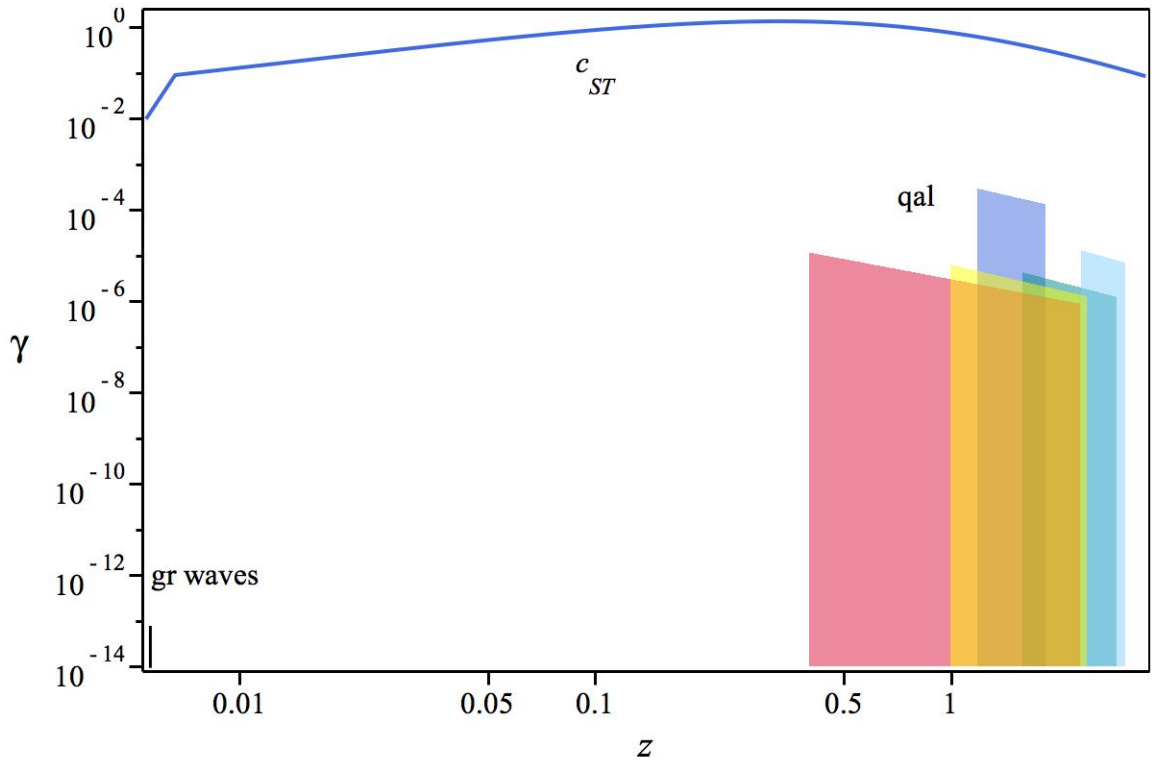


**Figure 5.27:**  $\gamma$  vs. redshift taken from SN distance modulus (for  $c_{ST}$ ), quasar absorption lines data and LIGO-Virgo results (for  $c_{EM}$ ). Again the single line on the left shows the result from the LIGO-Virgo observations at  $z = 0.0056$ . One can choose a single value for  $\gamma$  ( $\sim 10^{-14}$ ) for  $c_{EM}$ , except for the single redshift of MM2.

As it is shown in Figure 5.28, the dynamics of  $c_{ST}$  and  $c_{EM}$  are quite different. These dynamics are coming from the constraints on the model parameter shown in Figure 5.27.

At the end, we remind that the model we studied in this chapter, has only been fitted in cosmological scales. Therefore, the large  $F$  in the quadratic model considered here does not necessarily show conflict of this model with local gravity tests, in which a much smaller coupling constant is expected. In local scales, the effective gravitational theory could be very different from the one relevant to cosmic scales (Izadi et al., 2017). In other words, scales other than cosmological ones which have been studied here, have to be studied separately.

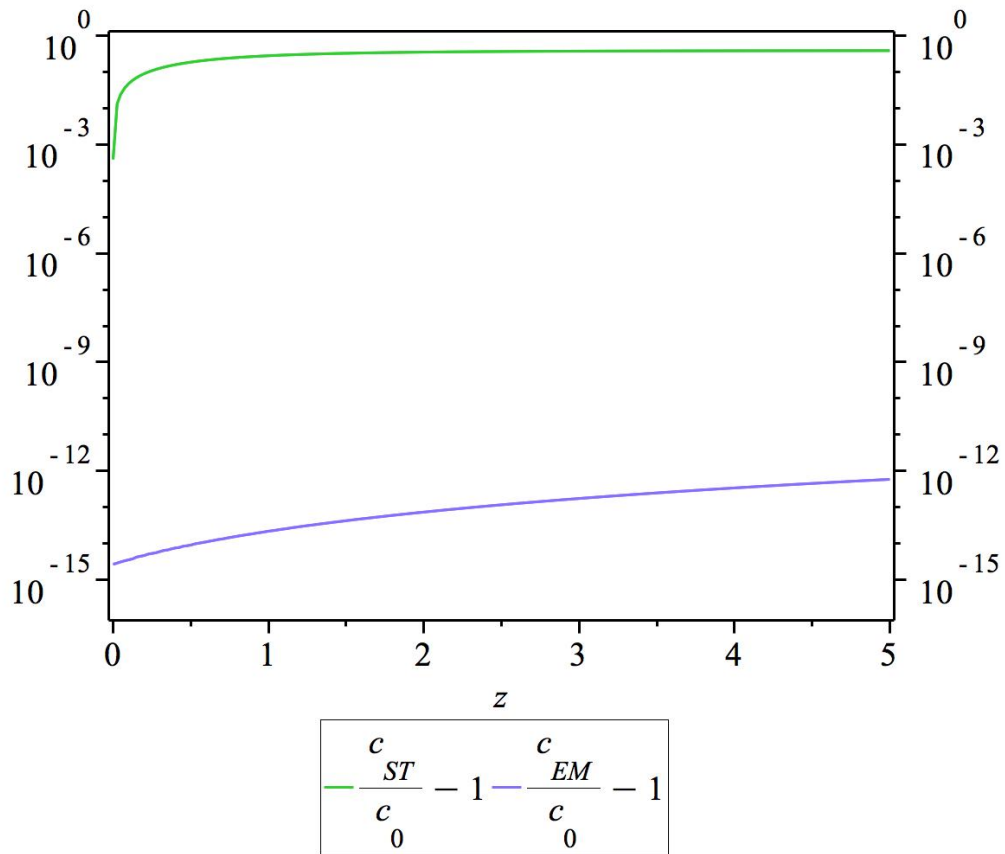


**Figure 5.28:**  $c_{ST}/c_0 - 1$  and  $c_{EM}/c_0 - 1$  vs. redshift. For  $c_{ST}$ , we used  $\gamma(z)$  from equation (5.22) which fits with the SN data. For the  $c_{EM}$ , we used  $\gamma = 7 \times 10^{-14}$  which fits with gravitational waves and quasar absorption lines data (except MM2). As it can be seen here,  $c_{ST}$  is always larger than  $c_{EM}$  in each redshift.

# 6

## Conclusion and outlook

In recent years, the value and dynamics of the constants of our universe has perhaps become more puzzling than ever. The whole dynamical space time that Einstein encouraged us to use, makes us think there might be a connection between taking the constants of the nature as completely "constants" and "rigid" and using standard dynamical General Relativity (without cosmological constant) to explain our universe (see e.g (Damour, 2009)). Different theoretical and experimental attempts have been carried out to examine this possibility (e.g see (Magueijo, 2003; Murphy et al., 2001a; Uzan, 2004, 2011; Webb et al., 2001; Balcerzak & Dabrowski, 2014; Zhang & Meng, 2014)) Dynamical couplings and in particular dynamical speed of light can also used to look for solutions for some cosmological ambiguities, including the recent expansion of the universe. Moreover, speed of light itself is a puzzling subject of interest. In principle, this fundamental constant enters several different physical equations related to distinct origins and plays various roles; including the speed of electromagnetic waves and gravitational waves, which are physically of distinct nature (Ellis & Uzan, 2005).

On the other hand, thinking about the causal structure used in GR, one might notice that the standard metric formalism used in GR, is one of the least general geometric formalisms one can have on a manifold. Inspired by the EPS formalism (Fatibene & Francaviglia, 2012), we choose Palatini formalism which become different from the metric formalism when using a Lagrangian different than Einstein-Hilbert Lagrangian. It was shown that different facets of the speed of light can become dynamical in an affine connection vanishing frame in Palatini formalism (Izadi & Shojai, 2009).

Motivated by ideas above, we used a modified gravity model in Palatini formalism which directly results in dynamics of the speed of light in an affine connection vanishing frame. We aim for putting constraints on the dynamics of different notions of the speed of light. In addition,

we examine the effect of a dynamical causal structure constant (as one of the different notions of speed of light) on the universe's recent acceleration.

Meanwhile, as being interested in studying the possibility of eliminating the cosmological constant with geometric terms, we consider a pure matter dominated universe for the recent time.

The results of this study are summarized and listed below:

- Using the  $f(\mathcal{R}^{\mu\nu}\mathcal{R}_{\mu\nu})$  correction in Palatini formalism, the Hubble parameter is modified. This new Hubble parameter is used in our study and is consistent with Observable Hubble Data coming from differential age method.
- The causal structure constant has dynamics within redshift. It enters the line element and has a direct effect on length measurements. We used this to study the possibility of compensating the cosmological constant in the luminosity distance of SN Ia and also redshift drift.

Our results show that this dynamic is consistent with observations and the difference between dynamical causal structure constant and a cosmological constant cannot be detected. It was also shown that regarding the causal structure constant ( $c_{ST}$ ), a constant model parameter is not consistent and the model parameter shows also dynamics in time (or redshift).

- When using this model, there is a slight difference between the redshift drift of this model and the standard model. However, when translating this to the relative velocity, one finds much more difference between these two models. On the other hand, the observable is redshift drift and this validates the view that there is no observable difference available.
- Contrary to the standard gravitational model, possible dynamics for the speed of electromagnetic waves ( $c_{EM}$ ) is allowed in this modified model and confirmed by data.  $c_{EM}$  which has a different origin compared to  $c_{ST}$ , also shows a different dynamic and different value in the redshift range we have studied.

Several observational data coming from quasar absorption lines and also the LIGO-Virgo event are also consistent with a non-varying speed of electromagnetic waves.

- Here, in order to fit the causal structure constant of the Hubble parameter with observations, we tried to use observations which are not dealing with electromagnetic waves; meaning that for the Observable Hubble Data we only used the differential age method and for the causal structure constant, we tried to compare the model with  $\Lambda$ CDM model. The distance modulus of the SN Ia has also been compared statistically with observations done with electromagnetic waves and we are aware that any dynamics in the speed of electromagnetic waves can change the data. However, we also compared our results with the  $\Lambda$ CDM model which in this case is more acceptable than only comparing the model with observational data. The comparison between the distance modulus coming from this model and the  $\Lambda$ CDM model shows they are in good agreement.

- In this model, no dynamics for the speed of gravitational waves ( $c_{GW}$ ) is achieved (Izadi & Shojai, 2009). Also, using SN data, one concludes that  $c_{ST}$  is different from  $c_{GW}$ . Unlike the standard theory, in which both these facets of the speed of light coincide, the difference between these two facets shows that gravitational waves are not the ripples of space time anymore. Therefore, the speed with which the gravitational waves travel differs from the causal structure constant used for length measurements.
- The constancy of the speed of gravitational waves makes them a useful tool for measuring distances.  
Using observational data from LIGO and LIGO-Virgo events, the distance taken from the observed gravitational waves ( $r_g$ ) differs slightly from the one taken from  $c_{ST}$  ( $d_L$ ). However, it was shown that this difference is not detectable within today's observational precision.
- As there is only one GW event (LIGO-Virgo) in which there is an electromagnetic coalescence involved, using gravitational waves, we can only put constraints on  $c_{EM}$  in one specific redshift. This event makes a very small possible range for the value of  $c_{EM}$  and accordingly  $\gamma$ , in this redshift.

All in all, the findings of this thesis provide support for possible difference between several facets of the speed of light.

Obviously, we could not cover many of the cosmological observations in this thesis. However, we tried to find out what constraints these observational data can put on the dynamics of different notions of the speed of light.

Here we emphasize that an ultimate model requires to match with as much observations as we have today. This of course needs more time and effort and can be considered as a future possible work.



# Bibliography

- Abbott, B. P., Abbott, R., Abbott, T. D., Abernathy, M. R., Acernese, F., Ackley, K., Adams, C., Adams, T., Addesso, P., Adhikari, R. X., & et al., GW151226: Observation of Gravitational Waves from a 22-Solar-Mass Binary Black Hole Coalescence. 2016a, *Physical Review Letters*, 116, 241103
- , Observation of Gravitational Waves from a Binary Black Hole Merger. 2016b, *Physical Review Letters*, 116, 061102
- Abbott, B. P., Abbott, R., Abbott, T. D., Acernese, F., Ackley, K., Adams, C., Adams, T., Addesso, P., Adhikari, R. X., Adya, V. B., & et al., Gravitational Waves and Gamma-Rays from a Binary Neutron Star Merger: GW170817 and GRB 170817A. 2017a, *Astrophysical Journal, Letters*, 848, L13
- , GW170104: Observation of a 50-Solar-Mass Binary Black Hole Coalescence at Redshift 0.2. 2017b, *Physical Review Letters*, 118, 221101
- , GW170817: Observation of Gravitational Waves from a Binary Neutron Star Inspiral. 2017c, *Physical Review Letters*, 119, 161101
- Albrecht, A. & Magueijo, J., Time varying speed of light as a solution to cosmological puzzles. 1999, *Physical Review D*, 59, 043516
- Amendola, L. & Tsujikawa, S. 2010, *Dark Energy: Theory and Observations*
- Balcerzak, A. & Dabrowski, M. P., Redshift drift in varying speed of light cosmology. 2014, *Physics Letters B*, 728, 15
- Barrow, J. D., *Constants and Variations: From Alpha to Omega*. 2003, *Astrophysics and Space Science*, 283, 645
- Barrow, J. D. & Lip, S. Z. W., Generalized theory of varying alpha. 2012, *Physical Review D*, 85, 023514
- Capozziello, S. & de Laurentis, M., *Extended Theories of Gravity*. 2011, *Physics Reports*, 509, 167

- Capozziello, S., De Laurentis, M., Fatibene, L., & Francaviglia, M., The physical foundations for the geometric structure of relativistic theories of gravitation. From General Relativity to Extended Theories of Gravity through Ehlers-Pirani-Schild approach. 2012, *Int.J.Geom.Meth.Mod.Phys*, 09, 1250072
- Chand, H., Petitjean, P., Srianand, R., & Aracil, B., Probing the time-variation of the fine-structure constant: Results based on Si IV doublets from a UVES sample. 2005, *Astronomy and Astrophysics*, 430, 47
- Chand, H., Srianand, R., Petitjean, P., & Aracil, B., Probing the cosmological variation of the fine-structure constant: Results based on VLT-UVES sample. 2004, *Astronomy and Astrophysics*, 417, 853
- Clifton, T., Ferreira, P. G., Padilla, A., & Skordis, C., Modified gravity and cosmology. 2012, *Physics Reports*, 513, 1
- Coles, P. & Lucchin, F. 2002, *Cosmology: The Origin and Evolution of Cosmic Structure*, Second Edition
- Damour, T., The Equivalence Principle and the Constants of Nature. 2009, *Space Science Reviews*, 148, 191
- de Felice, A. & Tsujikawa, S., *f(R) Theories*. 2010, *Living Reviews in Relativity*, 13
- D’Inverno, R. A. 1992, *Introducing Einstein’s relativity*
- Ellis, G. F. R., Maartens, R., & MacCallum, M. A. H. 2012, *Relativistic Cosmology*
- Ellis, G. F. R. & Uzan, J.-P., *c is the speed of light, isn’t it?* 2005, *American Journal of Physics*, 73, 240
- Faraoni, V. & Capozziello, S. 2011, *Beyond Einstein Gravity*
- Farooq, O. & Ratra, B., Hubble Parameter Measurement Constraints on the Cosmological Deceleration-Acceleration Transition Redshift. 2013, *Astrophysical Journal, Letters*, 766, L7
- Fatibene, L. & Francaviglia, M., *Extended Theories of Gravitation and the Curvature of the Universe – Do We Really Need Dark Matter?* 2012, *Open Questions in Cosmology*, Dr. Gonzalo J. Olmo (Ed.)
- Fatibene, L. & Garruto, S., *Extended theories of gravitation*. 2016, *International Journal of Geometric Methods in Modern Physics*, 13, 1650070
- Hobson, M. P., Efstathiou, G. P., & Lasenby, A. N. 2006, *General Relativity*, 590

- Izadi, A., Sajedi Shacker, S., Olmo, G. J., & Banerjee, R., Observational effects of varying speed of light in quadratic gravity cosmological models. 2017, ArXiv e-prints
- Izadi, A. & Shojai, A., The speed of light in extended gravity theories. 2009, *Classical and Quantum Gravity*, 26, 195006
- , Measurement of the space-time interval in modified gravity theories in Palatini formalism. 2013, *General Relativity and Gravitation*, 45, 229
- Joyce, A., Jain, B., Khoury, J., & Trodden, M., Beyond the cosmological standard model. 2015, *Physics Reports*, 568, 1
- Kotuš, S. M., Murphy, M. T., & Carswell, R. F., High-precision limit on variation in the fine-structure constant from a single quasar absorption system. 2017, *Monthly Notices of the RAS*, 464, 3679
- Li, B., Barrow, J. D., & Mota, D. F., Cosmology of Ricci-tensor-squared gravity in the Palatini variational approach. 2007, *Physical Review D*, 76, 104047
- Liske, J., Grazian, A., Vanzella, E., Dessauges, M., Viel, M., Pasquini, L., Haehnelt, M., Cristiani, S., Pepe, F., Avila, G., Bonifacio, P., Bouchy, F., Dekker, H., Delabre, B., D’Odorico, S., D’Odorico, V., Levshakov, S., Lovis, C., Mayor, M., Molaro, P., Moscardini, L., Murphy, M. T., Quéloz, D., Shaver, P., Udry, S., Wiklind, T., & Zucker, S., Cosmic dynamics in the era of Extremely Large Telescopes. 2008a, *Monthly Notices of the RAS*, 386, 1192
- Liske, J., Grazian, A., Vanzella, E., Dessauges, M., Viel, M., Pasquini, L., Haehnelt, M., Cristiani, S., Pepe, F., Bonifacio, P., Bouchy, F., D’Odorico, S., D’Odorico, V., Levshakov, S., Lovis, C., Mayor, M., Molaro, P., Moscardini, L., Murphy, M., Quéloz, D., Udry, S., Wiklind, T., & Zucker, S., E-ELT and the Cosmic Expansion History - A Far Stretch? 2008b, *The Messenger*, 133, 10
- Magueijo, J., New varying speed of light theories. 2003, *Reports on Progress in Physics*, 66, 2025
- Martínez Fiorenzano, A. F., Vladilo, G., & Bonifacio, P., Search for alpha variation in UVES spectra: Analysis of CIV and Si IV doublets towards QSO 1101-264. 2003, *Memorie della Societa Astronomica Italiana Supplementi*, 3, 252
- Mohr, P. J., Newell, D. B., & Taylor, B. N., CODATA recommended values of the fundamental physical constants: 2014\*. 2016, *Reviews of Modern Physics*, 88, 035009
- Murphy, M. T., Malec, A. L., & Prochaska, J. X., Precise limits on cosmological variability of the fine-structure constant with zinc and chromium quasar absorption lines. 2016, *Monthly Notices of the RAS*, 461, 2461

- Murphy, M. T., Webb, J. K., Flambaum, V. V., Dzuba, V. A., Churchill, C. W., Prochaska, J. X., Barrow, J. D., & Wolfe, A. M., Possible evidence for a variable fine-structure constant from QSO absorption lines: motivations, analysis and results. 2001a, *Monthly Notices of the RAS*, 327, 1208
- Murphy, M. T., Webb, J. K., Flambaum, V. V., Prochaska, J. X., & Wolfe, A. M., Further constraints on variation of the fine-structure constant from alkali-doublet QSO absorption lines. 2001b, *Monthly Notices of the RAS*, 327, 1237
- Olmo, G. J., Hydrogen atom in Palatini theories of gravity. 2008, *Physical Review D*, 77, 084021
- Olmo, G. J., Introduction to Palatini Theories of Gravity and Nonsingular Cosmologies, *Open Questions in Cosmology*. 2012, *Open Questions in Cosmology*, Dr. Gonzalo J. Olmo (Ed.)
- Padmanabhan, T. 1993, *Structure Formation in the Universe*, 499
- Perlmutter, S., Aldering, G., Goldhaber, G., Knop, R. A., Nugent, P., Castro, P. G., Deustua, S., Fabbro, S., Goobar, A., Groom, D. E., Hook, I. M., Kim, A. G., Kim, M. Y., Lee, J. C., Nunes, N. J., Pain, R., Pennypacker, C. R., Quimby, R., Lidman, C., Ellis, R. S., Irwin, M., McMahon, R. G., Ruiz-Lapuente, P., Walton, N., Schaefer, B., Boyle, B. J., Filippenko, A. V., Matheson, T., Fruchter, A. S., Panagia, N., Newberg, H. J. M., Couch, W. J., & Project, T. S. C., Measurements of  $\Omega$  and  $\Lambda$  from 42 High-Redshift Supernovae. 1999, *Astrophysical Journal*, 517, 565
- Planck Collaboration, Ade, P. A. R., & et al., Planck intermediate results. XXIV. Constraints on variations in fundamental constants. 2015, *Astronomy and Astrophysics*, 580, A22
- Qi, J.-Z., Zhang, M.-J., & Liu, W.-B., Observational constraint on the varying speed of light theory. 2014, *Physical Review D*, 90, 063526
- Riess, A. G., Filippenko, A. V., Challis, P., Clocchiatti, A., Diercks, A., Garnavich, P. M., Gilliland, R. L., Hogan, C. J., Jha, S., Kirshner, R. P., Leibundgut, B., Phillips, M. M., Reiss, D., Schmidt, B. P., Schommer, R. A., Smith, R. C., Spyromilio, J., Stubbs, C., Suntzeff, N. B., & Tonry, J., Observational Evidence from Supernovae for an Accelerating Universe and a Cosmological Constant. 1998, *Astronomical Journal*, 116, 1009
- Sandage, A., The Change of Redshift and Apparent Luminosity of Galaxies due to the Deceleration of Selected Expanding Universes. 1962, *Astrophysical Journal*, 136, 319
- Sotiriou, T. P. 2007, PhD thesis, PhD Thesis, 2007
- Sotiriou, T. P. & Faraoni, V.,  $f(R)$  theories of gravity. 2010, *Reviews of Modern Physics*, 82, 451
- Srianand, R., Petitjean, P., Chand, H., & Aracil, B., Constraining the time variation of the fine structure constant. 2004, *The Messenger*, 116, 25

- Suzuki, N. & et. al., The Hubble Space Telescope Cluster Supernova Survey. V. Improving the Dark-energy Constraints above  $z > 1$  and Building an Early-type-hosted Supernova Sample. 2012, *Astrophysical Journal*, 746, 85
- Tsujikawa, S., Modified Gravity Models of Dark Energy. 2010, in *Lecture Notes in Physics*, Berlin Springer Verlag, Vol. 800, *Lecture Notes in Physics*, Berlin Springer Verlag, ed. G. Wolschin, 99–145
- Tsujikawa, S., Dark Energy: Investigation and Modeling. 2011, in *Astrophysics and Space Science Library*, Vol. 370, *Astrophysics and Space Science Library*, ed. S. Matarrese, M. Colpi, V. Gorini, & U. Moschella, 331
- Tsujikawa, S., Dark Energy: Observational Status and Theoretical Models. 2013, in *Lecture Notes in Physics*, Berlin Springer Verlag, Vol. 863, *Lecture Notes in Physics*, Berlin Springer Verlag, ed. G. Calcagni, L. Papantonopoulos, G. Siopsis, & N. Tsamis, 289
- Uzan, J.-P., Variation of the Constants of Nature in the Early and Late Universe. 2004, in *American Institute of Physics Conference Series*, Vol. 736, *Phi in the Sky: The Quest for Cosmological Scalar Fields*, ed. C. J. A. P. Martins, P. P. Avelino, M. S. Costa, K. Mack, M. F. Mota, & M. Parry, 3–20
- Uzan, J.-P., Varying Constants, Gravitation and Cosmology. 2011, *Living Reviews in Relativity*, 14, 2
- Webb, J. K., Flambaum, V. V., Churchill, C. W., Drinkwater, M. J., & Barrow, J. D., Search for Time Variation of the Fine Structure Constant. 1999, *Physical Review Letters*, 82, 884
- Webb, J. K., Murphy, M. T., Flambaum, V. V., Dzuba, V. A., Barrow, J. D., Churchill, C. W., Prochaska, J. X., & Wolfe, A. M., Further Evidence for Cosmological Evolution of the Fine Structure Constant. 2001, *Physical Review Letters*, 87, 091301
- Weinberg, S. 2008, *Cosmology* (Oxford University Press)
- Zhang, P. & Meng, X., SNe data analysis in variable speed of light cosmologies without cosmological constant. 2014, *Modern Physics Letters A*, 29, 1450103
- Zhang, T.-J., Ma, C., & Lan, T., Constraints on the Dark Side of the Universe and Observational Hubble Parameter Data. 2010, *Advances in Astronomy*, 2010, 184284